MALATYA TURGUT ÖZAL UNIVERSITY

NATURENGS

MTU Journal of Engineering and Natural Sciences

Volume: 2 Issue: 2 - December 2021

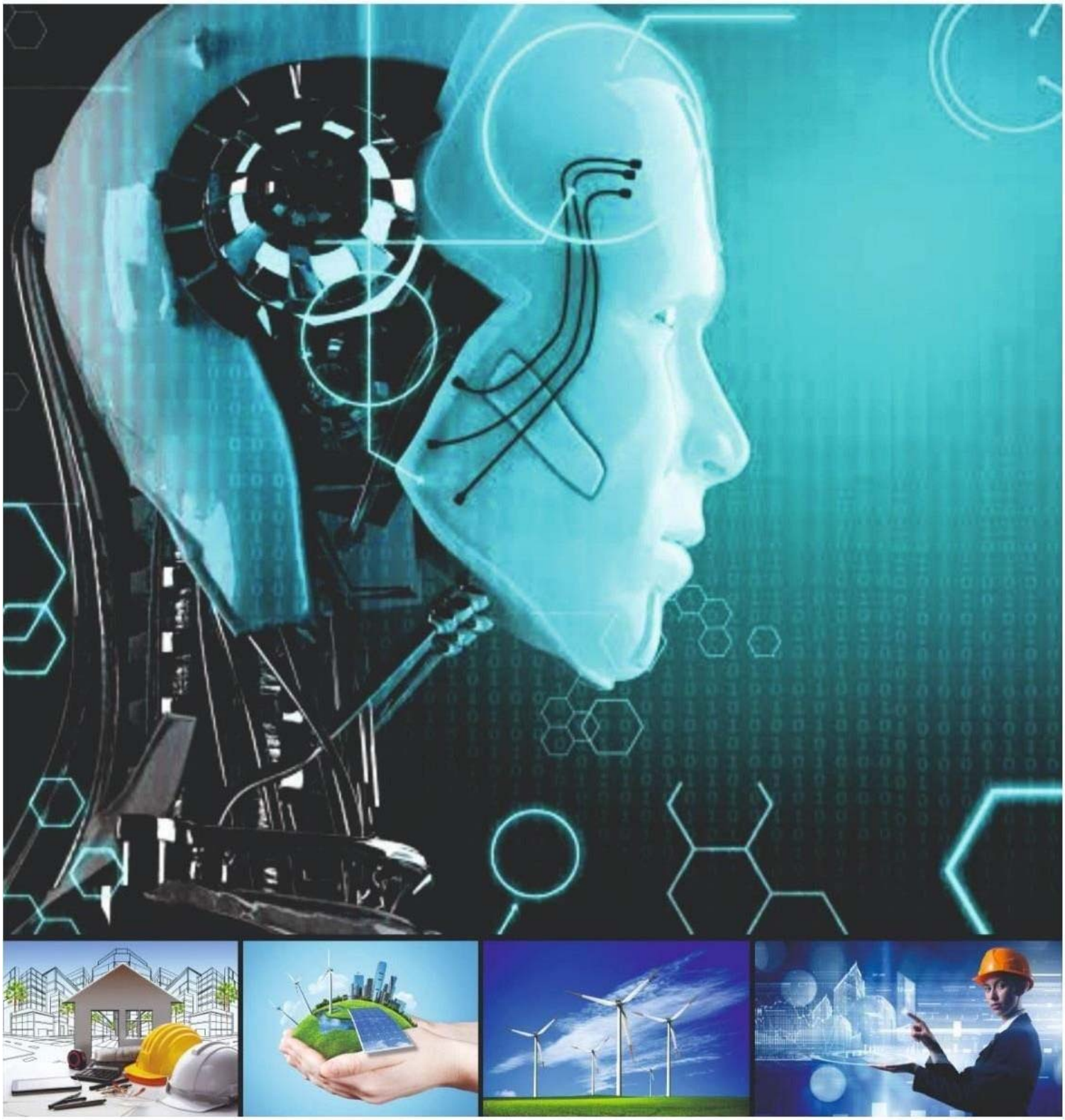

https://dergipark.org.tr/tr/pub/naturengs

www.naturengs.com

MALATYA TURGUT ÖZAL UNIVERSITY

NATURENGS

MTU Journal of Engineering and Natural Sciences

Volume: 2 / Issue: 2 / December - 2021

We are delighted to present the second volume of the journal NATURENGS owned by Malatya Turgut Özal University. MTU Journal of Engineering and Natural Sciences – NATURENGS is a double- blind peer-reviewed, open-access international journal which will publish electronically two times in a year by the Malatya Turgut Özal University from June 2020.

We set out with the desire to create an environment where scientific and/or technological studies carried out in universities, industry and other research institutions will be shared. We aim to advance by giving priority to studies involving scientific and / or technological originality.

Manuscripts submitted for publication are analyzed in terms of scientific quality, ethics and research methods in terms of its compliance by the Editorial Board representatives of the relevant areas. Then, the abstracts of the appropriate articles are sent to at least two different referees with a well-known in scientific area. If the referees agree to review the article, full text in the framework of the privacy protocol is sent. By the decisions of referees, either directly or corrected article is published or rejected. Confidential reports of the referees in the journal archive will be retained for ten years. All post-evaluation process is done electronically on the internet.

In the journal's publication policy, we would like to state that we will not compromise on quality. In this process, we know that we have undertaken important tasks, especially the selection of referees and monitoring of evaluations. Our journal is indexed in *Index Copernicus, CiteFactor, Google Scholar, Scientific Indexing Services, ASOS and ESJI* international databases. We will work with the devotion to get our journal into the TR-Index and then the Science Citation Index database as soon as possible.

We would like to thanks our Rector, Prof. Dr. Aysun Bay KARABULUT, who encouraged and supported the establishment of our journal. In addition, we would like to thank all the Authors and Referees who contributed to this issue.

Assist. Prof. Aydan AKSOĞAN KORKMAZ
On behalf of the Editorial Board

MALATYA TURGUT ÖZAL UNIVERSITY

NATURENGS

MTU Journal of Engineering and Natural Sciences

Volume: 2 / Issue: 2 / December- 2021

ISSN: 2717-8013

Owner / Publisher

Prof. Dr. Aysun BAY KARABULUT for Malatya Turgut Özal University

Editor

Assist. Prof. Aydan AKSOĞAN KORKMAZ

Malatya Turgut Özal University, 44210 Battalgazi/Malatya,

TURKEY Phone: +90-422-846 12 55 Fax: +90-422-846 12 25

e-mail: aydan.aksogan@ozal.edu.tr

Co-Editor

Assoc. Prof. Harun KAYA

Malatya Turgut Özal University, 44210 Battalgazi/Malatya,

TURKEY Phone: +90-422-846 12 55 Fax: +90-422-846 12 25

e-mail: harun.kaya@ozal.edu.tr

Contact Information

MTU Journal of Engineering and Natural Sciences – NATURENGS,

Malatya Turgut Özal University, 44210, Battalgazi/Malatya, TURKEY

Phone: +90-422 846 12 55, Fax: +90-422 846 12 25,

e-mail: naturengs@ozal.edu.tr

web: https://dergipark.org.tr/tr/pub/naturengs

CONTENTS

NATURENGS
MTU Journal of Engineering and Natural Sciences
https://dergipark.org.tr/tr/pub/naturengs
DOI: 10.46572/naturengs.949458

Research Article

Effects of Different Nose Cone Designs on Trajectory and Impact Angle of Smart Fire Extinguishing Ammunition

Murat TOPTAŞ [1*], Mehmet YILMAZ [2]

[1]Department of Mechanical Engineering, Faculty of Engineering, Inonu University, Malatya, Turkey.
[2]Department of Mechanical Engineering, Faculty of Engineering, Inonu University, Malatya, Turkey.

(**Received:** 08.06.2021; **Accepted:** 19.06.2021)

ABSTRACT: A nose cone is the conically shaped tip part of a missile, bomb or aircraft, used to regulate the behavior of oncoming airflow and minimize drag. In this study, the effects of different nose cone designs on the trajectory and impact angle of smart fire extinguishing ammunition were investigated. For this purpose, three different types of ammunition with different nose cone profiles were designed: spherically blunted conic nose cone, spherically blunted tangent ogive nose cone and truncated tangent ogive nose cone. A virtual wind tunnel was created in the computer environment and CFD software was used to calculate the drag coefficients for each design. By applying Newton's second law of motion, the horizontal distance the ammunition received before the striking fire, impact speed, and impact angle were calculated. The obtained results were compared using One-Way ANOVA (analysis of variance) to determine whether there is statistical evidence that the associated population means are significantly different. It was determined that the three types of nose cone designs examined did not have a significant effect on the impact speed, impact angle and horizontal distance of the ammunition at the investigated speeds and altitudes. On the other hand, flame detection, distance measurement and impact sensors, which should be in the smart fire extinguishing ammunition, should be on the plane at the front of the ammunition and in contact with the external environment. To place these sensors in the nose cone, a truncated tangent ogive nose cone was chosen as the nose cone for the smart fire extinguishing ammunition.

Keywords: Aerial Fire Fighting, Smart Fire Extinguishing Ammunition, Nose Cone, CFD.

1. INTRODUCTION

Aircraft, or any type of body moving through a fluid, encounter a drag force that decreases their performance. The drag force is due to the combined effects of pressure and wall shear forces in the flow direction. The part of drag that is due directly to wall shear stress τ_ω is called the skin friction drag (or just friction drag), and the part that is due directly to pressure P is called the pressure drag [1]. Pressure drags occurs by resultant pressure distribution over the surface [2]. Layer separation occurs when the flow slows down and static pressure increases in the direction of flow [3]. This situation is also known as adverse pressure gradient [4]. Adverse pressure gradients produce pressure drags. To improve performance, designers working in this area should identify where these resistance forces are dominant and eliminate or minimize them.

*Corresponding Author: murat.toptas@inonu.edu.tr
ORCID number of authors: [1] 0000-0001-9368-5675, [2] 0000-0001-5025-1842

The most important parts of a body exposed to these influences as it passes through a fluid are nose cones. A nose cone is the conically shaped tip part of a missile, bomb or aircraft, used to regulate the behavior of oncoming airflow and minimize drag. Nose cone profiles have a significant impact on aerodynamic characteristics [5]. Because they are the first parts that meet the resistance forces, arising from pressure and friction drags. Nose cones serve to regulate the behavior of the oncoming airflow and minimize drag. However, at velocities below 0.8 Mach, the pressure drag for all kinds of the nose cone is zero and the main resistance factor is the friction drag [6]. To reduce the drag forces and increase the performance of the design, the most appropriate nose cone type should be chosen. Conic, spherically blunted conic, bi-conic, tangent ogive, spherically blunted tangent ogive, secant ogive, elliptic, parabolic, power series and Haack series are the cone designs generally used for aerospace applications [6].

Smart fire extinguishing ammunition (SFEA) is a new and effective product we have designed for use in aerial firefighting (Figure 1a). This product was called smart fire extinguishing ammunition, taking into account some electronic equipment and software that makes the product autonomous. To realize the design goals and requirements, and also to ensure the practicality and cheapness of its use, the ammunition was designed with the dimensions of MK-82 air-to-ground general-purpose NATO ammunition (Figure 1b). There is a boron-based extinguishing agent in the ammunition and the ammunition is thrown onto the fires from an air vehicle. The explosive placed in the ammunition center detonates when it reaches the fire area and the extinguishing agent is scattered over the fire area.

(a) (b)

Figure 1. (a) Smart fire extinguishing ammunition (SFEA) **(b)** Low drag general-purpose bomb Mark-82

SEFA is expected to do its job successfully regardless of the type of fire. For this to happen, the spread of the extinguishing agent on the fire must occur in different patterns. One way to achieve this result is to drop the ammunition on the fire at different angles. Figures 2 and 3 show what the angles of impact of SFEA should be for different types of fires and what the dispersion of the extinguishing agent should be.

Figure 2. Circular scattering template of SFEA

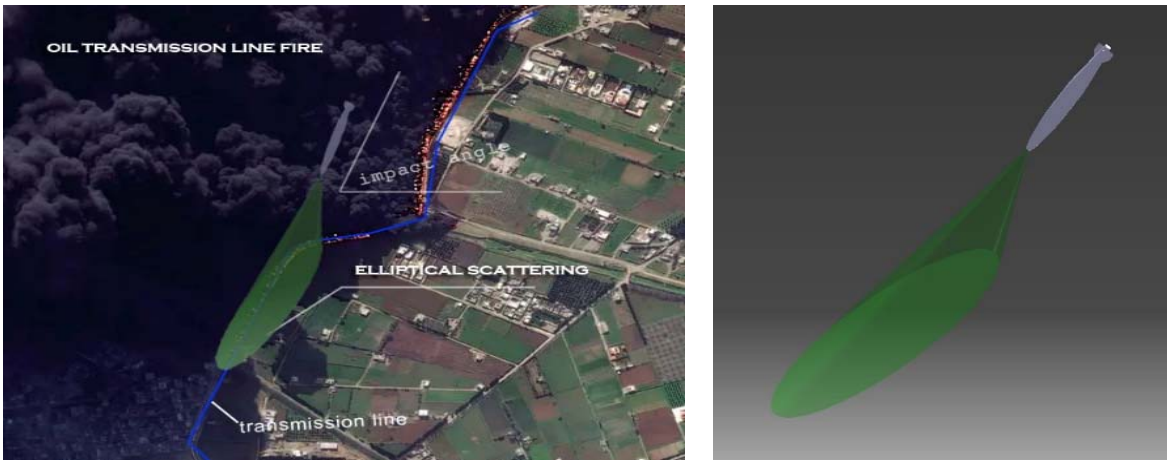

Figure 3. Elliptical scattering template of SFEA

This study aims to determine the most appropriate type of nose cone for SFEA and to examine the effects of different nose cone designs on the trajectory and impact angle of SFEA. For this purpose, three different types of ammunition with different nose cone profiles were designed: spherically blunted conic nose cone, spherically blunted tangent ogive nose cone and truncated tangent ogive nose cone. A virtual wind tunnel was created in the computer environment and Ansys Fluent 16.0 was used to calculate the drag coefficients for each design. By applying Newton's second law of motion, the horizontal distance the ammunition received before the striking fire, impact speed, and impact angle were calculated. The obtained results were compared using One-Way ANOVA (analysis of variance) to determine whether there is statistical evidence that the associated population means are significantly different. As a result of the study, the most appropriate type of nose cone for SFEA was determined.

2. SMART FIRE EXTINGUISHING AMMUNITION (SFEA)

Aerial firefighting methods are complementary to land firefighting methods. In aerial firefighting methods, extinguishing agents such as water, foam and soil are left on fires by an air vehicle. However, because of the air resistance and also airflows caused by the heated air, the appropriate amount of extinguishing material can not reach its target. Therefore, an innovative and effective product, which can be used in aerial firefighting, has been designed. This product was called smart fire extinguishing ammunition (SFEA), taking into account several electronic equipment and software that make the product autonomous. SFEA is an effective product that has not been designed before. To realize the design goals and requirements, and also to ensure the practicality and cheapness of its use, the ammunition was designed with the dimensions of MK-82 air-to-ground general-purpose NATO ammunition (Figure 4). In this way, it will be possible to load the SFEA without the need for any change on the aircraft which will carry ammunition. This means that no extra infrastructure investment costs will arise for the countries that will purchase the SFEA. The target of the SFEA is open area fires such as forests, petrochemical plants, oil and gas transmission lines and ammunition depots outside of residential areas. The purpose of SFEA is to deliver the extinguishing agent in the ammunition to the fire point with minimum deviation without being affected by weather conditions. Having the appropriate sensors, electronic equipment and software, the SFEA can determine the most suitable point where the explosion will occur after the ammunition is dropped from the aircraft.

The SFEA consists of ammunition body, nose cone, tail-wing assembly, extinguishing - cooling material, explosive substance, fuze, electronic equipment and software. Figure 5 shows the components of the smart fire extinguishing ammunition.

The SFEA is a new product for both the fire-fighting industry and the aviation industry. If the product goes into mass production, a combat tool that will make significant contributions in fighting fires will be obtained. Extinguisher-coolant can be left on the fire in the correct amount so that while the fires are extinguished, there will be no damage to the environment due to the use of excessive chemicals. In addition, considering both the efficiency of the product and the speed factors of the aircraft, fires can be controlled without spreading over large areas as before.

To design and create the three-dimensional product, computer-aided design software (Catia V.5) was used. Structural, flow and explosion analyses of the product were performed with ANSYS software. The software of the product was written in the C programming language.

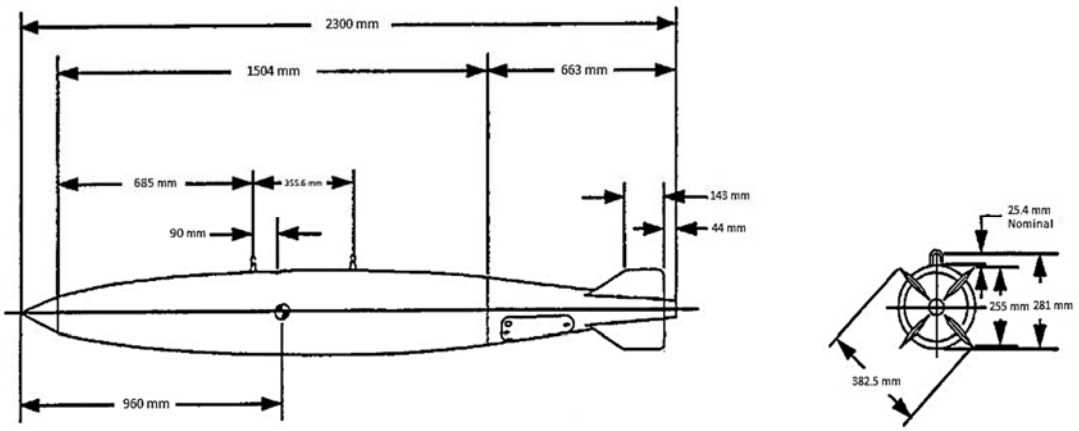

Figure 4. Dimensions of MK-82 ammunition [7]

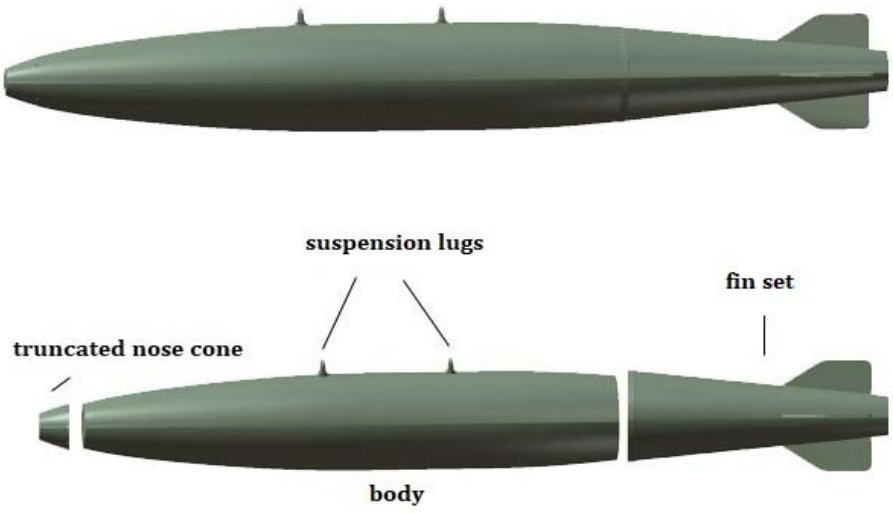

Figure 5. The smart fire extinguishing ammunition (SFEA)

3. MATERIAL AND METHODS

3.1. Design of Nose Cones

Various types of nose cones and their aerodynamics performances have been investigated in the literature [5,6,8]. Three nose cone types have been selected and designed to suit the ammunition so that the SFEA will achieve the expected objectives and create a low drag coefficient. The nose cones examined are spherically blunted conic, spherically blunted tangent ogive and truncated tangent ogive type nose cones (Figure 6).

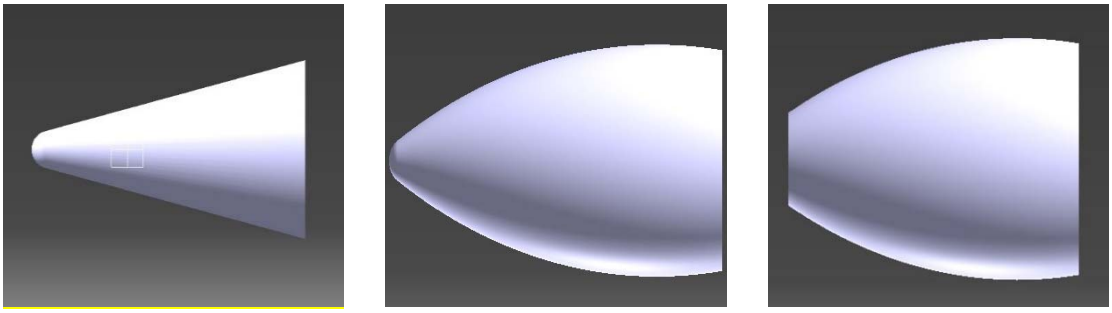

(a (b) (c)

Figure 6. Types of nose cones studied: (a) Spherically blunted conic nose cone; (b) Spherically blunted tangent ogive nose; (c) Truncated tangent ogive nose cone

Spherically blunted conic nose cones are created by blunting conic cones with a sphere (Figure 7-8). The point where the sphere meets the cone (tangent point) can be found from the following equations [7]:

$$x_t = \frac{L^2}{R}\sqrt{\frac{r_n^2}{R^2 + L^2}} \tag{1}$$

$$y_t = \frac{x_t R}{L} \tag{2}$$

here "L" is the total length of the nose cone, R is the radius of the base, r_n is radius of sphere which used for blunting. The center point (x_o) and apex point (x_a) of the blunting sphere can be found using Eqs. (3) and (4), respectively:

$$x_0 = x_t + \sqrt{r_n^2 - y_t^2} \tag{3}$$

$$x_a = x_0 - r_n \tag{4}$$

The second type of nose cone examined is the spherically blunted tangent ogive nose cone (Figure 9-10). Tangent ogive shape profiles are created by a segment of a circle tangent to the curve of the nose cone at the base of the missile, bomb, or aircraft. If this nose cone profile is blunted by capping it with a segment of a sphere, the point where the sphere meets the cone (tangent point) (Figure 10) can be found from the following equations:

$$\rho = \frac{R^2 + L^2}{2R} \tag{5}$$

$$y = \sqrt{\rho^2 - (L - x)^2} + R - \rho \tag{6}$$

$$x_0 = L - \sqrt{(\rho - r_n)^2 - (\rho - r)^2} \tag{7}$$

$$y_t = \frac{r_n(\rho - R)}{\rho - r_n} \tag{8}$$

$$x_t = x_0 - \sqrt{r_n^2 - y_t^2} \tag{9}$$

The apex point can be found using the same equation for the spherically blunted conic nose cone:

$$x_a = x_0 - r_n \tag{10}$$

The third type of nose cone examined is the truncated tangent ogive nose cone (Figures 11 and 12). This type of nose cone is the same as the spherically blunted tangent ogive nose cone, except that the nose part is not spherically blunted, but is truncated directly after a certain length (Figure 12). The design equations for the truncated tangent ogive nose cone are the same as for the spherically blunted conic nose cone, except that the truncated tangent ogive nose cones are cut at a distance x_a from the tip and are not blunted by any geometric shape (Figure 12).

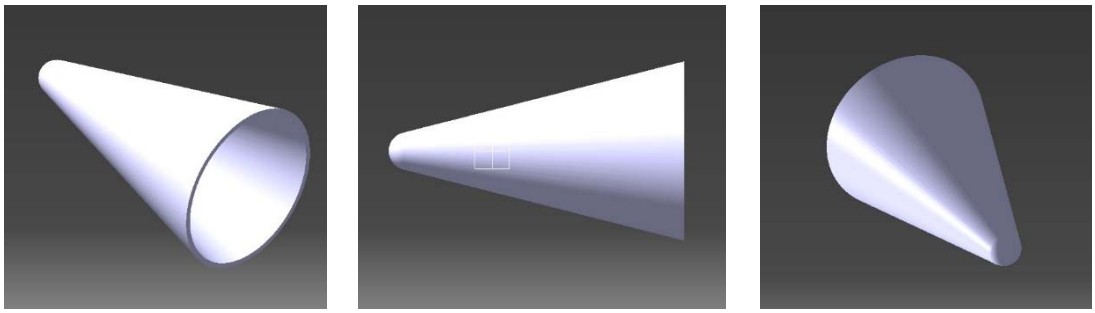

Figure 7. Spherically blunted conic nose cone

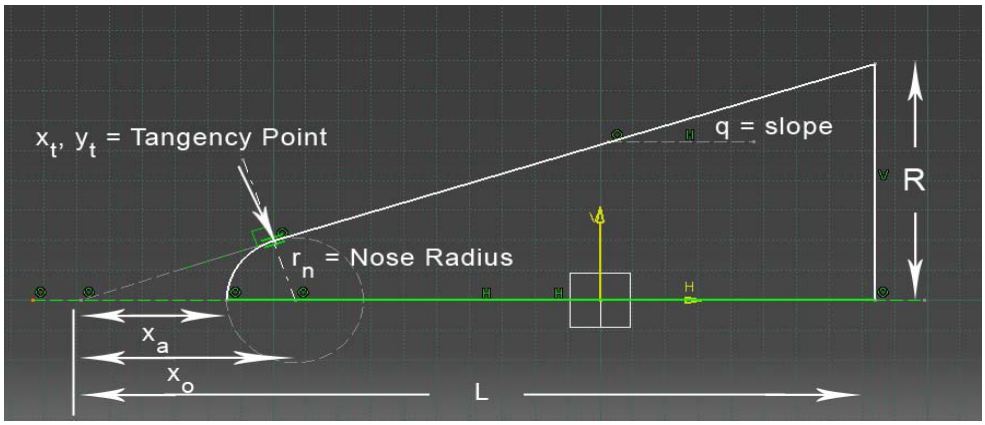

Figure 8. Spherically blunted conic nose cone profile [9]

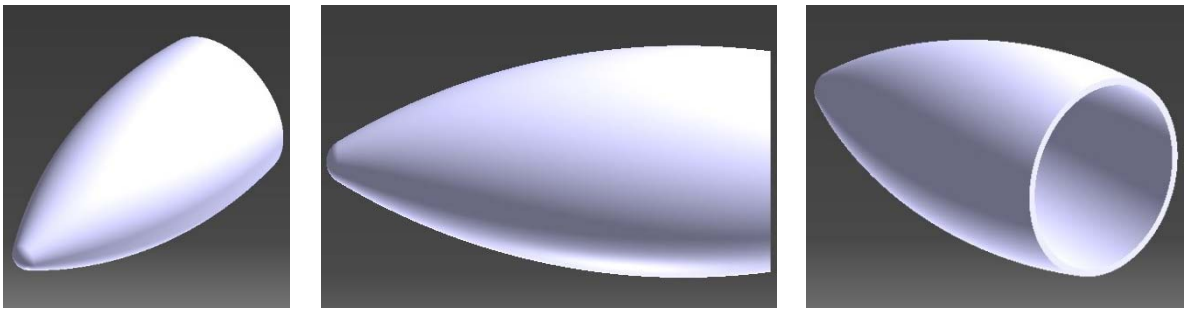

Figure 9. The spherically blunted tangent ogive nose cone

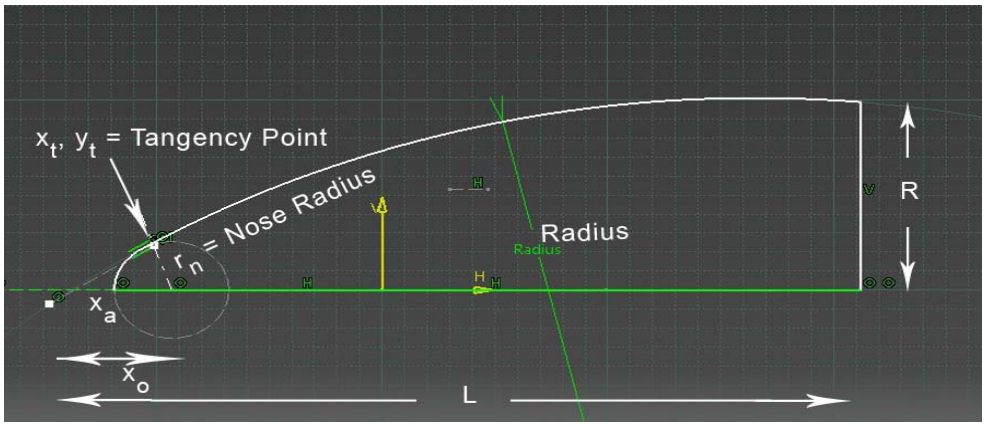

Figure 10. Spherically blunted tangent ogive nose cone profile [9]

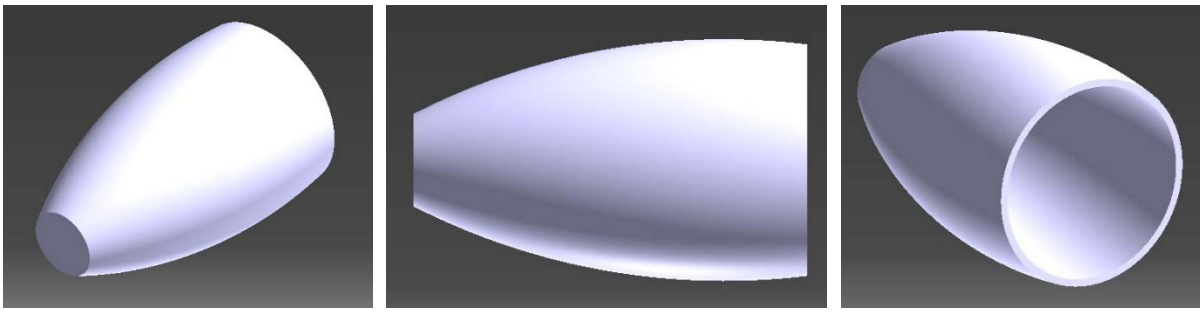

Figure 11. The truncated tangent ogive nose cone

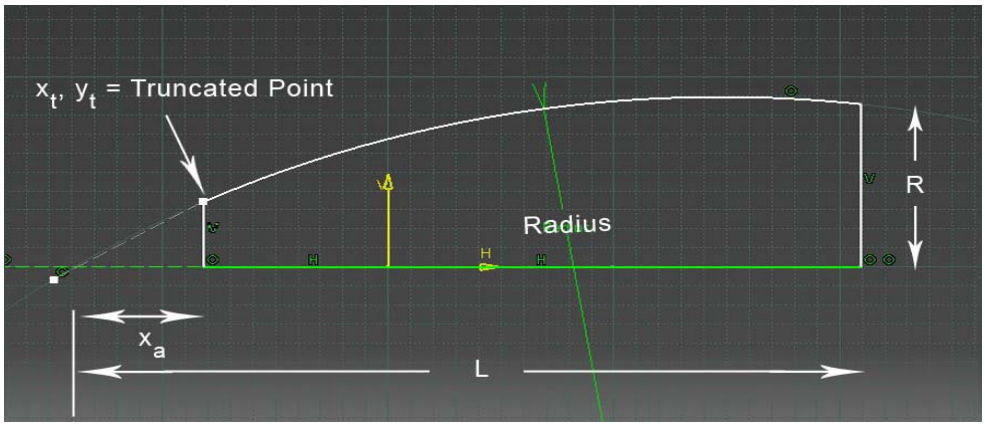

Figure 12. The truncated tangent ogive nose cone profile [9]

3.2. Creating Solid Models of Nose Cones

To realize the design goals and requirements, three suitable nose cone types were selected from the literature and modeled for the ammunition. Using Eqs. (1)-(10), the x and y coordinates for each nose cone were determined. Then, these coordinates were transferred to a 3D design software (Catia V5.R.20) and solid models of the objects were created. This solid model of nose cones was mounted to the body of SFEA. These models are given in Fig. 13.

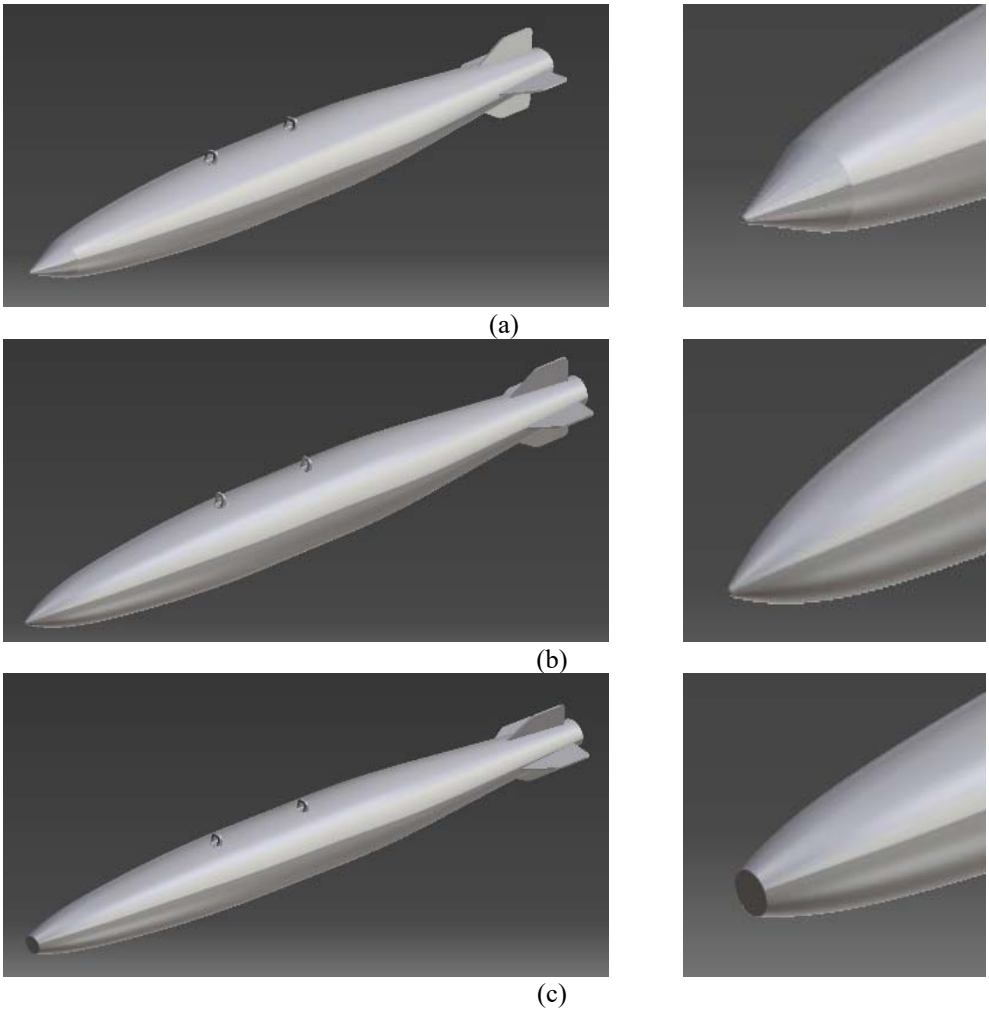

Figure 13. Different nose cones assemblies on ammunition body: (a) Spherically blunted conic nose cone; (b) Spherically blunted tangent ogive nose; (c) Truncated tangent ogive nose cone

3.3. Creating The Mesh Structures

The generated mesh structures and inflation layers associated with the ammunition geometries are shown in Figure 14.

3.4. Ammunition Trajectory and Impact Angle Calculations

The motion and path of the SFEA dropped from the aircraft can be described by Newton's second law of motion. If the trajectory of the SFEA dropped from the aircraft under the effect of drag force is expressed by force equations, the following equations are obtained. Here, the direction of the ammunition is taken as "+x" and the direction of fall (direction of gravity) is taken as "-y":

$$F_x = ma_x = -m\left(\frac{V_x}{V}\right)bV^2 \tag{11}$$

$$F_y = ma_y = -mg + m\left(\frac{V_y}{V}\right)bV^2 \tag{12}$$

$$b = C_d \rho_a A/m \tag{13}$$

b: air resistance (m^{-1})

m: mass of ammunition

ρ_{air}: density of air (kg/m^3)

A: cross-sectional area of ammunition (m^2)

C_d: drag coefficient

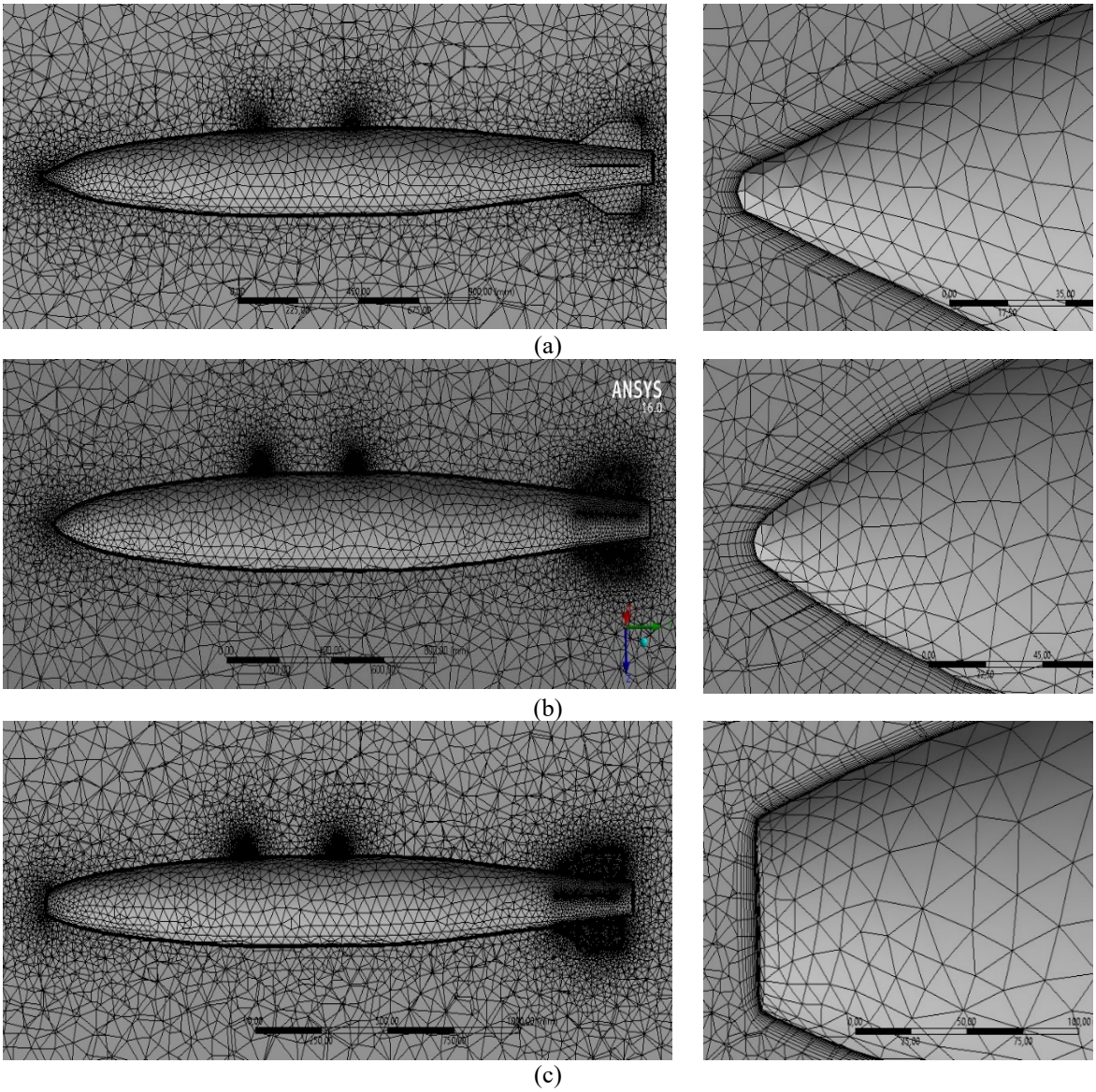

(a)

(b)

(c)

Figure 14. Mesh structures and inflation layers of nose cones: (a) Spherically blunted conic nose cone; (b) Spherically blunted tangent ogive nose; (c) Truncated tangent ogive nose cone

If Eqs. (11) and Eq. (12) are divided by mass, substituting dV_x/dt for ax, dV_y/dt for ay, and Δt for dt, the following equations are obtained:

$$V_x(t+\Delta t) = V_x(t) - bV_xV\Delta t \tag{14}$$

$$V_y(t+\Delta t) = V_y(t) - g\Delta t - bV_yV\Delta t \tag{15}$$

When equations (14) and (15) are entered into a spreadsheet, V_x, V_y velocities, a path taken by the ammunition in the x-direction, and total travel time can be calculated for different heights (h) and drag coefficients (C_d). Using the obtained velocities V_x and V_y, the impact angle (θ) is calculated by the following equation:

$$\theta = tan^{-1}\left(V_y/V_x\right) \tag{16}$$

3.5. Extinguishing Agent Release Rate Calculation

The velocity vector on the third axis also should be known to determine the distribution of the extinguishing material with the explosion of the ammunition at the appropriate altitude. For this purpose, the Gurney equation was used, which gives the shrapnel speed resulting from the explosion of cylindrical-shaped ammunition. The Gurney equation for cylindrical ammunition [11]:

$$V\sqrt{2E} = \left[\left(M/C_{exp}\right) + 1/2\right]^{-0.5} \tag{17}$$

V: Initial fragment velocity (m/s)
$\sqrt{2E}$: Gurney constant for a given explosive
M: Mass of the fragment (kg)
C_{exp}: Explosive charge mass (kg)

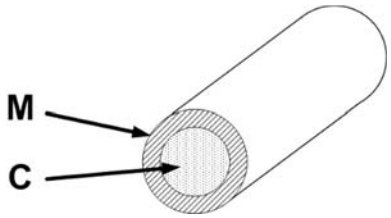

√2E value is generally very close to 1/3 of the detonation speed of explosives (Table 1). However, it is necessary to look at the relative effect factor (R.E.) of the explosive for the exact value. The relative effect factor is the ratio of the energy value of the same amount of explosives to the energy value of the TNT. Dynamite was used as an explosive in the SFEA. According to this:

$$R.E. = \frac{E_{dynamite}}{E_{TNT}} \tag{18}$$

Table 1. Gurney constants of some explosives [12]

Explosive	Density (kg/m^3)	Detonation Velocity (m/s)	Gurney Constant $\sqrt{2E}$ (m/s)
Octol 75/25	1.81	8640	2896
PETN	1.78	8260	2926
RDX	1.81	8700	2926
RDX/TNT 60/40 (Cyclotol)	1.68	7800	2402
Tetryl	1.71	7570	2499
TNT	1.61	6900	2438
Tritonal	1.70	5480	2316

4. RESULTS AND DISCUSSION

Drag coefficients were calculated for each nose cone type by performing flow analysis. Using the obtained drag coefficients, impact speed and impact angle calculations were made for the ammunition dropped with different speeds, jettison angles and altitudes.

4.1. Analysis Parameters

Flow analysis was performed by transferring the mesh structures to the Ansys Fluent environment and the drag coefficients for each model were numerically analyzed. Flow analysis was made according to the values in Table 2.

Table 2. Analysis parameters

Input Parameters	Value
Air Velocity (m/s)	86
Air Density (kg/m^3)	1.205
Air Dynamic Viscosity (kg/m.s)	$1.82x10^{-5}$
Ammunition Length (m)	2.3
Flow Type	Incompressible
Turbulence Model	SST k-ω
Mach sayısı	0.25

4.2. Drag Coefficients

As a result of the CFD analysis performed in the Ansys Fluent environment, the drag coefficients for each type of the three nose cones were calculated. The drag coefficients for each nose cone are given in Figure 15 and Table 8. The drag coefficient was found to be 0.136 for the spherically blunted conic nose cone, 0.138 for the spherically blunted tangent ogive nose cone, and 0.154 for the truncated tangent ogive nose cone. As can be seen, the drag coefficients for the spherically blunted conic nose cone and the spherically blunted tangent ogive nose cone are very close to each other, while the drag coefficient for the truncated tangent ogive nose cone is slightly higher (+11.76%). The higher coefficient of drag in the truncated tangential ogive nose cone is due to the deterioration of the flow structure and the formation of a separation zone. This causes the pressure drag to increase.

Table 8. Drag coefficients for a different types of nose cones

Nose Cone Type	Drag Coefficient
Spherically Blunted Conic	0.136
Spherically Blunted Tangent Ogive	0.138
Truncated Tangent Ogive	0.152

4.3. Ammunition Trajectory and Impact Angle

With the drag coefficients obtained, impact speed and impact angle calculations were made for ammunitions dropped from different speeds, jettison angles and altitudes. Ammunition trajectory and impact angle for spherically blunted conic nose cone are given in Table 3, ammunition trajectory and impact angle of spherically blunted tangent ogive nose cone in Table 4, and ammunition trajectory and impact angle of truncated tangent ogive nose cone in Table 5.

The one-way analysis of variance (ANOVA) was performed on the results using Minitab software to numerically show the effect of different nose cone designs on the impact angle and impact speed. Table 6 shows the results of a one-way analysis of variance for the impact angle versus nose cone type. In Table 7, the results of a one-way analysis of variance for the impact speed versus nose cone type are given. Since the p-values were greater than 0.05 in the ANOVA analysis, the nose cone difference did not have any effect on the impact angle and impact speed. On the other hand, flame detection, distance measurement and impact sensors, which should be in the smart fire extinguishing ammunition, should be on the plane at the front of the ammunition and in contact with the external environment. To place these sensors in the nose cone, a truncated tangent ogive nose cone was chosen as the nose cone for the smart fire extinguishing ammunition.

Table 3. Trajectory and impact angle for the ammunition with spherically blunted conic nose cone

Aircraft Speed (m/s)	Drop Angle (above horizontal)	Altitude (m)	Impact Speed (m/s)	Impact Angle	Distance (m)
25	0	180	63.61	69.16	244
50	0	180	70.92	56.95	367
75	0	180	76.41	51.08	469
50	**-15**	180	71.52	56.29	301
50	**0**	180	70.92	56.95	367
50	**15**	180	71.35	60.52	421
50	0	**180**	70.92	56.95	367
50	0	**300**	85.04	64.59	463
50	0	**500**	104.90	71.00	581

Table 4. Trajectory and impact angle for the ammunition with spherically blunted tangent ogive nose cone

Aircraft Speed (m/s)	Drop Angle (above horizontal)	Altitude (m)	Impact Speed (m/s)	Impact Angle	Distance (m)
25	0	180	63.49	69.15	251
50	0	180	84.83	64.61	471
75	0	180	105.70	51.00	474
50	**-15**	180	71.53	56.40	296
50	**0**	180	70.77	56.97	360
50	**15**	180	71.10	60.50	412
50	0	**180**	70.77	56.97	360
50	0	**300**	84.83	64.61	471
50	0	**500**	104.86	71.08	570

Table 5. Trajectory and impact angle for the ammunition with truncated tangent ogive nose cone

Aircraft Speed (m/s)	Drop Angle (above horizontal)	Altitude (m)	Impact Speed (m/s)	Impact Angle	Distance (m)
25	0	180	63.33	56.40	217
50	0	180	70.11	57.69	337
75	0	180	74.54	52.65	433
50	**-15**	180	70.92	56.92	278
50	**0**	180	70.11	57.69	337
50	**15**	180	70.58	61.40	383
50	0	**180**	70.11	57.69	337
50	0	**300**	84.52	65.50	424
50	0	**500**	104.11	71.78	528

Table 6. The results of one-way analysis of variance for impact angle versus nose cone type

Source	DF	Adj SS	Adj MS	F- Value	P- Value
Nose Cone Type	2	10.31	5.153	0.13	0.879
Error	24	956.41	39.850	-	-
Total	26	966.72	-	-	-

Table 7. The results of one-way analysis of variance for impact speed versus nose cone type

Source	DF	Adj SS	Adj MS	F-Value	P-Value
Nose Cone Type	2	159.1	79.56	0.45	0.645
Error	24	4282.7	178.45	-	-
Total	26	4441.9	-	-	-

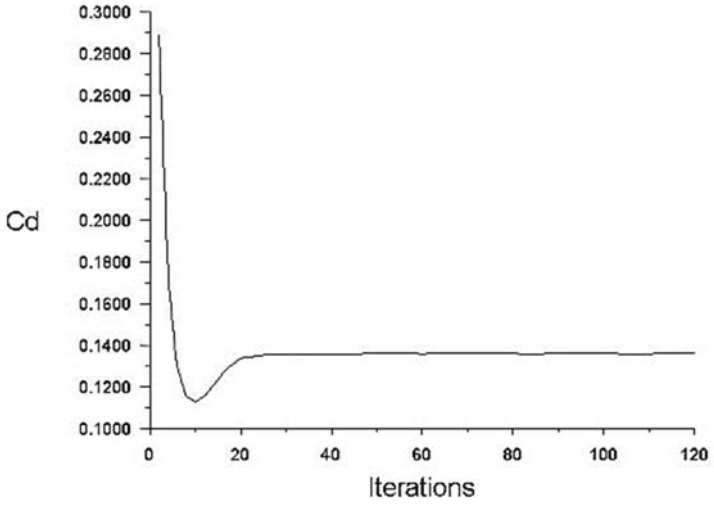

(a)

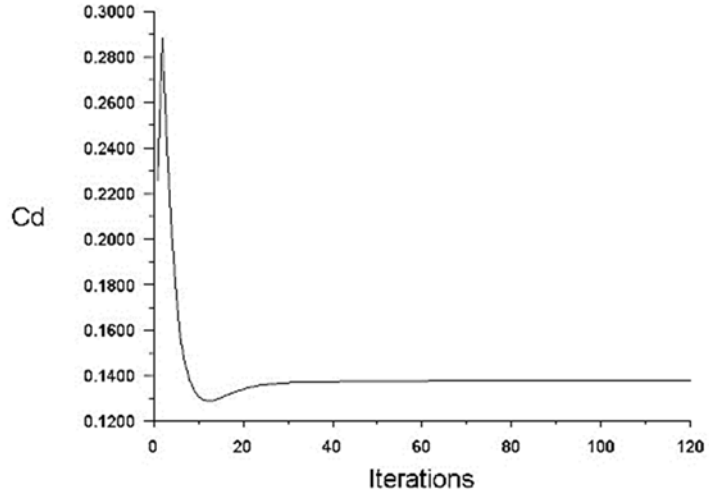

(b)

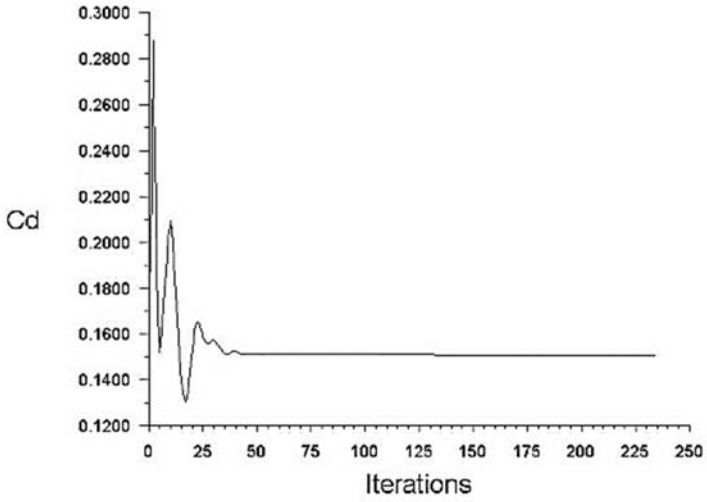

(c)

Figure 15. Nose cone drag coefficients: (a) Spherically blunted conic nose cone; (b) Spherically blunted tangent ogive nose; (c) Truncated tangent ogive nose cone

5. CONCLUSIONS

Smart fire extinguishing ammunition (SFEA) is a new and effective product we have designed for use in aerial firefighting. This product was called smart fire extinguishing ammunition, taking into account several electronic equipment and software that make the product autonomous. The effects of different nose cone designs on the trajectory and impact angle of the SFEA were investigated. Three different types of nose cones, namely spherically blunted conic, spherically blunted tangent ogive and truncated tangent ogive type nose cones were studied. The following findings were obtained in the study:

(a) The drag coefficient was found to be 0.136 for the spherically blunted conic nose cone, 0.138 for the spherically blunted tangent ogive nose cone, and 0.154 for the truncated tangent ogive nose cone.
(b) The drag coefficients for the spherically blunted conic nose cone and the spherically blunted tangent ogive nose cone are very close to each other, while the drag coefficient for the truncated tangent ogive nose cone is slightly higher (+11.76%).
(c) The higher coefficient of drag in the truncated tangential ogive nose cone is due to the deterioration of the flow structure and the formation of a separation zone. This causes the pressure drag to increase.
(d) The one-way analysis of variance (ANOVA) showed that the nose cone difference did not have a significant effect on the impact speed, impact angle and horizontal distance of the ammunition at the investigated speeds and altitudes.
(e) Flame detection, distance measurement and impact sensors, which should be in the smart fire extinguishing ammunition, should be on the plane at the front of the ammunition and in contact with the external environment. To place these sensors in the nose cone, a truncated tangent ogive nose cone was chosen as the nose cone for the SFEA.

Acknowledgments

The design proposed in this study participated in the 2242 University Students Research Project Competitions organized by TÜBİTAK Scientist Support Programs in the category of Defense, Space and Aviation, and won the Second Prize in Turkey in the Final Competition held between 17-22 September 2019. A patent application was made to the Turkish Patent and Trademark Office for the design. We would like to thank the Rectorate of İnönü University for their support for the patent application.

REFERENCES

[1] Çengel, Y. A. (2015). *Heat Transfer 5th ed.*, McGraw Hill, New York.

[2] Gudmundsson, S. (2014). *Aircraft Drag Analysis (Chapter 15)*, General Aviation Aircraft Design, Butterworth-Heinemann, 661-760.

[3] White, M., F. (2010). *Fluid Mechanics 7th ed.*, Flow Past Immersed Bodies, McGraw-Hill New York.

[4] Schlichting, H. 1960. *Boundary Layer Theory*, McGraw-Hill New York.

[5] Subha, R., Drozario, A. M., Sreeshin, M. (2020). Study on Various Types of Nose Cone Profiles at Supersonic Speed through Analytical, Experimental and Numerical Simulation Methods, *Journal of Xidian University*, 14(6): 2651-2675.

[6] Iyer, A. R., Pant, A. (2020). A Review On Nose Cone Designs for Different Flight Regimes, *International Research Journal of Engineering and Technology (IRJET)*, 7(8): 3546-3554.

[7] GICHD. (2017). Characterization of explosive weapons study, annex E – Mk 82 aircraft bomb, Geneva International Centre for Humanitarian Demining, Geneva, Switzerland.

[8] Watts, A., Curtis S., Braswll J., Underwood M. (2014). Missile Design Tool (MDT) User's Guide, Commander, U.S. Army Research, Development, and Engineering Command, Redstone Arsenal.

[9] Crowell S., Gary A. (1996). The descriptive geometry of nose cones, https://web.archive.org/web/20110411143013/http://www.if.sc.usp.br/~projetosulfos/artigos/NoseCone_EQN2.PDF Retrieved: 24.04.2021.

[10] ANSYS, Inc. (2011). Ansys Fluent 14.0: Theory Guide, 275 Technology Drive Canonsburg, PA 15317.

[11] Gurney, R. W. (1943). The Initial Velocities of Fragments from Bombs, Shells and Grenades, BRL-405. Ballistic Research Laboratory, Aberdeen, Maryland. USA.

[12] United Nations Office for Disarmament Affairs. (2015). International Ammunition Technical Guideline (2nd ed.). New York, NY: United Nations Headquarters.

NATURENGS
MTU Journal of Engineering and Natural Sciences
https://dergipark.org.tr/tr/pub/naturengs
DOI: 10.46572/naturengs.931954

Research Article

Activation and Characterization of Unye (Ordu) Clay with Nitric Acid

Yeliz AKBULUT[1*], Yunus ÖNAL [2]

[1]Department of Chemical Engineering, Faculty of Engineering, Inönü University, Malatya, Turkey.

(**Received:** 03.05.2021; **Accepted:** 10.07.2021)

ABSTRACT: In this study, clay belonging to the Ordu Unye region was activated by different concentrations of the acid solution by analytical methods. It is intended to remove adsorbed components between layers found in the structure of the clay. As a result, the activation process was performed with nitric acid (HNO_3) to enable the expansion of the distance between layers. Determination of structural changes of natural clay and activated clays have been characterized by XRD, SEM, FTIR and BET analyses. Characterization results showed that acid activation caused significant increases in surface area and pore volumes by changing both morphological and surface properties on clay. As a result of activation, the highest surface area of the clay was determined as 205.08 m^2/g with 2N HNO_3. Acid activation is more efficient in improving the surface properties of clay.

Keywords: Acid Activation, Clay, Surface Area.

1. INTRODUCTION

Clay is a sedimentary mineral formed by the decomposition of soft and very fine-grained feldspar, mica and other silicates, which contains high levels of Al_2O_3 and SiO_2 components as the main component in its structure together with MgO, CaO, Fe_3O_4, Na_2O, K_2O and TiO_2. Clay minerals are filtration components of nature, provide rain and snow water to be filtered underground and transform into drinking water quality. Adsorption, hence the filtration property, has a major significance in the industrial usage of clay. Acid activation is often used to modify and/or improve the structural properties of clay minerals by adsorption [1]. Defining the chemical and physical properties of the surface layers of a material is called surface analysis [2]. High surface area, number, and size of pores, as well as the number of acidic zones in the structure, are important for clay minerals. Acids such as HCl, H_2SO_4, HNO_3 are therefore preferred for activation processes in different concentrations [3-7]. All clay minerals can be physically and chemically altered by acid activation [8-10]. Although these changes are adsorptive properties, they are an increase in surface acidity, surface area, porosity, and pore volume. It has been determined by many scientists that the charges on the surface and the distances between silica layers can be changed. [11-13]. With the acid treatment, the formation of Si-OH groups already present in the structure is promoted and the interaction of minerals with different species in solution can be increased. In this case, applications can become diverse. As a result, acid-activated clays are used in different application areas in the industry. Acid-activated clays are used in environmental improvement processes, wastewater treatment,

*Corresponding Author: yelizzakbulut@gmail.com
ORCID number of authors: [1] 0000-0002-0703-7055, [2] 0000-0001-6342-6816

catalysis, sorption areas, oil refining, casting sand, drilling, filling, chemistry, detergent, cosmetics, paper, ceramic, pottery, faience, glass, porcelain, paint industries. [14-16]. Acid activation is easy as well as low cost. For this reason, many studies have used nitric acid as well as hydrochloric acid and sulfuric acid for the acid activation of vermiculite. [17-19]. Understanding the effect of acid activation on the structural properties of Unye bentonite is important for the use of clay-based commercial adsorbents or solid acid catalysts. [20-21]. As the main input agent in liquid oil refining and many other industrial areas, clays create a great economic potential. Acid activation improves the absorption properties of the clay by increasing the specific surface area as well as the active region. These changes depend on several factors, such as acid concentration, the nature of the clay, the duration of activation, and temperature.

This study aims to investigate the effect of different acid types (HCl and H_2SO_4 preferred in the literature) using HNO_3 at 0.5-3 N concentrations and to compare the final structural properties. XRD, SEM, FTIR, and BET analyses were used in the study. As a result of acid activation of bentonite taken from the Unye region of Ordu Province activated by nitric acid, it is aimed to improve the surface morphology and surface area changes of partially dissolved clay and contribute to the literature.

2. MATERIAL AND METHODS

2.1 Acid Activation of Vermiculite Samples

In the study, it was aimed to remove adsorbed components between the layers found in the structure of the clay. For this purpose, analytical techniques were preferred based on the needs of the industry that uses clay according to its surface area. Eventually, the activation process was performed with nitric acid to enable the expansion of the interlayer distance. Clay samples used in the present study were taken from Ordu / Unye region.

Figure 1. Raw Milled Unye Clay

Approximately 50 kg of natural clay samples were taken from this sample whose main mineral is vermiculite. This sample was mixed with a sufficient amount of distilled water and then sedimented. Later, the sedimentary clay was subjected to purification. After the sedimentation process, the non-precipitated clay was left to dry. The fully dried sample was ground and made ready for experiments. Using HNO_3 at different concentrations (0.5, 1.0, 1.5, 2.0, 3.0), 40 grams of clay was activated for each concentration. Three different acid groups were prepared (Table 1.).

Table 1. Composition of different acid groups

Sample Code	Composition
UCA 6	2.0 N (1.0 N 200 ml HCl & 1.0 N 200 ml HNO_3)
UCA 7	2.0 N (1.0 N 200 ml H_2SO_4 & 1.0 N 200 ml HNO_3)
UCA 8	2.0 N (1.0 N 200 ml HCl & 1.0 N 200 ml H_2SO_4)

The samples obtained were subjected to the activation process for 1 hour by refluxing. The mixture was centrifuged at 4000 rpm for 6 hours to make the phase separation of the samples cooled to room temperature. This process was continued until the nitrate ion in the structure was completely removed. The active solid clay samples were dried and ground (under a 200 mesh sieve) and stored in sealed containers for experiments.

2.2. Characterization of Active Vermiculite Samples

X-Ray Diffraction method (XRD) was used to determine the mineralogical composition and structural change of the raw and active clay samples. Surface morphologies were visualized by scanning electron microscopy (SEM). Fourier Transform Infrared Spectrophotometer (FTIR) method was used to determine the structural-functional groups. The surface areas of the raw and active clay samples were measured by the Bruneur - Emmet - Teller (BET) method (77 K). Pore distributions were determined with Density Functional Theory Plus (DFT Plus). Surface area measurements of clays were determined on TriStar II Plus device, XRD measurements were determined on Rigaku RadB-DMAX II (Cu K-alpha) device, and SEM measurements were determined by Leo EV040 brand scanning electron microscope.

3. RESULTS AND DISCUSSION

The surface areas of clays activated with different concentrations of HNO_3 are given in Table 2. As given in the table, it was determined that the total surface areas of the activated clay samples varied between 110.30-205.08 m^2/g. Unactivated raw clay has a surface area of 82.77 m^2/g. The minimum surface area was obtained at a concentration of 0.5 N HNO_3. The maximum surface area was obtained with 2 N HNO_3 and its value is 205.08 m^2/g. When the acid concentration was increased, the surface area also increased significantly. At a very high acid concentration, the surface area is partially reduced. When the acid concentration was 3.0 N, the structural collapse occurred and the surface area decreased to 187.22 m^2/g. Clay contains some impurities depending on the geological structure of the region where it is formed. With acid activation, the components between the layers, which are in the structure as impurities, are removed. At this stage, the aim is to increase the structural stability, to remove M^+, M^{++} and M^{+++} ions and organic impurities adsorbed between layers. In addition, as a result of increasing the distance between the layers by the activation process, the adsorption capability of the clay was increased by removing the adsorbed anions existing in the structure from between the layers. The increase in surface area is closely related to the separation of interlayer adsorbed components from the structure. The surface area values determined in our study were compared with similar studies in the literature (H_2SO_4, HNO_3 and HCl activated clay) in terms of surface area measurements. Turabik and Kumbur activated the clay surface area by changing the sulfuric acid ratio between 10 and 60%, and the specific surface area increased by a maximum of 40% [22]. Chmielarz et al. kiln-dried the clay sample with a crude surface area of 8 m^2/g using nitric acid for 24 hours at 900°C, and the specific surface area reached a maximum value of 162 m^2/g [23]. Guerra et al. Activated the specific surface area of 44 m^2/g in non-treated clay

with hydrochloric acid to maximize the surface area to 199 m^2/g [24]. Literature knowledge and the experiments carried out in this study have clearly shown the significance of nitric acid on acid activation. In the activation of clay acid, nitric acid is more effective than sulfuric and hydrochloric acid. The surface areas formed consist of micropores between 46.82 – 34.60 m^2/g and mesopores between 169.78 – 45.71 m^2/g. The increase of mesopore pores is very effective in the large surface areas of clays. In addition, the variation of average pore diameters between 3 - 6 nm proves that the clays contain high mesopores.

Table 2. BET analysis results of samples

Clay Samples	Surface Area (m^2/g)	S_{micro} (m^2/g)	S_{meso} (m^2/g)	V_T (cm^3/g)	V_{micro} (cm^3/g)	V_{meso} (cm^3/g)	dp (nm)
UCAH	82.77	53.47	29.30	0.11	0.02	0.09	5.40
UCA1 (0.5 N)	110.29	45.92	72.38	0.14	0.03	0.12	4.70
UCA2 (1 N)	114.46	45.19	78.89	0.15	0.03	0.12	4.54
UCA3 (1.5 N)	118.39	46.82	75.86	0.15	0.03	0.11	4.58
UCA4 (2 N)	205.08	36.11	169.78	0.21	0.02	0.18	3.94
UCA5 (3 N)	172.17	35.21	152.02	0.18	0.02	0.15	3.68
UCA6	161.16	43.62	121.36	0.11	0.03	0.08	2.77
UCA7	170.85	43.17	140.64	0.18	0.02	0.16	3.88
UCA8	148.07	45.60	100.33	0.15	0.02	0.13	4.25

The change in the pore size distribution of raw and acid-activated clay samples is given in Figures 2, 3 and 4, respectively. The pore size distribution of raw clay belongs to pores with maximum 1.6, 2.0, 3.0, 3.5 and 9 nm. According to the results, there is a very heterogeneous pore size distribution between 0-10 nm. Unlike the raw clay sample, it is seen that new pores with 4.0, 5.0 and 8.0 nm diameter are formed although the pores at 0.5 N HNO_3 concentration are in the range of 0-10 nm. At 1 N nitric acid concentration, new pores with 5.0 nm pore diameter are formed compared to the raw sample, while peaks of other pores are seen to be sharpened. In other words, the distribution is seen in a more regular structure. The 1.5 N nitric acid concentration and the raw clay sample were compared. As a result, new pores with 0.9, 1.5, 4.5 nm pore sizes were determined. Compared to 2.0 N nitric acid concentration, while new pores of 2.8 and 8.5 nm diameters occurred, pores of 3.0 and 9.0 nm diameters disappeared in the raw clay sample. The 3 N nitric acid concentration has new pores of 1.0, 2.2 and 3.2 nm in diameter compared to the raw clay sample. The destruction that occurs in the macromolecular structure of clay can be explained by the formation of new pores in small diameters. Indeed, the smaller surface area is proof of this. In the activation with different acid groups, the pore size distribution in all three acid groups was changed compared to the raw sample, and it was determined that the active clays had pores in the range of 1-10 nm. However, it was determined that the pore size distribution was more regular in the mixture of HCl-H_2SO_4.

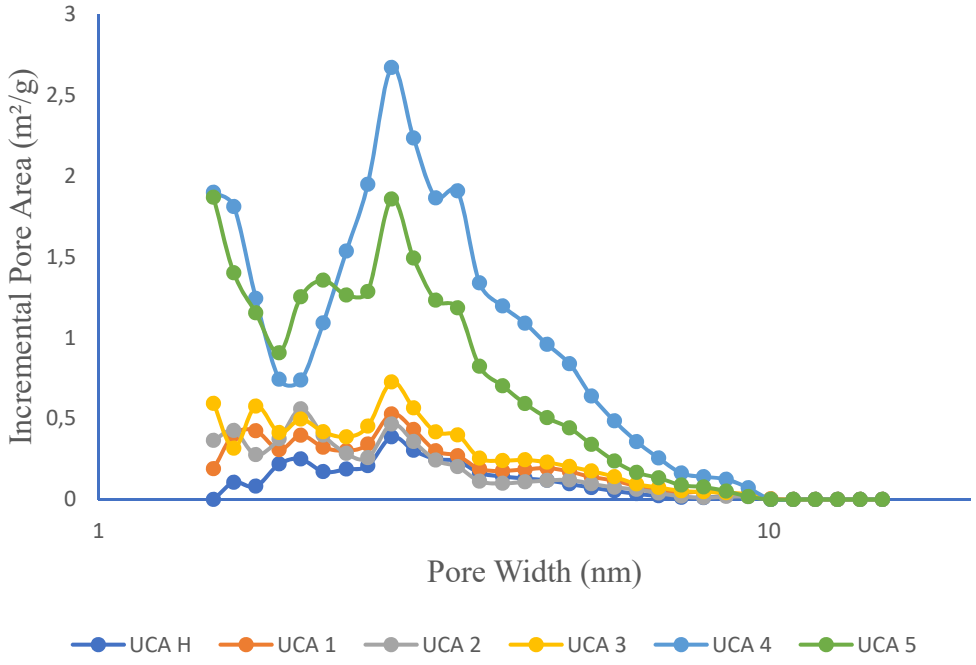

Figure 2. Pore size distribution of raw and HNO_3 activated samples DFT Plus isotherm

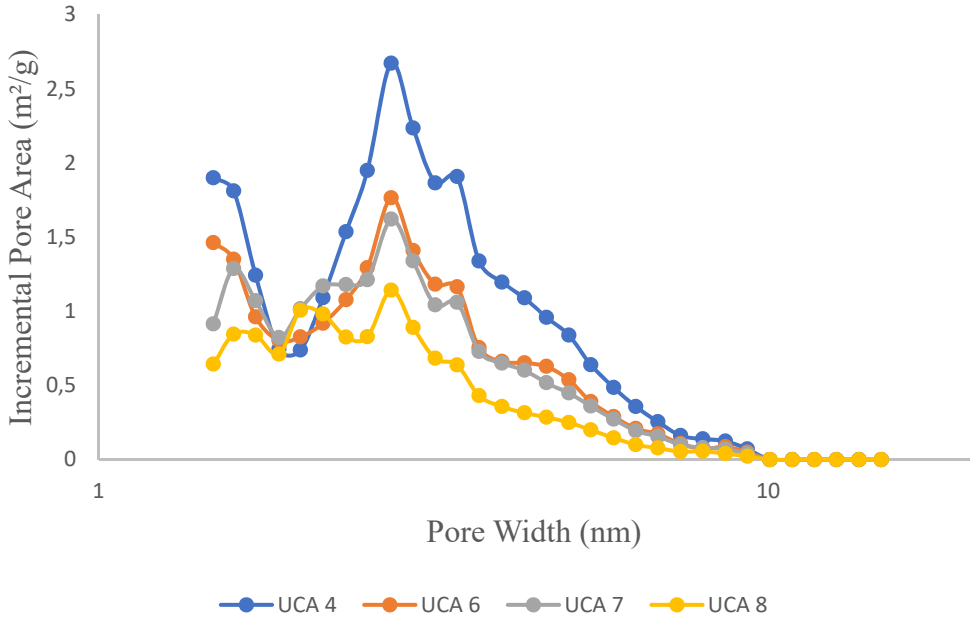

Figure 3. Pore size distribution of samples with high surface area (UCA 4) and activated by different acids DFT Plus isotherm

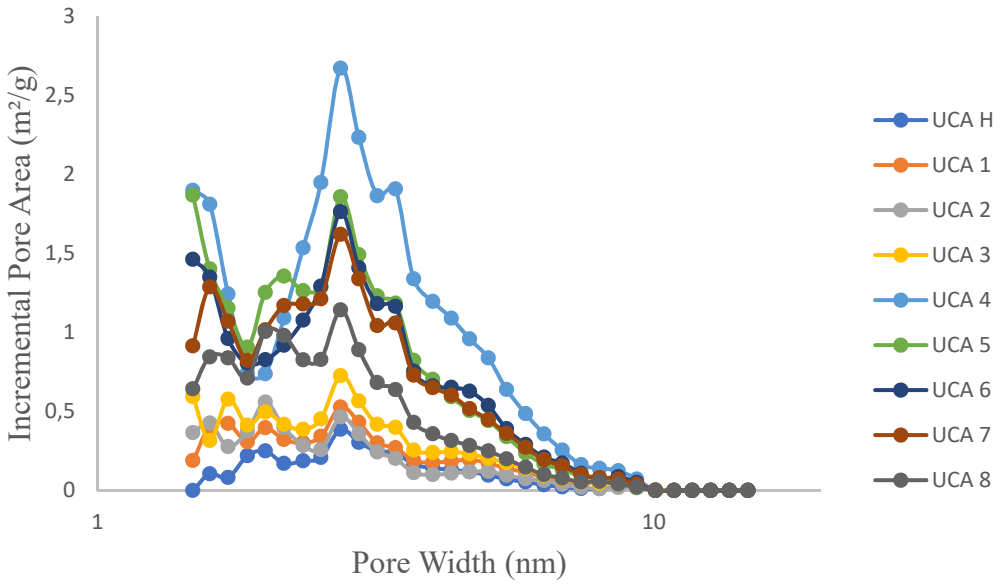

Figure 4. Pore size distribution of samples DFT Plus isotherm

When the nitrogen adsorption isotherm is examined, it is seen that the amount of nitrogen adsorption per gram of clay is seen against the relative pressure P/P_0. Relative pressure ranges from 0 to 1. The amount of nitrogen adsorption varies according to the surface area of the clay. This change is generally related to the type of porous structure of the clay. When the adsorption isotherms of clays activated with nitric acid are examined, it is observed that they conform to Type 2. This supports the presence of a high amount of mesopore in the isothermal structure. The nitrogen sent to the structure was adsorbed for a while. Type2 is the S-shaped (sigmoidal) isotherm. The isotherm of nitrogen (77 K) on many macroporous solids is of this type. BET isotherms are in Type 2 form. According to the BET theory, the adsorbed amounts are the same in all layers except the first layer. Here, the second layer is partially filled before the first layer is filled. The point at the beginning of the midline region is defined as the situation where the monolayer cover is complete and multilayer adsorption is about to begin. However, adsorption continues at all relative pressures.

As a result of the analysis made; while acid concentration increased the surface area increased first, then the surface area decreased at the 3N acid concentration. Raw and active clay samples were measured according to Surface Energy Distribution by Modified Density Functional Theory Model: N_2 - Modified Density Function software. In addition to being similar to the incremental area-energy change graph, the peak occurring at 40-46 e/k in the entire surface area is similar in all samples. Surface energy remains the same regardless of the increase in surface area. For example, while the raw clay incremental area value shows 42-44 surface energy in the range of 42.051-62-882, UCA4 sample with the highest surface area gives the same surface energy value between 205.323-56.960 m^2/g. As the active surface area increases as a result of acid activation, the surface energy remain constant can be explained as follows; As a result of the removal of interlayer adsorbed atoms, ions and/or molecules from the structure, negative and positive charge spaces are freed.

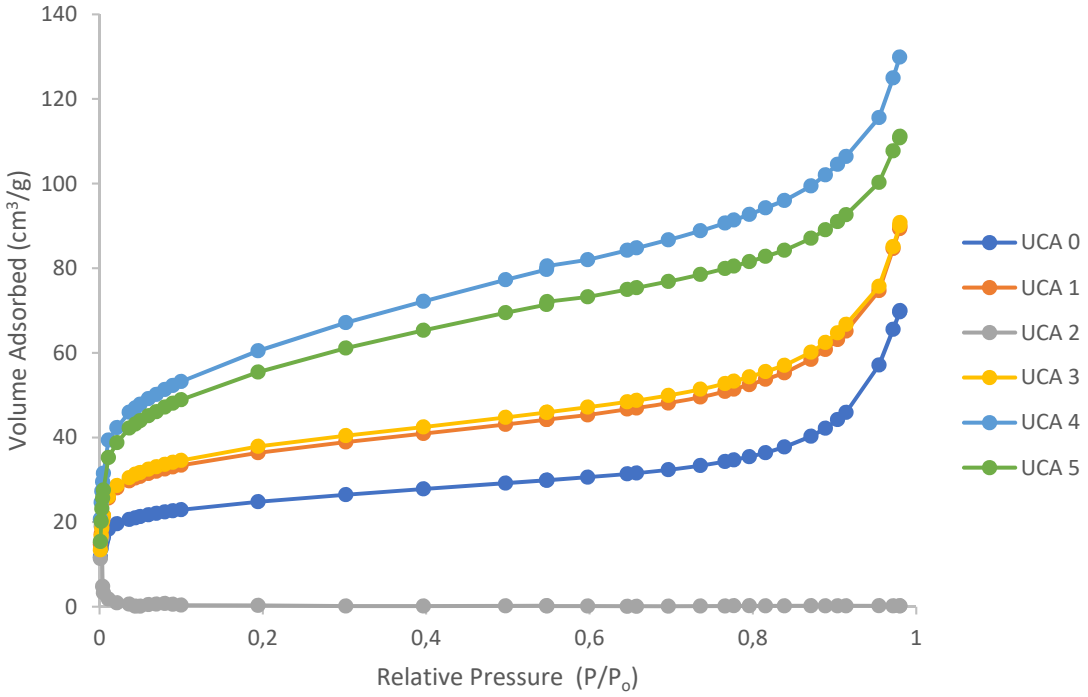

Figure 5. Adsorption isotherms of N_2

Table 3. Incremental Surface Area vs. Energy

Sample	Energy (e/k)	Sample	Energy (e/k)
UCAH	62	**UCA6**	145
UCA1 (0.5 N)	85		
UCA2 (1 N)	88	**UCA7**	136
UCA3 (1.5 N)	98		
UCA4 (2 N)	200	**UCA8**	106
UCA5 (3 N)	158		

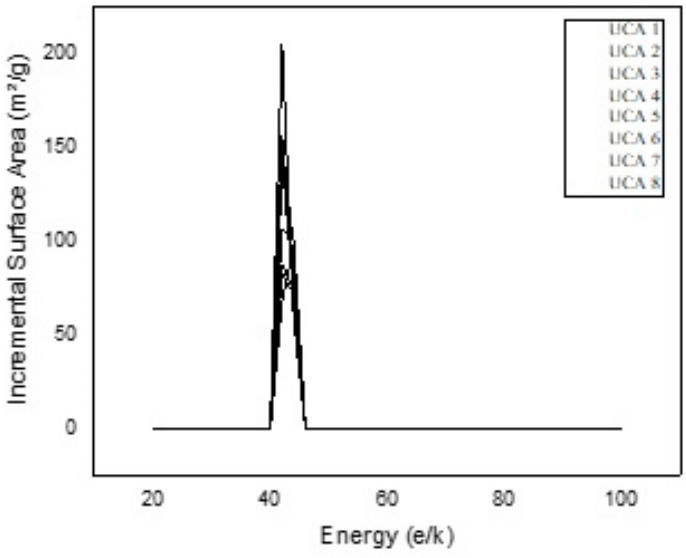

Figure 6. Incremental Surface Area vs. Energy

XRD patterns of crude and acid-activated clay samples are given in Figures 7 and 8. When the figure is examined, the distance between the layers of the raw sample of 7.219 2Θ was 12.2334 Å, while this value was obtained as 16.2300 Å in the sample with the highest surface area. This peak area is widening and its height increasing. As a result of the activation, the distance between the layers has increased by 33%. The acid treatment causes a serious change in the crystal structure of the minerals. When Figures 6 and 7 are examined, the high and sharp intensity of around 15.274 Å emerges as a result of 12.883 Å wide and splay peak acid activation in the XRD trace of raw clay. As the cations and other impurities between the layers are removed as a result of the acid treatment, the increase in the d value between the layers is an expected result. However, as a result of structural degradation in 3N HNO_3 concentration, the peak decreases to 14.772 Å also the maximum peak value is decreased. When the XRD patterns of a similar study by Chaari et al. [25] are examined, the main impurities in the raw clay are seen with an intense reflection at 2Θ = 30.5° (2.90 Å) and this reflection is dolomite. The pattern shown by sharp (101) basal reflection at 3.34 Å is quartz. The associated minerals detected in small amounts in the same study are basal reflection at 9.99 Å (001), feldspar (feldspars) at 3.23 Å and calcite at 3.03 Å. It has been observed that acid activation causes a significant decrease in crystallinity by decreasing the density of smectite and kaolinite. When the XRD traces of Turabik and Kumbur's [22] similar studies were examined, the smectite group was found at 5.88° and it was understood that it contained crystallite, a silica polymorph, at 21.48°. In addition, d (001) = 15.02 Å, 18.98 Å and 9.84 Å were obtained. Thus it was found that the original sample was montmorillonite.

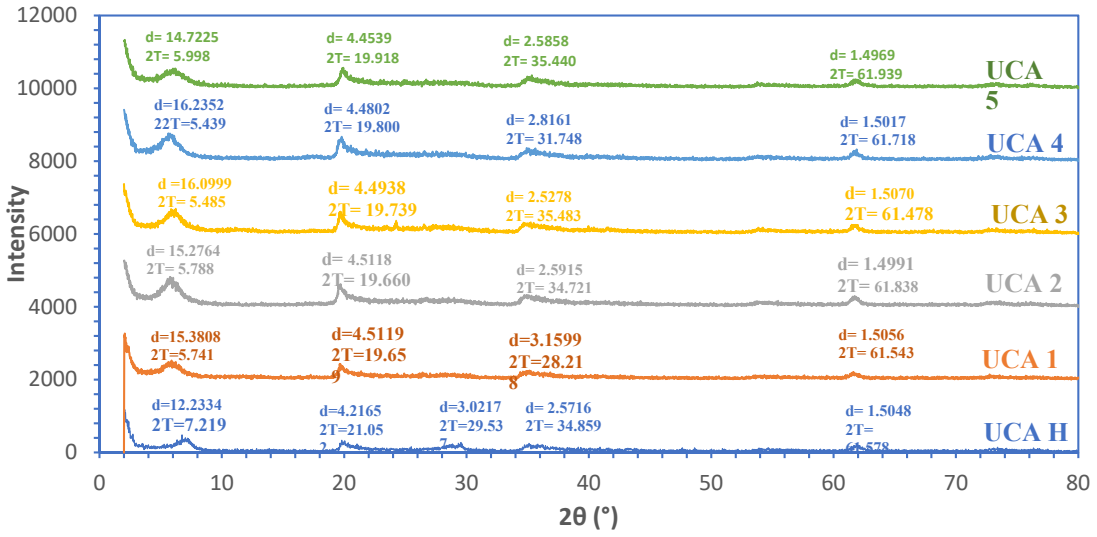

Figure 7. XRD graph of raw and HNO_3 activated clays

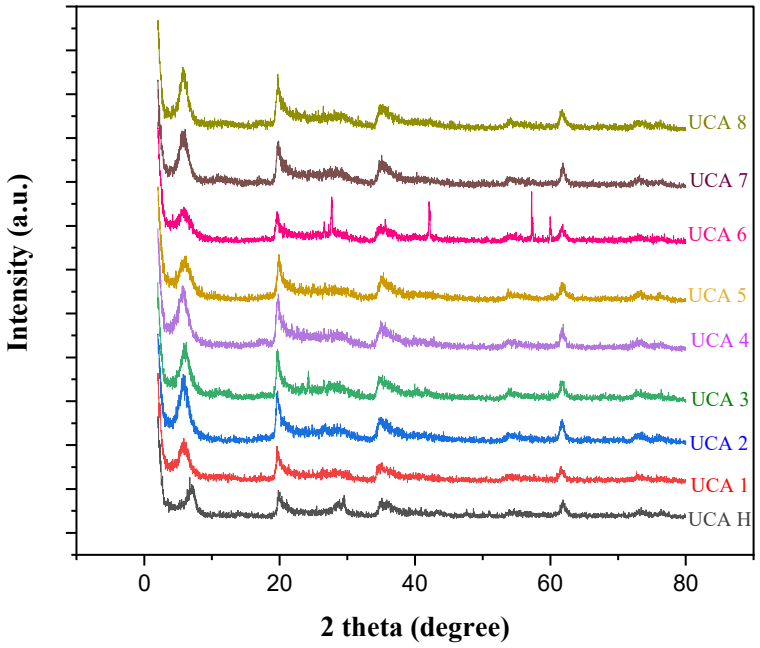

Figure 8. XRD graph of examples

FTIR spectra of the raw and active clay samples are given in Figure 9. When the figure is examined, the bending stress of the 915 cm^{-1} Al-AlOH structure and the 1035 in-plane Si-O stress are seen for the raw sample. The peak occurring in this region is wide. This expansion is explained by the 1113 cm^{-1} out-of-plane Si-O structures in the clay structure and the hydration peak of the 1635 cm^{-1} -OH bending. The –OH stress in the macromolecular main structure of clay minerals is observed in the 3621 cm^{-1} bands. As the acid concentration increases, the peak in the 700-1300 cm^{-1} region of the M-O-M stretch in the structure contains 3 shoulders in the range of 711-1189 cm^{-1} in the raw sample, and also the peak is high and sharp. As the acid concentration increases with acid activation, the peak width of 735-1214 cm^{-1}, 728-1214 cm^{-1}, 744-1222 cm^{-1}, 744-1271 cm^{-1} and 735-1271 cm^{-1} bands are the same, respectively. However, its sharpness and length are different. Since the FTIR traces in this region are related to structures such as Si-O, Si-O-Si, Al-O, Al-O-Al and these groups are the basic building blocks of clay, it is an expected result that these peaks remain largely unchanged. The –OH stretching observed around 1630 cm^{-1} is a group in the mineralogical structure of the clay mineral and is observed in all acid concentrations. It belongs to the –OH stress of water adsorbed by wide and flat peak clay around 3300 cm^{-1}. The -OH stress of 3630 cm^{-1} belonging to the mineralogical structure of clay is quite distinct and sharp in the raw sample, and it is partially deformed and shrunk as a result of acid activation [26-27].

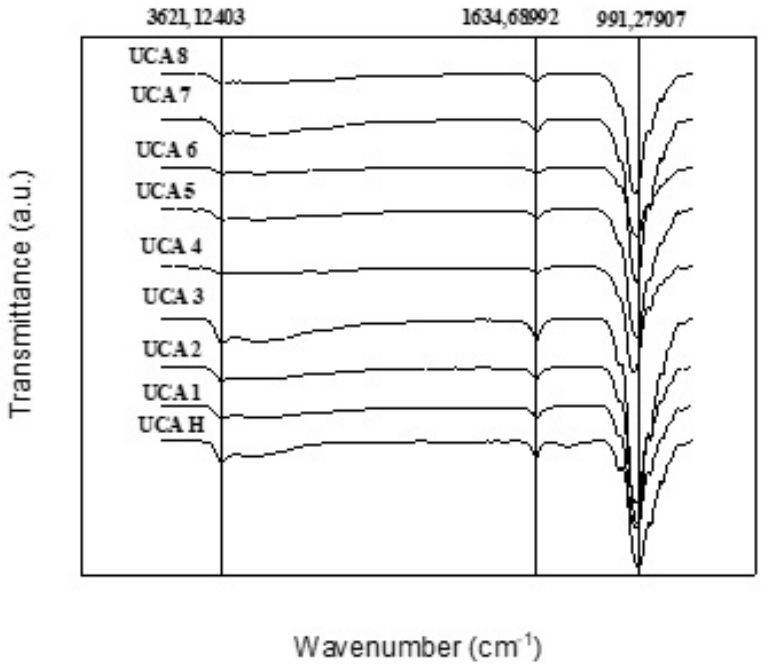

Figure 9. FTIR graph of examples

SEM images of raw and active clay samples are given in Figures 10 and 11. When SEM images are examined, it is seen that the raw clay sample has a very homogeneous structure and does not contain any impurities. This is an expected result as impurities are removed from the structure with sedimentation. Clay layers are visible and different grain sizes show the same structure with each other. It is seen that there are important changes within the structural units as a result of acid activation. In the example of UCA 4 (2N HNO_3) with the highest surface area, it was determined that the structural units shrunk, the inter-layer units were seen, and as a result, the surface area increased. However, in the example of UCA 5 (3N HNO_3), the surface area decreases as a result of high acid concentration and as seen in the SEM image, it is seen that cavities are formed between the units similar to the graphene structure. Although the concentration is low in the mixture of HCl-HNO_3, the structural units of the clay mineral are seen as a whole. The morphological structure of the UCA 7 sample is similar to the HNO_3 activation only. In the mixture of UCA 8, it is seen that the structural units are separated from each other and that graphene-like formations appear. This structure is similar to UCA 5, and when the acid is strong, the macromolecular structure is affected.

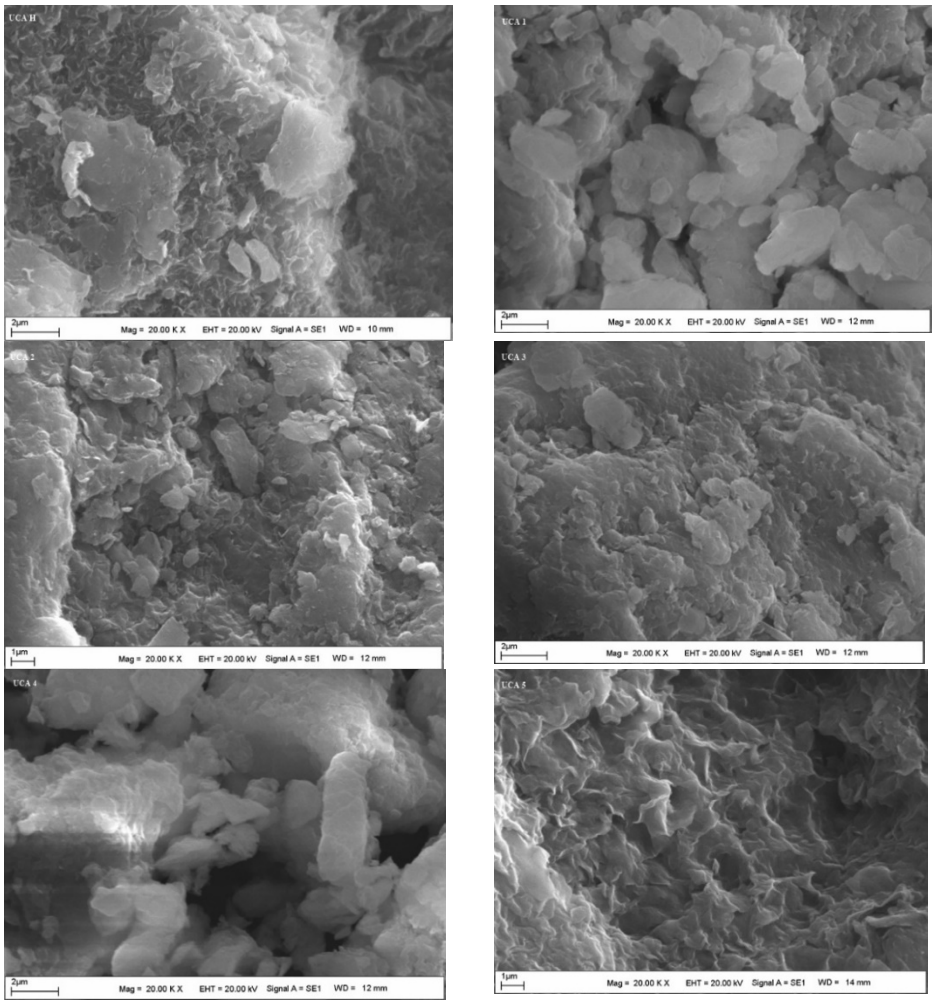

Figure 10. SEM images of raw and HNO_3 activated clays

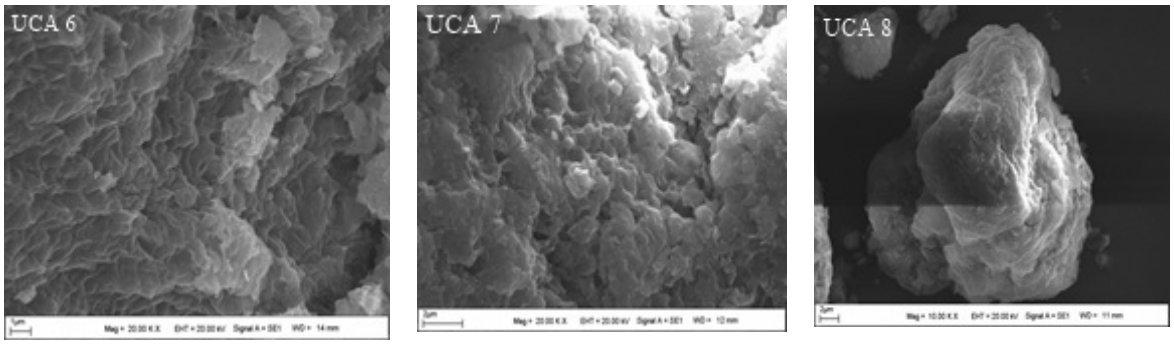

Figure 11. SEM images of clays activated by different acids
a. UCA 6 (HCl-HNO_3) **b.** UCA 7 (H_2SO_4-HNO_3) **c.** UCA 8 (HCl-H_2SO_4)

4. CONCLUSIONS

In this study, the highest surface area change in acid activation with nitric acid was obtained as 150% at 2N HNO_3 concentration. The smallest change was obtained at a concentration of 34% and 0.5N HNO_3. Generally, the higher the nitric acid concentration, the higher the surface area, and the lower the surface area at the 3N HNO_3 concentration. At this concentration, the mass loss by weight is 13.55%. Therefore, the macromolecular structure of the clay at high acid concentration is lost. Structural change is seen in XRD diffractograms. As the acid concentration increases, it is seen that the clay layers appear more clearly in SEM images. In addition, as the acid concentration increases, it has been determined that the structural degradation increases in the 3N HNO_3 concentration. Structural change in terms of functional groups with changing acid concentration gave similar results to XRD and SEM results in FTIR spectrum. The highest surface area in different acid groups was obtained in the mixture of 1N HCl and 1N HNO_3. Nitric acid is environmentally important in the acid activation of clay samples, and when diluted sufficiently at the end of the wash, it will not have any negative effects on the nitrate ion, on the contrary, it will be an important nutritional component for plants.

Acknowledgments

We would like to thank Altaş Oil industry company for the clay samples.

REFERENCES

[1] Santos, S.S.G., Silva, H.R.M., Souza, de A.G., Alves, A.P.M., Silva Filho, da E.C. and Fonseca, M.G. (2015). Acid-leached mixed vermiculites obtained by treatment with nitric acid, *Applied Clay Science*, 104: 286–294.

[2] Krupskayaa, V., Novikovad, L., Tyupinaee, E., Belousova, P., Dorzhievaa, O., Zakusina, S., Kimh, K., Roessneri, F., Badettij, E., Brunellij, A., and Belchinskayad, L. (2019). The influence of acid modification on the structure of montmorillonites and surface properties of bentonites, *Applied Clay Science*, 172: 1-10.

[3] Komadel, P. (2016). Acid activated clays: Materials in continuous demand, *Applied Clay Science*, 131: 84–99.

[4] Krupskaya, V., Novikovad, L., Tyupinae, E., Belousova, P., Dorzhievaa, O., Zakusina, S., Kimh, K., Roessneri, F., Badettij, E., Brunellij, A., and Belchinskayad, L. (2019). The influence of acid modification on the structure of montmorillonites and surface properties of bentonites, *Applied Clay Science,* 172: 1–10.

[5] Lycourghiotis, S., Makarouni, D., Kordouli, E., Bourikasa, K., Kordulis, C., and Dourtoglou, V. (2018). Activation of natural mordenite by various acids: Characterization and evaluation in the transformation of limonene into p-cymene, *Molecular Catalysis,* 450: 95–103.

[6] Guerra, D.L., Lemos, V.P., Airoldi, C., and Ange´lica, R.S. (2006). Influence of the acid activation of pillared smectites from Amazon (Brazil) in adsorption process with butylamine, *Polyhedron,* 25: 2880–2890

[7] Hussin, F., Aroua, M.K., and Wan Mohd Ashri Wan Daud, WMAW. (2011). Textural characteristics, surface chemistry and activation of bleaching earth: A review, *Chemical Engineering Journal,* 170: 90–106.

[8] Steudel, A., Batenburg, L.F., Fischer, H.R., Weidler, P.G., and Emmerich, K. (2009). Alteration of swelling clay minerals by acid activation, *Applied Clay Science,* 44: 105–115.

[9] Komadel, P., and Madejová, J. (2013). Acid Activation of Clay Minerals, Handbook of Clay Science, *Developments in Clay Science,* 5: 385-409.

[10] Juang, R.S., Wu, F.C., and Tseng, R.L. (2010). Acid activated clays: Materials in continuous demand, *Environmental Technology*, 18: 525-531.

[11] Carrado, K.A., and Komadel, P. (2009). Acid Activation of Bentonites and Polymer–Clay Nanocomposites, *Elements,* 5: 111–116.

[12] Vicente Rodríguez, M.A., López González, J.de D., and Bañares Muñoz, M.A. (1995). Preparation of microporous solids by acid treatment of a saponite, *Microporous Materials,* 4: 251-264.

[13] Komadel, P. (2003). Chemically modified smectites, *Clay Minerals*, 38: 127–138.

[14] Balcı, S. (2018). Structural Property Improvements of Bentonite with Sulfuric Acid Activation, *Journal of the Turkish Chemical Society Section B: Chemical Engineering*, 1(2): 201-212.

[15] Sabah, E. (2007). Decolorization of vegetable oils: Chlorophyll-a adsorption by acid-activated sepiolite, *Journal of Colloid and Interface Science,* 310: 1–7.

[16] Burst, J.F. (1991).The application of clay minerals in ceramics, *Applied Clay Science*, 5 (5–6): 421-443.

[17] Sousa, P. de E., Araujo, T. de D., Peixoto, G.V., Ferreira, F.B., Faria, H. de E., and Molina, F.E. (2020). Effect of sodium bentonite content on structural-properties of ureasil poly (ethylene oxide)-PEO hybrid: A perspective for water treatment, *Applied Clay Science*, 191: 105605.

[18] Chmielarz, L., Wojciechowska, M., Rutkowska, M., Adamski, A., Węgrzyn, A., Kowalczyk, A., Dudek B., Boroń, P., Michalik, M., and Matusiewicz, A. (2012). Acid-activated vermiculites as catalysts of the $DeNO_x$ process, *Catalysis Today,* 191(1): 25-31.

[19] Ravichandran, J., Lakshmanan, C.M., and Sivasankar, B. (1996). Acid Activated Montmorillonite and Vermiculite Clays as Dehydration and Cracking Catalysts, *Reaction Kinetics and Catalysis Letters,* 59: 301–308.

[20] Ravichandran, J., and Sivasankar, B. (1997). Properties and Catalytic Activity of Acid-Modified Montmorillonite and Vermiculite, *Clays and Clay Minerals,* 45: 854–858.

[21] Caglar, B., Afsin, B., Koksal, E., Tabak, A., and Eren, E. (2013). Characterization of Unye Bentonite After Treatment with Sulfuric Acid, *Química Nova*, 36(7): 955-959.

[22] Turabik, M., and Kumbur, H. (2002). Change in some Physicochemical properties of Ünye/Ordu bentonite with acid activation, *Cumhuriyet Üniversitesi Mühendislik Fakültesi Dergisi,* 19: 1-10.

[23] Chmielarz, L., Kowalczyk, A., Michalik, M., Dudek, B., Piwowarska, Z., and Matusiewicz, A. (2010). Acid-activated vermiculites and phlogophites as catalysts for the DeNOx process, *Applied Clay Science,* 49: 156–162.

[24] Guerra, D.L., Lemos, V.P., Airoldi, C., and Ange´lica, R.S. (2006). Influence of the acid activation of pillared smectites from Amazon (Brazil) in adsorption process with butylamine, *Polyhedron,* 25: 2880–2890.

[25] Chaari, I., Medhiou, M., Jamoussi, F., and Hamzaoui, A.H. (2021). Acid-treated clay materials (Southwestern Tunisia) for removing sodium leuco-vat dye: Characterization, adsorption study and activation mechanism, *Journal of Molecular Structure,* 1223: 128944.

[26] Tyagi, B., Chudasama, C.D., and Jasra, R.V. (2006). Determination of structural modification in acid activated montmorillonite clay by FT-IR spectroscopy, *Spectrochimica Acta Part A: Molecular and Biomolecular Spectroscopy,* 64(2): 273-278.

[27] Snoussi, Y., Khalil, A.M., Strzemiecka, B., Voelkel, A., and Chehimi, M.M. (2017). Surface Analysis of Clay Polymer Nanocomposites, *Clay Polymer Nanocomposite*, 11: 363-411.

NATURENGS
MTU Journal of Engineering and Natural Sciences
https://dergipark.org.tr/tr/pub/naturengs
DOI: 10.46572/naturengs.937010

Research Article

A Note on The Generalized k-Fibonacci Sequence

Yashwant K Panwar

Department of Mathematics, Government Model College, Jhabua, India.

(**Received:**14.05.2021; **Accepted:** 05.11.2021)

ABSTRACT: In this paper, we present a generalization of well-known k-Fibonacci sequence. Namely, we defined generalized k-Fibonacci sequence. This sequence generalizes others, k-Fibonacci sequence, classical Fibonacci sequence, Pell sequence and Jacobsthal sequence. We establish some of the interesting properties of generalized k-Fibonacci sequence. Also, we obtain a generating function for them.

Keywords: Generalized k-Fibonacci sequence, k-Fibonacci sequence, Fibonacci sequence, Binet's formula, Generating function.

1. INTRODUCTION

It is well-known that the Fibonacci sequence is most prominent examples of recursive sequence. The Fibonacci sequence is famous for possessing wonderful and amazing properties. The Fibonacci appear in numerous mathematical problems. Fibonacci composed a number text in which he did important work in number theory and the solution of algebraic equations. The book for which he is most famous in the "Liber abaci" published in 1202. In the third section of the book, he posed the equation of rabbit problem which is known as the first mathematical model for population growth. From the statement of rabbit problem, the famous Fibonacci numbers can be derived,

This sequence in which each number is the sum of the two preceding numbers has proved extremely fruitful and appears in different areas in Mathematics and Science.

The Fibonacci numbers F_n are terms of the sequence $\{0,1,1,2,3,5,...\}$ wherein each term is the sum of the two previous terms, beginning with the values $F_0 = 0$ and $F_1 = 1$.

The Fibonacci sequence [11], is defined by the recurrence relation

$$F_n = F_{n-1} + F_{n-2}\ ,\ n \geq 2\ \ with\ F_0 = 0,\ F_1 = 1 \tag{1}$$

*Corresponding Author: yashwantpanwar@gmail.com
ORCID number of authors: 0000-0002-7429-4043

The Lucas sequence [11],is defined by the recurrence relation

$$L_n = L_{n-1} + L_{n-2},\ n \geq 2\ with\ L_0 = 2,\ L_1 = 1 \tag{2}$$

The Fibonacci sequence, Lucas sequence, Pell sequence, Pell-Lucas sequence, Jacobsthal sequence and Jacobsthal-Lucas sequence are the most prominent examples of recursive sequences. The second-order recurrence sequence has been generalized in two ways mainly, first by preserving the initial conditions and second by preserving the recurrence relation.

Kalman and Mena [10], generalize the Fibonacci sequence by

$$F_n = aF_{n-1} + bF_{n-2},\ n \geq 2 \quad with \quad F_0 = 0,\ F_1 = 1 \tag{3}$$

Horadam [7], defined generalized Fibonacci sequence $\{H_n\}$ by

$$H_n = H_{n-1} + H_{n-2},\ n \geq 3\ with\ H_1 = p,\ H_2 = p + q \tag{4}$$

where p and q are arbitrary integers.

The k-Fibonacci numbers defined by Falcon and Plaza [2, 5], for any positive real number k, the k-Fibonacci sequence is defined recurrently by

$$F_{k,n} = k\,F_{k,n-1} + F_{k,n-2},\ n \geq 2 \quad with \quad F_{k,0} = 0,\ F_{k,1} = 1 \tag{5}$$

The k-Lucas numbers defined by Falcon [3],

$$L_{k,n} = k\,L_{k,n-1} + L_{k,n-2},\ n \geq 2 \quad with \quad L_{k,0} = 2,\ L_{k,1} = k \tag{6}$$

Most of the authors introduced Fibonacci pattern-based sequences in many ways which are known as Fibonacci-Like sequences and k-Fibonacci-like sequences [12, 13, 18, 20, 21].

Generalized Fibonacci sequence [6], is defined as

$$F_k = pF_{k-1} + qF_{k-2},\ k \geq 2 \quad with \quad F_0 = a,\ F_1 = b \tag{7}$$

(p,q) - Fibonacci numbers [15], is defined as

$$F_{p,q,n} = pF_{p,q,n-1} + bF_{p,q,n-2},\ n \geq 2 \quad with \quad F_{p,q,0} = 0,\ F_{p,q,n} = 1 \tag{8}$$

(p,q) - Lucas numbers [16], is defined as

$$L_{p,q,n} = pL_{p,q,n-1} + bL_{p,q,n-2},\ n \geq 2 \quad with \quad L_{p,q,0} = 2,\ L_{p,q,n} = p \tag{9}$$

Generalized (p,q) -Fibonacci-Like sequence [17], is defined by recurrence relation

$$S_{p,q,n} = pS_{p,q,n-1} + qS_{p,q,n-2},\ n \geq 2 \quad with \quad S_{p,q,0} = 2k,\ S_{p,q,n} = 1 + kp \tag{10}$$

Goksal Bilgici [1], defined new generalizations of Fibonacci and Lucas sequences

$$f_k = 2af_{k-1} + (b - a^2)f_{k-2},\ k \geq 2\ with\ f_0 = 0,\ f_1 = 1 \tag{11}$$

$$l_k = 2al_{k-1} + (b - a^2)l_{k-2},\ k \geq 2\ with\ l_0 = 2,\ l_1 = 2a \tag{12}$$

In this paper, we introduce a generalized $k-$Fibonacci sequence. The generalized $k-$Fibonacci numbers have lots of properties.

2. THE GENERALIZED k-FIBONACCI SEQUENCE

In this section, we define the generalized k-Fibonacci sequence and its particular cases.

Definition 1: Let k be any positive real number and p, q are positive integer. For $n \geq 2$, the generalized k-Fibonacci sequence $\{F_{k,n}\}$, is defined by

$$F_{k,n} = pkF_{k,n-1} + qF_{k,n-2} \tag{13}$$

with initial conditions $F_{k,0} = a$, $F_{k,1} = b$.

The first few generalized k-Fibonacci numbers are

$F_{k,2} = pkb + aq$

$F_{k,3} = p^2k^2b + pkqa + qb$

$F_{k,4} = p^3k^3b + p^2k^2qa + 2pkqb + aq^2$

$F_{k,5} = p^4k^4b + p^3k^3qa + 3p^2k^2qb + 2pkaq^2 + bq^2$

...

Particular cases of generalized k-Fibonacci sequence are

- If $a = 0$, $p = q = b = 1$, the k-Fibonacci sequence is obtained
  $F_{k,0} = 0$, $F_{k,1} = 1$ and $F_{k,n} = kF_{k,n-1} + F_{k,n-2}$, for $n \geq 2$:
  $\{F_{k,n}\}_{n\in N} = \{0, 1, k, k^2+1, k^3+2k, k^4+3k^2+1, ...\}$
- If $a = 0$, $k = p = q = b = 1$, the classic Fibonacci sequence is obtained
  $F_0 = 0$, $F_1 = 1$ and $F_n = F_{n-1} + F_{n-2}$, for $n \geq 2$:
  $\{F_n\}_{n\in N} = \{0, 1, 1, 2, 3, 5, 8, ...\}$
- If $a = 0$, $k = 2$, $p = q = b = 1$, the classic Pell sequence appears
  $P_0 = 0$, $P_1 = 1$ and $P_n = 2P_{n-1} + P_{n-2}$, for $n \geq 2$:
  $\{P_n\}_{n\in N} = \{0, 1, 2, 5, 12, 29, 70, ...\}$
- If $a = 0$, $q = 2$, $p = k = b = 1$, the classic Jacobsthal sequence appears
  $J_0 = 0$, $J_1 = 1$ and $J_n = J_{n-1} + 2J_{n-2}$, for $n \geq 2$:
  $\{J_n\}_{n\in N} = \{0, 1, 1, 3, 5, 11, 21, ...\}$
- If $a = 0$, $k = 3$, $p = q = b = 1$, the following sequence appears
  $H_0 = 0$, $H_1 = 1$ and $H_n = 3H_{n-1} + H_{n-2}$, for $n \geq 2$:

  $\{H_n\}_{n\in N} = \{0, 1, 3, 10, 33, 109, ...\}$

3. PROPERTIES OF THE GENERALIZED *k*-FIBONACCI SEQUENCE

In this section, we introduce and prove some interesting properties of the generalized *k*-Fibonacci sequence.

3.1. First Explicit Formula for The Generalized *K*-Fibonacci Sequence

In the 19th century, the French mathematician Binet devised two remarkable analytical formulas for the Fibonacci and Lucas numbers. In our case, Binet's formula allows us to express the generalized *k*-Fibonacci numbers in the function of the roots $\Re_1^n$ and $\Re_2^n$ of the following characteristic equation, associated with the recurrence relation (13):

$$x^2 = pkx + q \tag{14}$$

3.1.1. Binet's formula

Theorem 1: The nth generalized *k*-Fibonacci number is given by

$$F_{k,n} = A\Re_1^n + B\Re_2^n \tag{15}$$

where $\Re_1^n$ and $\Re_2^n$ are the roots of the characteristic equation (13) , $\Re_1 > \Re_2$ and

$$A = \frac{b - a\beta}{\sqrt{p^2k^2 + 4q}} \text{ and } B = \frac{a\alpha - b}{\sqrt{p^2k^2 + 4q}}.$$

Proof: The roots of the characteristic equation (13) are

$$\Re_1 = \frac{pk + \sqrt{p^2k^2 + 4q}}{2} \text{ and } \Re_2 = \frac{pk - \sqrt{p^2k^2 + 4q}}{2},$$

we use the Principle of Mathematical Induction (PMI) on n. The result is true for $n = 0$ *and* $n = 1$ by hypothesis. Assume that it is true for r such that $0 \le r \le s+1$, then

$$F_{k,r} = A\Re_1^r + B\Re_2^r$$

It follows from the definition of generalized *k*-Fibonacci numbers and equation (15)

$$F_{k,s+2} = pkF_{k,s+1} + qF_{k,s} = A\Re_1^{s+2} + B\Re_2^{s+2}$$

Thus, the formula is true for any positive integer.

Particular cases are:

- If $a = 0$, $p = q = b = 1$, we obtained *k*-Fibonacci numbers and then $\sigma = \frac{k + \sqrt{k^2 + 4}}{2}$ is known as the *k*-metallic ratio.
- If $a = 0$, $k = p = q = b = 1$, we obtained classic Fibonacci numbers and then $\tau = \frac{1 + \sqrt{5}}{2}$ is well known as the golden ratio, τ is also denoted by α .
- If $a = 0$, $k = 2$, $p = q = b = 1$, we obtained classic Pell numbers and then $\alpha = 1 + \sqrt{2}$ is well known as the silver ratio.

- If $a=0$, $k=3,\ p=q=b=1$, for the sequence $\{H_n\}$, and then $\sigma=\frac{3+\sqrt{13}}{2}$ is known as the bronze ratio.

Proposition 2: For any integer $n\geq 1$,

$$\begin{aligned}\Re_1^{n+2}&=pk\Re_1^{n+1}+q\Re_1^n\\ \Re_2^{n+2}&=pk\Re_2^{n+1}+q\Re_2^n\end{aligned} \tag{16}$$

Proof: Since $\Re_1^n$ and $\Re_2^n$ are the roots of the characteristic equation (13), then

$$\Re_1^2=pk\Re_1+q\ ,\ \Re_2^2=pk\Re_2+q$$

now, multiplying both sides of these equations by $\Re_1^n$ and $\Re_2^n$ respectively, we obtain the desired result.

Lemma 3: If r is a positive integer then $\frac{\Re_1^r-\Re_2^r}{\Re_1-\Re_2}=\frac{bF_{k,r}-aF_{k,r+1}}{b^2-a^2q-abpk}$ (17)

Proof: Using the Principle of Mathematical Induction (PMI) on n, the proof is clear.

Theorem 4: If $V=\left(\frac{\Re_1^n-\Re_2^n}{\Re_1-\Re_2}\right)^2-\left(\frac{\Re_1^{n-r}-\Re_2^{n-r}}{\Re_1-\Re_2}\right)\left(\frac{\Re_1^{n+r}-\Re_2^{n+r}}{\Re_1-\Re_2}\right)$, then

$$V=(-q)^{n-r}\left(\frac{bF_{k,r}-aF_{k,r+1}}{b^2-a^2q-abpk}\right)^2 \tag{18}$$

Proof: Using the roots of the characteristic equation (13), the proof is clear.

Proposition 5: $\left(A^2\Re_1^2+B^2\Re_2^2\right)\left(p^2k^2+4q\right)=\left(p^2k^2+2q\right)+2ab\left(aq+bpk\right)$ (19)

Proof: Since $\Re_1^n$ and $\Re_2^n$ are the roots of the characteristic equation (13) and

$A=\frac{b-a\beta}{\sqrt{p^2k^2+4q}}$ and $B=\frac{a\alpha-b}{\sqrt{p^2k^2+4q}}$, then

$$\left(A^2\Re_1^2+B^2\Re_2^2\right)=\frac{b^2\left(\Re_1^2+\Re_2^2\right)+2a^2\left(\Re_1\Re_2\right)^2+2ab\Re_1\Re_2\left(\Re_1+\Re_2\right)}{\left(p^2k^2+4q\right)}$$

$$\left(A^2\Re_1^2+B^2\Re_2^2\right)\left(p^2k^2+4q\right)=b^2\left\{pk\left(\Re_1+\Re_2\right)+2q\right\}+2a^2q+2abqpk$$

Finally, by simplifying the last expression, Eq. (19) is proven.

Theorem 6: If $T=\sum_{i=0}^{n}\frac{\Re_1^i-\Re_2^i}{\Re_1-\Re_2}$, then

$$T=\frac{1}{pk+q-1}\left(\frac{b\left(F_{k,n+1}+F_{k,n}\right)-a\left(F_{k,n+2}+F_{k,n}\right)}{b^2-a^2q-abpk}-1\right) \tag{20}$$

Proof: Since $\Re_1^n$ and $\Re_2^n$ are the roots of the characteristic equation (13), now by summing up the geometric partial sums $\sum_{i=0}^{n}\Re_j^i$ for $j=1,2$, we obtain

$$T=\frac{1}{\Re_1-\Re_2}\left(\frac{\Re_1^{n+1}-1}{\Re_1-1}-\frac{\Re_2^{n+1}-1}{\Re_2-1}\right)$$

$$=\frac{1}{pk+q-1}\left(\frac{\Re_1^{n+1}-\Re_2^{n+1}}{\Re_1-\Re_2}+\frac{\Re_1^{n}-\Re_2^{n}}{\Re_1-\Re_2}-1\right)$$

$$T=\frac{1}{pk+q-1}\left(\frac{b\left(F_{k,n+1}+F_{k,n}\right)-a\left(F_{k,n+2}+F_{k,n}\right)}{b^2-a^2q-abpk}-1\right)$$

This completes the proof.

3.1.2. Limit of the quotient of two consecutive terms

A useful property in these sequences is that the limit of the quotient of two consecutive terms is equal to the positive root of the corresponding characteristic equation.

Proposition 7: $\lim_{n\to\infty}\frac{F_{k,n}}{F_{k,n-1}}=\Re_1$ (21)

Proof: Using Eq. (13), $\lim_{n\to\infty}\frac{F_{k,n}}{F_{k,n-1}}=\lim_{n\to\infty}\frac{A\Re_1^r+B\Re_2^r}{A\Re_1^r+B\Re_2^r}=\lim_{n\to\infty}\frac{1+\frac{B}{A}\left(\frac{\Re_2}{\Re_1}\right)^n}{\frac{1}{\Re_1}+\frac{B}{A}\left(\frac{\Re_2}{\Re_1}\right)^n\frac{1}{\Re_2}}$

and taking into account that $\lim_{n\to\infty}\left(\frac{\Re_2}{\Re_1}\right)^n=0$, since $\left|\Re_2\right|<\Re_1$, Eq. (21) is obtained.

Particular cases are:

- If $a=0$, $k=p=q=b=1$, we obtained, $\lim_{n\to\infty}\frac{F_n}{F_{n-1}}=\tau$.
- If $a=0$, $k=2$, $p=q=b=1$, we obtained $\lim_{n\to\infty}\frac{P_n}{P_{n-1}}=\alpha$.
- If $a=0$, $k=3$, $p=q=b=1$, we obtained $\lim_{n\to\infty}\frac{H_n}{H_{n-1}}=\sigma$.

3.1.3. Catalan's identity

Catalan's identity for Fibonacci numbers was founded in 1879 by Eugene Charles Catalan a Belgian mathematician who worked for the Belgian Academy of Science in the field of number theory.

Proposition 8: (Catalan's identity) $F_{k,n}^2 - F_{k,n+r}F_{k,n-r} = (-q)^{n-r}\dfrac{(bF_{k,n} - aF_{k,r+1})^2}{(b^2 - a^2q - abpk)}$ (22)

Proof: By using Eq. (13) in the left-hand side (LHS) of Eq. (22), and taking into account that $\Re_1\Re_2 = -q$ it is obtained

$$\begin{aligned}
(\text{LHS}) &= \left(A\Re_1^n + B\Re_2^n\right)^2 - \left(A\Re_1^{n+r} + B\Re_2^{n+r}\right)\left(A\Re_1^{n-r} + B\Re_2^{n-r}\right) \\
&= AB\left(\Re_1\Re_2\right)^n\left(2 - \Re_1^r\Re_2^{-r} - \Re_1^{-r}\Re_2^r\right) \\
&= AB(-q)^n\left\{2 - \left(\frac{\Re_1^r}{\Re_2^r}\right) - \left(\frac{\Re_2^r}{\Re_1^r}\right)\right\} \\
&= (-AB)(-q)^n\frac{\left(\Re_1^r - \Re_2^r\right)^2}{(-q)^r} \\
&= (b^2 - a^2q - abpk)(-q)^{n-r}\left(\frac{\Re_1^r - \Re_2^r}{\Re_1 - \Re_2}\right)^2
\end{aligned}$$

Finally, by using Eq. (17),

$$= (-q)^{n-r}\frac{(bF_{k,n} - aF_{k,r+1})^2}{(b^2 - a^2q - abpk)}$$

This completes the proof.

3.1.4. Cassini's identity

This is one of the oldest identities involving the Fibonacci numbers. It was discovered in 1680 by Jean-Dominique Cassini a French astronomer.

Proposition 9: (Cassini's identity or Simpson's identity)

$$F_{k,n}^2 - F_{k,n+1}F_{k,n-1} = (-q)^{n-1}(b^2 - a^2q - abpk) \quad (23)$$

Proof: Taking $r = 1$ in Catalan's identity the proof is completed.

3.1.5. d'ocagnes's identity

Proposition 10: (d'ocagnes's Identity)

$$F_{k,m}F_{k,n+1} - F_{k,m+1}F_{k,n} = (-q)^{n-1}(bF_{k,m-n} - aF_{k,m-n+1}) \quad (24)$$

where $n \le m$ integers.

Proof: Using the Binet's formula, the proof is clear.

- If $a=0$, $k=p=q=b=1$, we obtained d'ocagnes's Identity for classic Fibonacci numbers, $F_m F_{n+1} - F_{m+1} F_n = (-1)^{n-1} F_{m-n}$.

3.2. Generalized İdentity for Generalized *K*-Fibonacci Sequence

In this section, we present generalized identity for generalized *k*-Fibonacci sequence, from which we obtain Catlan's identity, Cassini's identity and d'Ocagne's identity.

Theorem 11: If $Y = F_{k,m} F_{k,n} - F_{k,m-r} F_{k,m+r}$ and $F_{k,n}$ be the generalized k-Fibonacci numbers, then $Y = (-q)^{m-r} \dfrac{\left(bF_{k,r} - aF_{k,r+1}\right)\left(bF_{k,n+r-m} - aF_{k,n+r-m+1}\right)}{\left(b^2 - a^2 q - abpk\right)}$ (25)

where n, m, r nonnegative integers.

Proof: Using the Binet's formula, the proof is clear.

Eq. (25), is generalized of Catalan's, Cassini's and d'ocagnes's identities.

- If $a=0, k=p=q=b=1$, we have $F_m F_n - F_{m-r} F_{n+r} = (-1)^{m-r} F_r F_{n+r-m}$

which is given for Fibonacci numbers by Spivey in [14].

3.3. A Second Formula for The Generalized K-Fibonacci Sequence in Terms of Their Characteristic Roots

Theorem 12: $\mathfrak{R}_1^n - \mathfrak{R}_2^n = \dfrac{1}{2^n - 1} \sum_{i=0}^{\left\lfloor \frac{n-1}{2} \right\rfloor} \binom{n}{2i+1} (pk)^{n-1-2i} \left(p^2 k^2 + 4q\right)^i$ (26)

where $\lfloor a \rfloor$ is the floor function of a that is $\lfloor a \rfloor = \sup . \{ n \in N \mid n \le a \}$ and says the integer part of a, for $a \ge 0$.

Proof: Since $\mathfrak{R}_1^n$ and $\mathfrak{R}_2^n$ are the roots of the characteristic equation $x^2 - pkx - q = 0$, using the value of $\mathfrak{R}_1^n$ and $\mathfrak{R}_2^n$, we get $\mathfrak{R}_1^n - \mathfrak{R}_2^n = \left[\left(\dfrac{pk + \sqrt{p^2 k^2 + 4q}}{2} \right)^n - \left(\dfrac{pk - \sqrt{p^2 k^2 + 4q}}{2} \right)^n \right]$

from where, by developing the nth powers, it follows:

$$\mathfrak{R}_1^n - \mathfrak{R}_2^n = \frac{1}{2^n - 1} \sum_{i=0}^{\left\lfloor \frac{n-1}{2} \right\rfloor} \binom{n}{2i+1} (pk)^{n-1-2i} \left(p^2 k^2 + 4q\right)^i$$

Particular cases are:

- If $p=q=1$, for the classical Fibonacci sequence, we have

$$\mathfrak{R}_1^n - \mathfrak{R}_2^n = \frac{1}{2^n - 1} \sum_{i=0}^{\left\lfloor \frac{n-1}{2} \right\rfloor} \binom{n}{2i+1} (5)^i$$

- If $k=2,\ p=q=1$, for the Pell sequence, we have

$$\Re_1^n-\Re_2^n=\frac{1}{2^n-1}\sum_{i=0}^{\left\lfloor\frac{n-1}{2}\right\rfloor}\binom{n}{2i+1}(2)^{n-1-2i}(8)^i=\sum_{i=0}^{\left\lfloor\frac{n-1}{2}\right\rfloor}\binom{n}{2i+1}(2)^i$$

- If $k=3,\ p=q=1$, for the sequence $\{H_n\}$, we have

$$\Re_1^n-\Re_2^n=\frac{1}{2^n-1}\sum_{i=0}^{\left\lfloor\frac{n-1}{2}\right\rfloor}\binom{n}{2i+1}(3)^{n-1-2i}(13)^i=\left(\frac{3}{2}\right)^{n-1}\sum_{i=0}^{\left\lfloor\frac{n-1}{2}\right\rfloor}\binom{n}{2i+1}\left(\frac{13}{9}\right)^i$$

4. SUM OF FIRST TERMS OF THE GENERALIZED *k*-FIBONACCI SEQUENCE

Theorem 13: Let $F_{k,n}$ be the nth generalized *k*-Fibonacci number then

$$\sum_{s=1}^{n}F_{k,s}=\frac{F_{k,n}+qF_{k,n-1}+apk-a-b}{pk+q-1} \tag{27}$$

Proof: Using the Binet's formula for the generalized *k*-Fibonacci numbers,

$$\sum_{s=1}^{n}F_{k,s}=\sum_{s=1}^{n}A\Re_1^s+B\Re_2^s$$

$$=A\sum_{s=1}^{n}\Re_1^s+B\sum_{s=1}^{n}\Re_2^s$$

$$=A\left(\frac{1-\Re_1^s}{1-\Re_1}\right)+B\left(\frac{1-\Re_2^s}{1-\Re_2}\right)$$

$$=\frac{(A+B)-(A\Re_1^s+B\Re_2^s)-(A\Re_2+B\Re_1)+\Re_1\Re_2(A\Re_1^{s-1}+B\Re_2^{s-1})}{(1-\Re_1)(1-\Re_2)}$$

$$=\frac{F_{k,n}+qF_{k,n-1}+apk-a-b}{pk+q-1}$$

Particular cases are:

- If $a=0$, $k=p=q=b=1$, for the classic Fibonacci sequence, we have:

$$\sum_{s=1}^{n}F_s=F_{n+2}-1.$$

- If $a=0$, $k=2, p=q=b=1$, for the Pell sequence, we have:

$$\sum_{s=1}^{n}P_s=\frac{1}{2}\left(P_{n+1}+P_n-1\right).$$

- If $a=0$, $k=3, p=q=b=1$, the sum of the first elements of the sequence $\{H_n\}$ is:

$$\sum_{s=1}^{n}H_s=\frac{1}{3}\left(H_{n+1}+H_n-1\right)$$

5. GENERATING FUNCTION FOR GENERALIZED *k*-FIBONACCI SEQUENCE

The function is $F(x) = a_0 + a_1 x + a_2 x^2 + a_3 x^3 + ... + a_n x^n + ...$ called the generating function for the sequence $\{a_0, a_1, a_2, ...\}$. Generating functions provide a powerful tool for solving linear recurrence relations with constant coefficients.

Let $F_{k,n}(x) = \dfrac{a + x(b - apk)}{1 - pkx - qx^2}$ (28)

Particular cases are:

- If $a = 0$, $p = q = b = 1$, generating function of the *k*- Fibonacci sequence:
  $F_{k,n}(x) = \dfrac{x}{1 - kx - x^2}$.
- If $a = 0$, $k = p = q = b = 1$, generating function of the classic Fibonacci sequence:
  $F_n(x) = \dfrac{x}{1 - x - x^2}$.
- If $a = 0$, $k = 2, p = q = b = 1$, generating function of the Pell sequence:
  $P_n(x) = \dfrac{x}{1 - 2x - x^2}$.
- If $a = 0$, $k = 3, p = q = b = 1$, generating function of the sequence $\{H_n\}$:
  $H_n(x) = \dfrac{x}{1 - 3x - x^2}$.

6. CONCLUSIONS

In this study new generalized *k*-Fibonacci sequences have been introduced and studied. Many of the properties of these sequences are proved by simple algebra. Compactly and directly many formulas of such numbers have been deduced.

REFERENCES

[1] Bilgici, G. (2014). New Generalizations of Fibonacci and Lucas Sequences, *Applied Mathematical Sciences,* 8(29): 1429-1437.

[2] Falcon, S., and Plaza, A. (2007). On the k-Fibonacci Numbers, *Chaos, Solitons and Fractals*, 32(5): 1615-1624.

[3] Falcon, S. (2011). On the k-Lucas Numbers, *International Journal of Contemporary Mathematical Sciences*, 6(21): 1039-1050.

[4] Falcon, S., and Plaza, A. (2008). The k-Fibonacci hyperbolic functions, *Chaos, Solitons and Fractals*, 38(2): 409-420.

[5] Falcon, S., and Plaza, A. (2007). The k-Fibonacci sequence and the Pascal 2-triangle, *Chaos, Solitons and Fractals*, 33(1): 38-49.

[6] Gupta, V. K., Panwar, Y. K., and Sikhwal, O. (2012) Generalized Fibonacci Sequences, *Theoretical Mathematics & Applications*, 2(2): 115-124.

[7] Horadam, A.F. (1961). A Generalized Fibonacci Sequence, *American Mathematical Monthly*, 68(5): 455-459.

[8] Horadam, A. F. (1996). Jacobsthal Representation Numbers. *The Fib. Quart*, 34(1): 40-54.

[9] Horadam, A. F. (1971). Pell Identities, *The Fibonacci Quarterly*, 9(3), 245-252.

[10] Kalman, D., and Mena, R. (2002). The Fibonacci Numbers–Exposed, *The Mathematical Magazine*, 2.

[11] Koshy, T. (2001). *Fibonacci and Lucas numbers with applications*, New York, Wiley-Interscience.

[12] Panwar, Y. K., Rathore, G. P. S., and Chawla, R. (2014). On the k-Fibonacci-like numbers, *Turkish J. Anal. Number Theory*, 2(1): 9-12.

[13] Singh, B., Sikhwal, O., and Bhatnagar, S. (2010). Fibonacci-Like Sequence and its Properties, *Int. J. Contemp. Math. Sciences*, 5(18): 859-868.

[14] Spivey, M.Z. (2006). Fibonacci Identities via the determinant sum Property, *The College Mathematics Journal*, 37(2): 286-289.

[15] Suvarnamani, A., and Tatong, M. (2015). Some Properties of (p,q)-Fibonacci Numbers, *Science and Technology RMUTT Journal*, 5(2): 17-21.

[16] Suvarnamani, A., and Tatong, M. (2016). Some Properties of (p,q)-Lucas Numbers, *Kyungpook Mathematical Journal*, 56(2): 367-370.

[17] Taşyurdu, Y. (2019). Generalized (p,q)-Fibonacci-Like Sequences and Their Properties, *Journal of Mathematics Research*, 11(6): 43-52.

[18] Taşyurdu, Y., Cobanoğlu, N., and Dilmen, Z. (2016). On The a New Family of *k*-Fibonacci Numbers, *Erzincan University Journal of Science and Thechnology*, 9(1): 95-101.

[19] Vajda, S. (1989). *Fibonacci and Lucas numbers, and the golden section. Theory and applications*, Chichester: Ellis Horwood Limited.

[20] Wani, A. A., Catarino, P., and Rafiq, R. U. (2018) On the Properties of *k*-Fibonacci-Like Sequence, *International Journal of Mathematics And its Applications*, 6(1-A): 187-198.

[21] Wani, A. A., Rathore, G. P. S., and Sisodiya, K. (2016). On The Properties of Fibonacci-Like Sequence, *International Journal of Mathematics Trends and Technology*, 29(2), 80-86.

[22] Yazlik, Y. aand Taskara, N. (2012). A note on generalized k-Horadam sequence, *Computers and Mathematics with Applications*, 63(1): 36-41.

NATURENGS
MTU Journal of Engineering and Natural Sciences
https://dergipark.org.tr/tr/pub/naturengs
DOI: 10.46572/naturengs.959984

The Thermal and Mechanical Properties of the Building Stones in Eskisehir - Kayseri and Kırsehir regions

Ayşe Biçer

Department of BioEngineering, Faculty of Engineering and Natural Sciences, Malatya Turgut Özal University, Malatya, Turkey.

(**Received:** 30.06.2021; **Accepted:** 05.11.2021)

ABSTRACT: In this study, certain physical properties of Derbent (Eskisehir), Tomarza (Kayseri) and Mucur (Kırsehir) stones, which are used as building materials in the relevant regions, are subjected to analysis. For each stone, the samples were taken from two separate quarries, after which the chemical analysis, thermal conductivity, compression stress, water absorption, breathability and abrasion tests were carried out. The results obtained from the tests carried out are as follows: *i*) It is understood that Eskisehir Derbent tuff and Tomarza stones can be used as briquettes, bricks or aggregates as lightweight concrete thanks to their low thermal conductivity values (0.355 W/mK and 0.581 W/mK) and heat insulation properties. *ii*) Kırşehir Mucur stone shows that it can be used in load-bearing wall material and abrasion-resistant flooring with 88.46 MPa compressive strength and 0.4% volume abrasion values. *iii*) It has also been conferred that three stones have rich reserves and low costs. The results are compared with other building materials, especially in terms of energy-saving, strength and comfort conditions.

Keywords: Derbent tuff, Mucur stone, Tomarza stone, Building material.

1. INTRODUCTION

Natural stones are mineral assemblages formed by the combination of one or more minerals. A stone can be composed of a single mineral or a combination of several minerals. Calcite, Dolomite, Quartz, Orthose, Plagioclase, Biotite-Muscovite, Hornblende, Pyroxene-Olivine are some of the important minerals found in the combination of stones.
Natural stones have been utilized by humankind since the beginning of civilization up to date. The largest historical buildings that survive to date were made of stone. Typical examples include Egyptian Pyramids, Greek Acropolises, Roman Amphitheaters, Ottoman fountains and mosques, Artemis Temple and Halicarnassus Mausoleum. Additionally, roads, bridges, squares, monuments and obelisks are also other structures where natural stones are widely used [1]. The structures in question were built with stones brought from hundreds of kilometers away, as the result of years of effort.

Turkey is one of the richest countries in natural stone presence, while also having a great potential in terms of both reserve and diversity aspects. Today, stones are used in a wide range of areas such as road and paving, curbstone, wall material, coastal fortification, breakwater, dam construction and aggregate production. Stones maintain their importance in today's modern building industry [1]. Stones obtained from the quarries gain functionality by cutting in place, exploiting natural discontinuities and using explosives. The use of natural stones as building

*Corresponding Author: ayse.bicer@ozal.edu.tr
ORCID number of authors: 0000 -0003-4514-5644

and decoration materials has led to an increase in natural stone production across the world. Today, as a result of both the price increases in construction materials and the increase in housing demand, the use of natural stones as a carrier and filling element, depending on the geological structure of each region, is brought to the agenda.

Some studies on building blocks have been carried out in the literature in this area. Some of these studies are summarized as follows:

In the study they carried out, Taşlıgil and Sahin have investigated the determination of the characteristics and geographic distribution of wealth comprehensively along with the detection of natural stone used as building materials in Turkey [1]. Pivko conducted researches on the formation of Stones [2]. Gevrek & Kazanci ignimbrite formation [3]; Kazanci & Gurbuz [4], the geological formation of the natural stone of Turkey. Dinçer et al. conducted a study on the water absorption rates of ignimbrites [5], while Bakiş et al. carried out a study on the use of Ahlat Stone in the construction sector [6] and Bicer conducted a study determining the thermal and mechanical properties of Ahlat and Malazgirt Stones [7]. In a different study, Bicer investigated the thermal and mechanical properties of building blocks used as building construction materials in many regions of the Euphrates basin [8]. Similarly, in another study carried out by Biçer, the physical properties of the building stones used in buildings in the Elazığ and Nevşehir regions were determined accordingly [9]. Doran and Kaygisiz, in their dissertations on an individual basis, investigated the formation of Erciyes volcanism, the physicomechanical properties of the tuff and building stones from the eructation [10, 11]. Demir investigated the building blocks found in Kırşehir and its vicinity [12], and Çavumirza et al investigated the physicomechanical properties of Mucur stone [13]. Daloğlu & Emir investigated certain properties of Derbent tuff, as one of the building stones found in Eskişehir [14].

For these natural stones to be used as building materials in the best manner possible, all physicomechanical properties are required to be well known. In this study, Tomarza stone (Kayseri), Mucur stone (Kırşehir) and Derbent Tuff (Eskişehir), which are used extensively in the relevant regions, were examined and certain properties of the same were subjected to analysis. Stones have been preferred by the local people and used in old buildings up to date. This study sets forth the reasons for preference with the properties determined as a result of the tests carried out on the stones.

2. MATERIAL AND METHODS

2.1. Materials

Eskisehir Derbent Tuff:

It is quarried in blocks within the cut stone quarry located near Derbent Farm village, approximately 20 km southeast of Eskişehir. Compared to artificially produced counterparts, there is no product cost other than a cutting process in the quarry. It has been used as the most important material and building element in masonry buildings for many years. Derbent tuff has acidic magma characteristics and is a type of rock resistant to heat due to the minerals it contains. It also provides thermal insulation due to the porous structure of tuff. There are several examples of Ottoman architecture in which tuff was used as cut stone in Anatolia as can be seen in the recent past. Eskişehir Kurşunlu Complex, which was built in 1525 in connection with the same, is one of the structures that has survived to date (Figure 1). Today, it is produced and used as cut stone, especially in Kayseri and Nevşehir provinces. There are two separate cut

stone quarries in Derbent Farm in Eskişehir. While there is no production process carried out in the quarry that produces pink tuff, the quarry for white tuff continues its production process [14, 15].

Figure 1. Kursunlu complex [14]

Kayseri Tomarza Stone:

These are the tuff stones that are the ignimbrite of Erciyes Mountain, as the largest extinct volcano in Central Anatolia. The stone samples were obtained from natural stone quarries located in Tomarza District of Kayseri Province. It can be used as wall cladding, floor and stair flooring, road and pavement flooring, and it is frequently preferred to be used in structures such as fountains, fireplaces, barbecues and tombstones [11]. Because the colors of these stones are attractive, they are also used for decoration purposes, as well. The colors available are Dried Rose, Yellow, Tomarza Black, Brown, Antique Yellow colors (Figure 2). The properties of the stones can be summarized as follows: color, pattern, appearance, hardness, durability, resistance to external factors and ability to be cut and polished. Tomarza Stone can be used as a building block due to its ease of processing after being quarried, along with its ability to gain strength as long as it stays under atmospheric conditions. In addition, Tomarza Stone is especially preferred for decorative purposes due to its wide variety of colors, its ability to be polished on the surface and its aesthetic appearance.

a) b)

Figure 2. a) Akdeniz University Mosque (Tomarza yellow), b) Biga Government House (Dried rose and antique yellow) [10]

Kırsehir Mucur Stone:

The stone samples were obtained from the crushed stone production quarry located in the northeast of Kırşehir Province, within the boundaries of İnaç village at the 7th km of Kırşehir-Mucur highway. The chemical contents of the limestone marbles taken from the surface in the study area were determined accordingly and shown in Table 1. The stones are used as aggregate in the production of quality concrete in the region with a first-degree seismic zone [13]. Due to the roughness of crushed aggregate surfaces, it creates a strong adherence between cement paste and aggregate. The larger the rough surface is, the larger the contact surface of crushed aggregate and cement paste becomes. For this reason, it can be seen that the strength properties of concretes produced with crushed stone aggregate have improved accordingly.

Table 1. The chemical composition of the samples, (%)

Component / Material	SiO_2	Al_2O_3	Fe_2O_3	CaO	MgO	K_2O	Loss of ignition	Undefined
Derbent stone	68.9	12.11	1.19	1.03	2.91	4.66	5.72	3.60
Tomarza stone	61.88	15.95	1.82	6.38	3.18	1.22	7.13	2.51
Mucur stone	0.36	0.012	0.09	54.73	0.40	5.19	36.4	2.88

2.2. Methods

The samples of 150x60x20 mm for thermal tests and 100x100x100 mm for pressure and wear tests were prepared from the stones taken from the quarries and subjected to the following tests (Figure 3).

a) b) c)

Figure 3. Color samples of natural building stones a) Derbent tuff, b)Tomarza stone, c) Mucur stone

2.2.1. Thermal conductivity

The measurement procedures were carried out with "*Shotherm-QTM*", measuring in the temporary regime and operating in hot-wire method (Fig. 4). Measuring as per DIN 510406 norm, this device was used to carry out measurements from 3 different points on every sample under room temperature of 22-25 ºC, calculating the arithmetic mean of these 3 values. The thermal conductivity coefficient of the device has a tolerance of 5% between 0.02 to 6 W/mK [16, 17]. Measurement results are given in Table 2.

Figure 4. Shotherm-QTM unit

2.2.2. Compressive strength and abrasion tests

Endurance tests were carried out on the samples following TS 699 standard [18]. Compressive strength tests for the samples were carried out with Ele International branded device, bearing the following features: 3000 kN loading capacity; digital control panel; adjustable loading rate; applying uniaxial force.
Volume abrasion lost results for 88 rpm within the scope of frictional abrasion tests can be seen in Table 3.

2.2.3. Water absorption test

The objective of this test is to determine the presence of a dry volume, where the ice crystals within can expand, as the building materials -in direct contact with water- freeze [19]. This feature ensures a warranty for the material against freezing. The dry weight (W_k) of each sample was determined. Then the water level is gradually raised within the water tank, where the samples are placed, adding water into the tank in a manner allowing the samples to be submerged. The change of the samples' weight based on time can be seen in Figure 3. After keeping the samples in the water for 48 hours, they were removed out of the water and wiped, finding the water-absorbed weight (W_d), while on the other hand calculating the water absorption ratio with the Eq. 1.

$$\text{Water absorption percent} = \{[W_d - W_k]/ W_k \} x100 \quad (1)$$

2.2.4. Density test

Dry weights of the samples were taken with the weighing machine having a tolerance of 1%, while the density levels were calculated by identifying the sample volumes.

3. RESULTS AND DISCUSSION

The following findings were obtained in this study conducted to investigate the thermal and mechanical properties of some stones, which are used in the center and districts of Kayseri, Kırşehir and Eskişehir provinces located in the Central Anatolia Region, as well as having large reserves.

Eskisehir-Derbent Tuff:

Tuff is a natural building stone and is produced as cut stone. Derbent tuffs do not meet the requirements to be used as flooring and outer covering stone with 17.17% volume abrasion and 30.44% water absorption ratios (Table 2, Figure 5). Since tuff is a lightweight and easily processable material, it can be produced by being sliced on site. Therefore, according to their artificially produced counterparts, tuffs do not have any costs other than the cutting process in the quarry. Derbent tuff has similar properties with pumice concrete, concrete briquette/concrete block and less-hole brick, which is used as an artificial filling wall material and is a more cost-friendly alternative product. The lightness of tuffs compared to natural filling wall materials increases the resistance of the building against earthquakes as it reduces the dynamic loads on the structure in high-rise buildings.

Derbent tuff looks better than concrete, granite, marble, limestone and sandstone with its thermal conductivity coefficient of 0.355 W/mK. For this reason, it will provide heat and sound insulation where it is used as a filling material in brick, briquette and walls in buildings. Additionally, considering the compressive strength value of 11.39 MPa, it has approximately equivalent strength with artificial materials such as briquette, brick, aerated concrete although it is lower than high strength natural building stones.

Kayseri Tomarza Stone:

Tomarza Stone is included in the class of light building materials, while it greatly reduces the dead load of the buildings, such as Derbent tuff, and reduces energy costs by contributing to the thermal insulation of the buildings thanks to the closed pores in its internal structure. Tomarza Stone can be used both as a building stone and as a covering stone thanks to its high compressive strength compared to tuff-class rocks. The fact that the buildings in the Tomarza Region, where the climatic conditions are very heavy in winter, still maintain their durability is an indicator of the resistance of the stone to atmospheric conditions. Due to its high color variety and aesthetics, Tomarza Stone is preferred for decorative purposes, as well. The low water absorption rate indicates that it can be used as exterior cladding.

With its 0.581 W/mK thermal conductivity value, Tomarza stone seems to be better compared to the building materials given in Table 4. Additionally, considering the compressive strength of 22.58 MPa, it has approximately equivalent strength with artificial materials such as concrete, briquette, brick, aerated concrete although it is lower than high strength building blocks. Notwithstanding that it can be used as a wall covering material with a 5.8% abrasion loss, it can also be seen that it cannot be used as a building element subject to excessive wear such as stairs, parquet.

Kırşehir Mucur Stone:

Kırşehir Mucur Stone seems to bear better properties compared to granite, sandstone and marble with thermal conductivity of 1.483 W/mK. Its compressive strength and abrasion values appear to be more durable than other stones examined. The fact that the water absorption rate is less than 30% indicates that the stones can be used in humid environments.

Examining the drying rates seen in Figure 6, it can be seen that the three regional stones examined have respiration capability, albeit it is low.

Table 2. Thermal and mechanical properties of stones

Materials	Density (kg/m^3)	Thermal conductivity (W/mK)	Compressive strength (MPa)	Water absorption (%)	Volume abrasion (%)
Derbent tuff	1420	0.355	11.39	30.44	17.17
Tomarza stone	1740	0.581	22.58	17.09	5.18
Mucur stone	2720	1.483	88.46	10.13	0.4

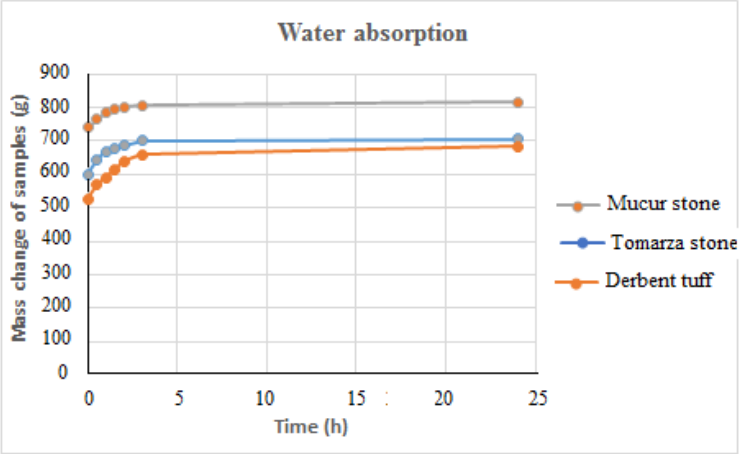

Figure 5. Mass change of stones according to time in water absorption test

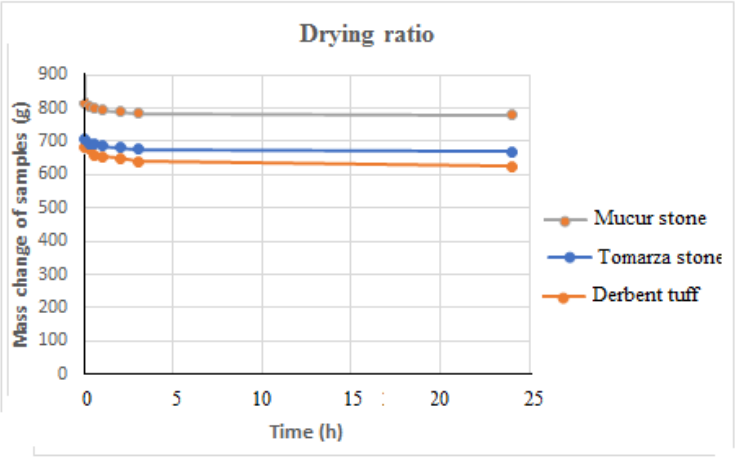

Figure 6. Mass change of stones according to time in drying test

Table 3. The physical properties of some building materials [20]

Materials	Density (kg/m^3)	Thermal conductivity (W/mK)	Compressive strength (MPa)
Concrete	1906	0.814	20
Granite	2643	1.73	120
Limestone	2483	1.16	35
Sandstone	2235	1.85	80
Marble	2603	2.77	50
Common brick	1602	0.692	16

4. CONCLUSIONS

The thermal and mechanical properties of the local stones used as construction elements in the center and districts of Kayseri, Kırşehir and Eskişehir provinces were experimentally subjected to examination, and the results obtained are given as follows:

✓ Eskişehir Derbent tuff can be used as a filling material in low-density concrete, briquette, brick making due to its lightweight (1420 kg/m^3) and its low thermal conductivity coefficient (0.355 W/mK). If it is used for this purpose, the heating costs of the building will decrease and also the dynamic loads on the building in high-rise buildings will decrease, and it will increase the resistance of the building against earthquakes. The high rate of water absorption indicates that it cannot be used as a building siding material.

✓ With its low density and thermal conductivity (1740 kg/m^3 and 0.581 W/mK), using Kayseri Tomarza stone instead of bricks on the outer walls of the building is advantageous in terms of the energy economy. Additionally, it can be used in load-bearing wall structures with its compressive strength value of 22.58 MPa and as an exterior wall covering material with a 17.09% water absorption ratio value. The fact that the stone is easy to process once it is quarried, and the variety of colors, along with the ability to be polished on its surface increase the appeal of using the stone.

✓ Kırşehir Mucur stone is a stone with a high thermal conductivity value (1.483 W/mK) among the stones examined, and no significant value has been conferred within the scope of the thermal properties of the same. On the other hand, the compressive stress of 88.46 MPa shows that it can be used in load-bearing wall material and abrasion-resistant flooring with a 0.4% wear rate.

✓ Along with the properties of the stones subjected to examination, the fact that the quarry reserves are rich, easy to supply, they can be cut and used directly and their cost is low can be considered as significant reasons for preference, based on these advantages.

REFERENCES

[1] Taşlıgil, N., and Şahin, G. (2016). Yapı malzemesi olarak kullanılan Türkiye doğal taşlarının iktisadi coğrafya odağında analizi, *Marmara Coğrafya Dergisi,* 33: 607-640.

[2] Pivko, D. (2003). Natural stones in earth's history, *Acta Geologica,* 58: 73-86.

[3] Gevrek, A.İ. and Kazancı, N. (1991). İgnimbrit: oluşumu ve özellikleri, *Jeoloji Mühendisliği Dergisi*, 38: 39-42.

[4] Kazancı, N., and Gürbüz, A. (2014). Jeolojik miras nitelikli Türkiye doğal taşları, *Türkiye Jeoloji Bülteni*. 57: 1-6.

[5] Dinçer, İ., Özvan, A., Akın, M., Tapan, M. and Oyan, V. (2012). İgnimbiritlerin kapiler su emme potansiyellerinin değerlendirilmesi: Ahlat Taşı örneği, *Yüzüncü Yıl Üniversitesi Fen Bilimleri Enstitüsü Dergisi*, 17(2): 64-71.

[6] Bakış, A., Işık, E., Hattatoğlu, F. and Akıllı, A. (2014). Jeolojik miras nitelikli Ahlat Taşı'nın inşaat sektöründe kullanımı, *III. Uluslararası Ahlat-Avrasya Bilim, Kültür ve Sanat Sempozyumu Bildiriler Kitabı* (Editörler Doğru M. ve Aksoy E.), 46-59, 22-24 Eylül Ahlat- Bitlis.

[7] Bicer A. (2019). Ahlat ve Malazgirt yapı taşlarının bazı fiziksel özellikleri, *Fırat Üniversitesi Müh. Bil. Dergisi*, 31(2): 301-307.

[8] Bicer, A. (2019). Some physical properties of the building stones from southeastern Anatolia region, *Bartın University International Journal of Natural and Applied Sciences,* 2(1): 9-15.

[9] Bicer, A. (2019). Some physical properties of the building stones from Elazıg-Nevsehir region, *Nevşehir Bilim ve Teknoloji Dergisi,* 8(2): 96-102.

[10] Duran, F. (2009). Erciyes Volkanizmasının Oluşumu, Koçcağız Köyü (Kayseri) Dolayının Stratigrafisi ve Tüflerin Yapı-Kaplama Taşı Olarak kullanılabilirliği. Çukurova Üniversitesi, Fen Bilimleri Enstitüsü*, Yüksek Lisans Tezi*, Adana.

[11] Kaygısız, H. (2010). Kayseri Yöresindeki Yapıtaşlarının Fiziko-Mekanik Özelliklerinin Belirlenmesi. Çukurova Üniversitesi, Fen Bilimleri Enstitüsü, *Yüksek Lisans Tezi*, Adana.

[12] Demir, I. (2005). The usage properties of Kırşehir regional rocks as crushed stone aggregate, *Journal of Polytechnic*, 8(1): 111-121.

[13] Çavumirza, M., Kılıç Ö., and Anıl M. (2003). Mucur (Kırşehir) yöresi kireçtaşı mermerleri ve travertenlerinin fiziko-mekanik özellikleri, *Türkiye IV. Mermer Sempozyumu (Mersem'2003) bildiriler kitabı 18-19 Aralık 2003*.

[14] Daloğlu, G., and Emir, E. (2010). The assessment of tuffs located at Eskisehir-Derbent region as the natural building stone, *Journal of Engineering and Architecture Faculty of Eskişehir Osmangazi University, Vol: XXIII, No:1.*

[15] Devecioglu, A.G. (2001). An investigation on the heat conduction parameters of porous building stones, *Master Thesis*, Firat University.

[16] Vysnıauskas, V.V, and Zıkas, A.A. (1988). Determination of the thermal conductivity of ceramics by the Hot-Wire Technique, *Heat Transfer Soviet Research*, 20(1): 137-142.

[17] Denko, S. (1990). Shotherm Operation Manual No 125-2. K.K. Instrument products department, 13-9, Shiba Daimon, Tokyo, 105, Japan.

[18] TS 699, (1978). The test and experiment methods of natural building stones, *TSE*, Ankara.

[19] Bicer, A. (2019). Influence of tragacanth resin on the thermal and mechanical properties of fly ash-cement composites, *Journal of Adhesion Science and Technology,* 33(10): 1019-1032.

[20] Toksoy, M. (1988). Thermal conductivity coefficients of industrial materials, *Journal of Engineers and Machinery,* 347: 12-15.

NATURENGS
MTU Journal of Engineering and Natural Sciences
https://dergipark.org.tr/tr/pub/naturengs
DOI: 10.46572/naturengs.845528

Research Article

Investigation of Hygiene Knowledge Levels of Kitchen Staff in Diyarbakir Provincial State Hospitals

Gurbet EREN [1*], Aylin SEYLAM KÜŞÜMLER [2]

[1,2] Department of Nutrition and Dietetics, İstanbul Okan University, İstanbul, Turkey.

(**Received:** 24.01.2021; **Accepted:** 10.07.2021)

ABSTRACT: This research was carried out to investigate the hygiene knowledge level of the personnel working in the nutrition/beverage service and kitchen of hospitals that provide mass feeding in Diyarbakır. For this purpose, a survey form of 94 questions was applied to a total of 150 people, 117 men and 33 women, working in three hospital kitchens in the central district of Diyarbakır. The study was initiated after the approval of the ethics committee of Okan University, dated 08.05.2019 with meeting number 108 and decision number 6. According to the data obtained from the research, 78% of the staff working in the institutional kitchens in Diyarbakir province were male and 22% were female. It was determined that the job duration in the profession was concentrated between 2-5 years (40.7%). Also, it is seen that the person who received hygiene training makes up the vast majority, such as 95.3%.

A significant difference was found between the groups in terms of personal hygiene and personnel hygiene competence and also between the age groups of the personnel who participated in our study. It has been observed that the knowledge of all those who got HACCP training at school is sufficient while others (who got training in a course or masters) have less knowledge. It has been observed that the knowledge of the staff on hand hygiene and HACCP system is low. Moreover, it has been observed that the personnel knowledge on hand hygiene and HACCP system is low.

Keywords: Hygiene, Food hygiene, Institutional kitchen, Mass feeding.

1. INTRODUCTION

Mass feeding is the feeding of people outside the home with nutrients and meals offered through institutions. Places that provide mass feeding are institutions that manage and program nutrition programs of a certain segment from a center. Research has shown that approximately 1/10 of Turkey's population is fed by mass feeding services [1,2].

Mass Feeding Systems (MFS) have developed in parallel with the development of technology since the middle ages [3]. Universities, schools, hospitals, workplaces, nursing homes for the elderly and needy, military, kindergartens, prisons, and correctional houses can be included for mass feeding institutions. Hotels, self-service restaurants, restaurants, fast-food restaurants, public transport enterprises, recreation and entertainment places are included in the group of commercial enterprises [4]. Due to its wide scope and complex structure, Mass Feeding Systems (MFS) services can have dangerous consequences for public health if hygiene/sanitation is not attached importance [5]. The issue is important in terms of nutrition,

*Corresponding Author: gurbeteren@gmail.com
ORCID number of authors: [1] 0000-0002-9503-5550, [2] 0000-0003-4705-8042

health, and the expectations of those who benefit from the service. Failure, carelessness that may occur at any step of the service can lead to food poisoning which can result in death [6]. The staff must be healthy when dealing with food to ensure hygienic cleaning of clothes, hands and bodies. Some unconscious practices while preparing meals can lead to mass food poisoning. Therefore, personnel interested in food processing should be given training that includes the main principles of healthy food preparation and personal hygiene matters. In particular, time and temperature control, personnel hygiene, sources of cross-contamination and factors affecting the proliferation of pathogens in food should be taught and this training should be given periodically [7]. Diseases that can be transmitted by food products, new production methods, genetically modified organisms (GMO), pesticides, and similar issues that constitute health risks have revealed the need to determine the main elements in food hygiene and safety. That's why, Law No. 5996 on Veterinary Services, Plant Health, Food and Feed and the provisions on food hygiene and safety in our country have been adapted to the European Union norms and minimum standards to be complied with have been regulated [8, 9]. In addition, provisions regarding the training to be received by personnel working on food hygiene are regulated by law and a Hygiene Training Regulation on the implementation of the provisions has been published. In the regulation, the procedures and principles regarding the planning of hygiene training for employees, delivering training, determining infectious diseases and skin diseases that prevent employees working in these workplaces, the treatment of these diseases and the responsibilities of the workplace owners, operators and employees are identified [10, 11]. In a study conducted on sanitation and hygiene training for protecting and improving health, the necessity to train those who deal with food for the control and prevention of foodborne diseases was reported [12, 13].

People are affected by many stimulants around them from birth to death. Due to the constant change of conditions, education has a great share in adapting to the new conditions. That's why education needs to be continuous [14]. Considering that education is a dynamic process, the continuity of the training to be given to the person should also be taken into account in institutions where mass feeding is provided [15].

Although most of the employees in the food production and distribution sector are given hygiene training, it is seen that the knowledge of the people about food and personal hygiene is often not sufficient. For this reason, there is a need for studies to measure the level of knowledge about the hygiene knowledge level of the personnel working in mass feeding establishments. This study, it was aimed to investigate the level of knowledge of food hygiene and personal hygiene of the employees in the kitchens of the institutions in Diyarbakır.

2. MATERIAL AND METHODS

This study aims to evaluate the up-to-date knowledge level of 117 male and 33 female personnel working in hospital kitchens in Diyarbakır city center, which constitutes the population of the study, on food hygiene and safety, personal and personnel hygiene, equipment hygiene, and HACCP to determine the knowledge level of the personnel on food and personnel hygiene.

This study is descriptive and cross-sectional research and was carried out by the staff of food companies that provide food production and distribution services to three state hospitals in the central districts (Yenisehir, Sur) of Diyarbakir. In the selection of the study population, these districts were chosen as research regions because of the large number of institutional kitchens in these regions. It was determined that a total of 400 kitchen personnel were working. Volunteerism was taken as a basis in personnel selection. The participation of 150 (M+F) personnel was ensured. The formula given below was used to determine the sample volume.

$N.p.$q

n = $(N-1).(Z \propto 2 \setminus d)\ 2 + p.$q (1)

N: Research material (main mass)

n: Sample volume

Zα/2: Confidence coefficient

d: Sampling error

p: Incidence (probability) of the studied event

q: Frequency of the absence of the studied event (probability; 1-p)

When the formula was applied, the sample size was found to be 150. In the formula applied, 90% confidence coefficient and 20% margin of error were taken into account. The general rule applied in this type of sampling was accepted as (p) = (q) = 0.5. In this case, the largest possible sample volume was obtained with a fixed sampling error [16].

To test our hypotheses and meet the study objectives at the best possible level, the questionnaire was prepared by considering the issues stated by the experts in this field and the previous empirical studies.

The questions in the questionnaire form were created based on food hygiene, personnel hygiene and equipment hygiene [17, 18]. When the formula was applied, the sample size was found to be 150. In the formula applied, 90% confidence coefficient and 20% margin of error were taken into account. The general rule applied in this type of sampling was accepted as (p) = (q) = 0.5. In this case, the largest possible sample volume was obtained with a fixed sampling error [16].

To test the developed hypotheses and to realize the research objectives at the best possible level, the questionnaire questions were prepared by considering the issues stated by the experts in this field and the previous empirical studies. The questions in the questionnaire form were created by making use of food hygiene, personnel hygiene and equipment hygiene [17, 18]. A questionnaire consisting of 94 questions in which information about economic and social (demographic) characteristics, hygiene education, food hygiene and food safety, personal and personnel hygiene, equipment hygiene, and HACCP system were asked to be evaluated was applied. In the analysis, the correct answer was evaluated as 1 (one), the wrong answer as -1 (minus one) and “I don't know” as 0 (zero) points, and the triple Likert scale was used. The knowledge points of the participants in the study were obtained. By taking the average of their knowledge scores, those who are at or below the average score are deemed to have insufficient knowledge, and those with above-average scores are deemed to have sufficient knowledge. The results were evaluated in 2 groups as sufficient and insufficient knowledge levels [19]. The collected data were analyzed using the Statistical Package for Social Sciences (SPSS), version 24.0. In its statistical evaluation; percentage (%), frequency distribution (f), arithmetic mean, standard deviation, Pearson Chi-Square, Fisher's exact test and Chi-square statistical analysis were used to compare knowledge competencies with other variables. Results were evaluated at a 95% confidence interval and $p < 0.05$ significance level.

3. RESULTS AND DISCUSSION

78.0% of the participants are men and 22.0% are women. It was observed that 44.0% of the participants were between the ages of 31-40. Looking at the marital status of the participants, it is seen that the majority (75.3%) are married. Considering the distribution by educational status, it was seen that 12.0% of them were higher education graduates. Considering the distribution according to their titles, the largest group in the institutional kitchens is the other group with 47. 3%, while 12.7% are the chefs, 16.0% are the section chiefs and 4.7% are the master chefs. Considering the distribution by professional seniority, 58.0 % of them are between 1-5 years. Those with professional seniority over 10 years are 15.3% and those between 6-10 years are 26.7%. Considering the distribution of the participants according to their smoking status, it is seen that more than half (65.4%) of the kitchen workers of the institution do not smoke. The distribution of the average scores of the participants from the questionnaires and the hygiene knowledge sufficiency ratios according to the surveys are given in Table 1.

Table 1. Evaluating the scores of the participants from surveys

		n	%
Food hygiene and safety qualification	Sufficient	86	57.3
	Insufficient	64	42.7
Personal hygiene and staff hygiene qualification	Sufficient	70	46.7
	Insufficient	80	53.3
Equipment hygiene qualification	Sufficient	85	56.7
	Insufficient	65	43.3
HACCP system knowledge sufficiency	Sufficient	69	43.0
	Insufficient	81	57.0

When looking at the calculation made using the triple Likert scale of the participants, the hygiene score average is 32.6. Those below this average were considered insufficient, and those above this average were considered sufficient. During the evaluation, the total score they should get was evaluated as 100%, and other averages and percentage calculations were made. It was determined that food hygiene and safety knowledge of 56.4% of the personnel, personal hygiene and personnel hygiene knowledge of 38% of the personnel, equipment and tools hygiene knowledge of 41.8% of the personnel, and HACCP knowledge of 71% of the personnel were above the average level. When Table 1 is examined, food hygiene and safety sufficiency, personal hygiene and personnel hygiene sufficiency, equipment hygiene sufficiency scored above average. The distribution of food hygiene and safety sufficiency ratios according to the demographic characteristics of the participants is given in Table 2 in numbers and percentage values.

Table 2. Food hygiene and food safety sufficiency ratios according to the demographic characteristics of the participants

Demographic features		Food Hygiene and Food Safety				X^2	P
		Sufficient		Insufficient			
		N	%	n	%		
Gender	Male	68	58.1	49	41.9	0.134	0.714
	Female	18	54.5	15	45.5		
Age	Age 30 and under	20	54.1	17	45.9	1.183	0.553
	31-40 age	36	54.5	30	45.5		
	Over 40 years old	30	63.8	17	36.2		
Educational status	Literate	17	54.8	14	45.2	4.809	0.307
	primary school	17	56.7	13	43.3		
	middle School	19	46.3	22	53.7		
	High school	20	66.7	10	33.3		
	Higher education	13	72.2	5	27.8		
Type of employment	Full-time	80	58	58	42	0.287	0.592
	Part-time	6	50	6	50		
	Intern	2	100	-	-		
Title	Assistant Chef	14	51.9	13	48.1	6.341	0.256
	Chef	15	78.9	4	21.1		
	Section chief	12	50	12	50		
	Masterchef	3	42.9	4	57.1		
	Other	40	56.3	31	43.7		
Experience	1 year	15	57.7	11	42.3	1.854	0.603
	2-5 year	34	55.7	27	44.3		
	6-10 year	21	52.5	19	47.5		
	More than 10 years	16	69.6	7	30.4		
Where he/she learned his/her job	At school	7	100	-	-	6.513	0.080
	In a course	7	50	7	50		
	On-the-job training	56	57.7	41	42.3		
	Other	16	50	16	50		
Average working time per week	40 hours and less	57	60.6	37	39.4	1.124	0.289
	More than 40 hours	29	51.8	27	48.2		
Cooking profession certificate status	Yes	37	63.8	21	36.2	1.613	0.204
	No	49	53.3	43	46.7		
Average monthly income	Minimum wage and below	65	55.6	52	44.4	0.687	0.407
	More than the minimum wage	21	63.6	12	36.4		

In Table 2, when the distribution of food hygiene and safety competence results is examined according to the demographic characteristics of the participants, no statistically significant difference was found between the participants in the questionnaire ($p>0.05$).

The distribution of personal hygiene and personnel hygiene sufficiency ratios according to the demographic characteristics of the kitchen employees of the participating institution is given in Table 3 in numbers and percentage values.

Table 3: Personal hygiene and staff hygiene sufficiency ratios according to the demographic characteristics of the participants

Demographic features		**Personal Hygiene and Personnel Hygiene**				**X^2**	**P**
		Sufficient		**Insufficient**			
		n	**%**	**n**	**%**		
Gender	Male	52	44.4	65	55.6	1.055	0.304
	Female	18	54.5	15	45.5		
Age	Age 30 and under	18	48.6	19	51.4	6.020	**0.049***
	31-40 Age	24	36.4	42	63.6		
	Over 40 years old	28	59.6	19	40.4		
Educational status	Literate	15	48.4	16	51.6	5.610	0.230
	Primary school	9	30.0	21	70.0		
	Middle School	19	46.3	22	53.7		
	High school	18	60.0	12	40.0		
	Higher education	9	50.0	9	50.0		
Type of employment	Full-Time	68	49.3	70	50.7	4.717	**0.030***
	Part- Time	2	16.7	10	83.3		
	Intern	1	50.0	1	50.0		
Title	Assistant Chef	13	48.1	14	51.9	4.111	0.550
	Chef	5	26.3	14	73.7		
	Section chief	12	50.0	12	50.0		
	Masterchef	3	42.9	4	57.1		
	Other	36	50.7	35	49.3		
Experience	1 year	13	50.0	13	50.0	1.816	0.611
	2-5 year	25	41.0	36	59.0		
	6-10 year	19	47.5	21	52.5		
	More than 10 years	13	56.5	10	43.5		
Where he/she learned his/her job	At school	6	85.7	1	14.3	4.444	0.215
	the course	6	42.9	8	57.1		
	at the workplace next to the master	43	44.3	54	55.7		
	Other	15	46.9	17	53.1		

Average working time per week	40 hours and less	41	43.6	53	56.4	0.941	0.332
	More than 40 hours	29	51.8	27	48.2		
Cooking profession certificate status	Yes	27	46.6	31	53.4	0.001	0.982
	No	43	46.7	49	53.3		
Average monthly income	Minimum wage and below	54	46.2	63	53.8	0.056	0.813
	More than the minimum wage	16	48.5	17	51.5		

The distribution of personal hygiene and staff hygiene sufficiency ratios according to the demographic characteristics of the participants was examined; a statistically significant difference was found between the groups in terms of age and type of employment ($p<0.05$).

According to the demographic characteristics of the participants, the distribution of equipment hygiene qualification ratios is given in Table 4 in numbers and percentage values.

Table 4. Equipment hygiene qualification according to the demographic characteristics of the participants

Demographic features		**Equipment Hygiene**					
		Sufficient		**Insufficient**			
		n	**%**	**n**	**%**	**X^2**	**P**
Gender	Male	65	55.6	52	44.4	0.267	0.605
	Female	20	60.6	13	39.4		
Age	Age 30 and under	20	54.1	17	45.9	0.275	0.872
	31-40 years	37	56.1	29	43.9		
	Over 40 years old	28	59.6	19	40.4		
Educational status	Literate	16	51.6	15	48.4	3.866	0.424
	Primary school	14	46.7	16	53.3		
	Middle School	23	56.1	18	43.9		
	High school	19	63.3	11	36.7		
	Higher education	13	72.2	5	27.8		
Type of employment	Full-Time	78	56.5	60	43.5	0.015	0.903
	Part-Time	7	58.3	5	41.7		
	Intern	1	50.0	1	50.0		
Title	Assistant Chef.	15	55.6	12	44.4	4.757	0.446
	Chef	7	36.8	12	63.2		
	Section chief	13	54.2	11	45.8		
	masterchef	4	57.1	3	42.9		
	Other	45	63.4	26	36.6		
Experience	1 years	13	50.0	13	50.0	0.978	0.807
	2-5 years	36	59.0	25	41.0		

Where he/she learned his/her job	6-10 years	24	60.0	16	40.0	5.124	0.166
	More than 10 years	12	52.2	11	47.8		
	At school	5	71.4	2	28.6		
	the course	11	78.6	3	21.4		
	at the workplace next to the master	49	50.5	48	49.5		
	Other	20	62.5	12	37.5		
Average working time per week	40 hours and less	50	53.2	44	46.8	1.238	0.266
	More than 40 hours	35	62.5	21	37.5		
Cooking profession certificate status	Yes	32	55.2	26	44.8	0.086	0.769
	No	53	57.6	39	42.4		
Average monthly income	Minimum wage and below	63	53.8	54	46.2	1.723	0.189

When the data to find the questions sufficient according to the demographic characteristics of the participants according to the sufficiency of equipment hygiene, it was determined that there was no statistically significant difference between the groups (p>0.05).

The distribution of knowledge sufficiency ratios regarding the HACCP system according to the demographic characteristics of the participants is given in Table 5 in numbers and percentage values.

Table 5. Sufficiency of HACCP System knowledge according to the demographic characteristics of the participants

Demographic features		**HACCP System knowledge sufficiency**				**X^2**	**P**
		Sufficient		**Insufficient**			
		n	**%**	**n**	**%**		
Gender	Male	57	48.3	61	51.7	0.502	0.479
	Female	12	37.5	20	62.5		
Age	Age 30 and under	19	52.8	17	47.2	6.364	**0.042***
	31-40 years	35	47.9	38	52.1		
	Over 40 years old	11	26.8	30	73.2		
Educational status	Literate	11	37.9	18	62.1	3.640	0.457
	Primary school	12	40	18	60		
	Middle School	14	35.9	25	64.1		
	High school	19	52.7	17	47.3		
	Higher education	9	56.3	7	43.8		
Type of employment	Full-Time	61	44.2	78	55.8	0.212	0.758
	Part-Time	4	36.4	7	63.6		
Title	İntern	2	100	-	-	3.080	0.730
	Assistant Chef.	11	42.3	15	57.7		
	Chef	7	41.2	10	58.8		

	Section chief	8	34.8	15	65.2		
	masterchef	3	42.9	4	57.1		
	Other	32	45.0	39	55.0		
Experience	1 years	13	52	12	48	5.760	0.135
	2-5 years	29	47.5	32	52.5		
	6-10 years	19	43.1	25	56.9		
	More than 10 years	4	20	16	80		
Where he/she learned his/her job	At school	6	100	-	-	12.891	**0.004***
	the course	10	45.4	12	54.6		
	at the workplace next to the master	31	34.4	59	65.6		
	Other	18	56.3	14	43.8		
Average working time per week	40 hours and less	51	51.5	48	48.5	7.809	**0.005***
	More than 40 hours	14	27.5	37	72.5		
Cooking profession certificate status	Yes	28	48.2	30	51.8	0.958	0.328
	No	37	40.2	55	59.8		
Average monthly income	Minimum wage and below	51	43.5	66	56.5	0.037	0.847
	More than minimum wage	14	42.4	19	57.6		

When the distribution of HACCP System knowledge sufficiency ratios according to the demographic characteristics of the personnel is examined, a statistically significant difference was found between the groups in terms of age, where he learned his job and the average working time per week ($p<0.05$).

The ratio of women included in our study was found to be 22%. When examining the data, the findings were consistent with the findings of the studies of Berber (2008) and Eser (2017) who stated that Eastern and Southeastern regions of Turkey had the lowest woman employment rates [20, 21]. The low rate of woman employees compared to man employees can be explained by the fact that the women in these two regions are profoundly affected by the sociological and cultural factors of the society in which they live.

When the age distribution of the personnel working in the kitchens of the institutions was examined, it was found that 44% of the personnel were between the ages of 31-40, 24.7% were under 30 years old, and 31.3% were over 40 years old. It is thought that the accumulation of the largest age group between 31 and 40 is due to the demand for more experienced chefs and master chefs for quality products in the food industry.

When the survey data are analyzed according to the education level of the personnel, it was determined that 20.7% were literate, 20% were primary school, 27.3% were secondary school, 20% were high school graduates, and 12% were higher education graduates. Çakıroğlu et al. (2008) [22] found that 27.8% of the employed personnel were primary school graduates, 67.4% were secondary and high school graduates, and 4.8% were university graduates. The findings of this study about mass feeding personnel were similar to Çakıroğlu's findings.

When the professional seniority and hygiene knowledge level of the employees who participated in the survey were examined, the total hygiene, food and personal scores of employees with more than 10 years of work experience were found to be higher than those who

had less than 1 year of work experience. However, it was stated that the difference between them was not statistically significant ($p > 0.05$). When the job duration and food, personal, culinary and total hygiene knowledge scores of the individuals were examined, it was found that there was no statistically significant difference between the groups ($p > 0.05$). Although the difference between the employees participating in the survey is not found to be statistically significant, it has been stated that the knowledge of food safety and hygiene rules changes depending on the occupational seniority and working time of the personnel. In a study conducted by Bıyıklı (2011) [23], no statistically significant difference was found among the results of the data obtained from the food hygiene, personnel hygiene, kitchen hygiene, equipment hygiene, and total scores according to the professional experiences of the cooks participating in the study. ($p > 0.05$). In a study by Ulusoy et al. (2018) [24], the scores of employees with 3-6 years of work experience were found to be lower than those of employees with 2 years or less work experience ($p < 0.05$).

In hygiene, which is one of the vital issues in mass feeding systems, two issues come to the fore especially. The first of these is the health of the personnel working in food production and the cleanliness of the place where the food is made. The second is that the food is healthy and of good quality and preserved under appropriate conditions. Employees should have an understanding and awareness of personal cleanliness and hygiene and should be trained regularly. The continuity of this training should be monitored because continuous and effective training will help to eliminate the deficiencies [25, 26].

When the data about whether the personnel participating in the survey received hygiene training were analyzed, it was seen that 95.3% got training and 4.7% did not. It is important to receive training on the subject for employees in places where mass feeding is provided. In the study conducted by Clayton et al. (2002) [15] in England, they reported that even if the people received hygiene training, most of them did not practice hygiene rules. In a study conducted by Eksen et al. (2004) [27] in Muğla, it was reported that 75.6% of employees working in food production establishments did not receive hygiene training. In another study, it was found that 48% of some delicatessen and butchers in Istanbul did not receive hygiene training [28]. In addition, as a result of a study conducted by Babür (2007) [29] in Muğla, it was pointed out that there is a parallelism between the high ratio of personnel receiving hygiene training and the detection of good sanitation status. In a study conducted by Erçişli (2005) [30] to find out the knowledge of the personnel working in the institutions that produce and offer mass feeding in Konya, 44% of the personnel could not even define the concept of hygiene and this was associated with the insufficiency of the in-service training of these institutions.

It is important whether the personnel working in places where mass feeding is provided receive training or not. The ratios obtained in this study are similar to the ratios determined for staff working in hotel kitchens in studies conducted by Siau et al. (2015) and Abdul-Mutalip et al. (2012) in Malaysia [31, 32]. In these studies, it was seen that most of the personnel received hygiene training. The reason why the training ratio (58.4%) obtained by Demirel in mass feeding establishments in Istanbul is higher than the rate obtained by Siau et al. in Malaysia (27.8%) and the rate obtained in the study conducted by Baş et al. can be explained by the fact that the requirement of the personnel working in food establishments to receive hygiene training was made mandatory after the studies conducted by Baş et al. and Demirel [33, 34]. However, although it has become obligatory to receive hygiene training in institutions in Turkey from 2013 onwards [35], it was determined that among the personnel working in the institutions surveyed in this study, few people have not received this training yet (Table 2).

4. CONCLUSIONS

44% of the personnel participating in the survey are between the ages of 31-40. 78.0% of the personnel surveyed are men and 22.0% are women. It is seen that the majority of the employees (75.3%) participating in the survey are married. 20.7% of the personnel participating in the survey are literate, 20.0% are primary school graduates and 27.3% are secondary school graduates. These are followed by high school graduates with 20.0% and higher education graduates with 12.0%. The families of slightly more than half (54.7%) of the personnel consist of 4-6 people, while 27.3% of the personnel consist of 1-3, and 18.0% of the personnel consist of 6 and more people. While 65.3% of the employees participating in the survey have a nuclear family structure, it was determined that 27.3% have extended families and 7.3% have broken families. While the other staff (houseman, dishwasher, waiter, and cleaner) comprised 47.3% of the personnel participating in the survey, 12.7% were chefs, 18.0% were assistants, 16.0% were section chiefs and 4.7% of them were master chefs and 1.3% were interns. 40.7% of the personnel's professional seniority in the kitchen was between 2-5 years. Those with a seniority of 10 years or more in the kitchen were 15.3%, those between 6-10 years were 26.7% and those for 1 year were 17.3%. It has been observed that the weekly average working hours of 62.7% of kitchen personnel were 40 hours or less, and 37.3% of those were more than 40 hours. It is seen that 65.4% of the personnel do not smoke and 34.6% of the personnel smoke.

When the distribution of personal hygiene and personnel hygiene sufficiency ratios is examined according to the demographic characteristics of the personnel, a statistically significant difference was found between the age groups ($p<0.05$). In the analysis performed, it was determined that the difference in age groups was between cases "over 40" and "31-40 years old". It is seen that those under the age of 40 have a higher percentage of qualification in the HACCP information system than those over the age of 40. It was determined that most of those with insufficient knowledge (73.2%) were over 40 years old. While it is observed that the HACCP knowledge of those who work more than 40 hours a week is insufficient, it is seen that all of those who received HACCP knowledge at school have sufficient knowledge, others (such as who received it in a course or masters) have less knowledge. The reason for this can be that the hygiene education given at school is more instructive.

The necessary environment and facilities should be provided for the personnel to perform the hygiene training in the simplest manner and by using visual training tools according to their education levels. Dieticians or food engineers trained in this field should be included. When choosing dieticians or food engineers, priority should be given to those with formation training. While the training continue, the person should also be inspected during the production. It is necessary to make the hygiene practices of the personnel a habit, especially the concept of hand hygiene.

It has been observed that the level of knowledge of the personnel on hand hygiene and HACCP system is low. Attention should be paid to these hygiene problems and a realistic approach should be followed in solving these problems. Personnel should also be trained in the subjects they are lacking, and their progress should be checked by re-measuring or observing their hygiene knowledge level.

This section should summarize the main findings and also link to the recommendations. Previous findings in the discussion should not be repeated, the author's results in a broader context of other studies on the subject interpreting them with a minimum of speculation. The conclusion should integrate with the research findings of other studies to provide the readers with a broad base for understanding whether the hypotheses tested were accepted or rejected.

REFERENCES

[1] Kutluay, M.T., Birer, S. (1997). *Kurum Beslenmesi (5 baskı)*, Milli Eğitim Basımevi, Ankara.

[2] Sneed, J., Strohbehn, C.H. (2008). Trends Impacting Food Safety in Retail Foodservice: Implications for Dietetics Practice, *Journal of the American Dietetic Association,* 108: 1170–1177.

[3] Birer, S. (2002). Yemek Hazırlama, Pişirme ve Servisinde Dikkat Edilmesi Gereken Sağlık ve Temizlik Kuralları, *Turizmde Sağlık ve Beslenme Sorunları ve Çözümler Sempozyumu*, Alanya*,* 172-183.

[4] Demirci, M. (2005). *Beslenme. II. Baskı*, Onur Grafik, İstanbul.

[5] Merdol, T.K., Beyhan, Y., Ciğerim, N., Sağlam, F., Tayfur, F., Baş, M., Dağ, A. (2000). *Toplu beslenme yapılan kurumlarda çalışan personel için sanitasyon/hijyen eğitimi rehberi*, Hatiboğlu Yayınevi, Ankara.

[6] Bulduk, S. (2010). *Gıda ve personel hijyeni*, Detay Yayıncılık, Ankara.

[7] Ciğerim, N., Beyhan, Y., Çeliktaş, N. (1995). Ankara'da Yüksek Öğretim Kredi ve Yurtlar Kurumu'na Bağlı Yurt Mutfaklarında Hijyen Durumunun Değerlendirilmesi, *Beslenme ve Diyet Dergisi*, 24(2): 273-278.

[8] Oğur, S., Aksoy, A., Yılmaz, Z. (2017). Üniversite Öğrencilerinin Genetiği Değiştirilmiş Organizmalar ve Gıdalar Hakkındaki Bilgi Düzeyleri ve Tutumları: Bitlis Eren Üniversitesi Örneği, *Food and Health*, 3(3): 97-108.

[9] Internet: 5996 Sayılı Veteriner Hizmetleri, Bitki Sağlığı, Gıda ve Yem Kanunu. http://www.resmigazete.gov.tr/ Eskiler/2010/06/20100613-12.Htm. (Erişim Tarihi: 15.12.2015).

[10] Aksoy, A., Arıkan, F.B. (2016). Diş Hekimlerinin Bazı Bulaşıcı Hastalıklar (AIDS, Hepatit B, Tüberküloz, Grip, Kabakulak) Konusundaki Farkındalık ve Davranışları. *BEÜ Fen Bilimleri Dergisi*, 5(2): 113-122.

[11] Internet: Hijyen Eğitimi Yönetmeliği. http://www. Resmigazete. Gov.Tr/ Eskiler/ 2013/07/2013 0705-3. Htm. (Erişim Tarihi: 15.12.2015).

[12] Cevizci, S., Önal, A.E. (2009). Halk sağlığı açısından hijyen ve iyi üretim uygulamaları, *Türk Hijyen ve Deneysel Biyoloji Dergisi*, 66(2): 73-82.

[13] Angelillo, I.F., Viggiani, N.M., Rizzo, L., Bianco, A. (2000). Food handlers and foodborne diseases: knowledge, attitudes, and reported behavior in Italy, *Journal of Food Protection*, 63(3): 381-385.

[14] Elmacıoğlu, F., Dündar, C., Topbaş, M., Peşken, Y. (2000). Samsun İl Merkezindeki Hastane Mutfaklarının Hijyen Durumunun Değerlendirilmesi, *Türk Hijyen Ve Deneysel Biyoloji Dergisi*, 57(2):1-6.

[15] Clayton, D.A., Griffith, C.J., Price, P., Peters, A.C. (2002). Food handlers' beliefs and self-reported practices, *International Journal of Environmental Health Research*, 25-39.

[16] Köksal, Ş., Soysal, A., Ergör, G., Kaner, G. (2016). İzmir'de Sağlık Kurumlarına Yemek Üretim ve Dağıtım Hizmeti Veren Bir Firmada Çalışanların Gıda Hijyeni İle İlgili Bilgi Ve Davranışları, *Türk Hij.Den.Biyol. Derg.*, 73(2); 139-148.

[17] West, B., Wood, L., Harger, V.F. (1998). *Food Service in Institutions,* Millan Publishing, New York.

[18] Internet: WHO. Food Safety and Foodborne Illness, Fact sheet No.237, Reviewed March 2007. http://www.who.int/mediacentre/factsheets/fs237/en/print.html, (17.10.2007)

[19] Ulusoy, B.H., Çolakoğlu, N. (2018). What Do They Know About Food Safety? A Questionnaire Survey On Food Safety Knowledge of Kitchen Employees in İstanbul, *Food and Health*, 4(4): 283-292.

[20] Berber, M., Eser, B.Y. (2008). Türkiye'de Kadın İstihdamı: Ülke Ve Bölge Düzeyinde Sektörel Analiz, *ISGUC The Journal of Industrial Relations and Human Resources*, 10(2): 1-16.

[21] Özaydınlı, K. (2014). Toplumsal cinsiyet temelinde Türkiye'de kadın ve eğitim, *Sosyal Politika Çalışmaları Dergisi*, (33): 93-112.

[22] Çakıroğlu, F.P., Uçar, A. (2008). Employees Perception of Hygiene in The Catering Industry in Ankara (Turkey), *Food Control*, (19): 9-15.

[23] Bıyıklı, A.E. (2011). *Hastane Mutfaklarında Çalışan Aşçıların Gıda Güvenliği Bilgi ve Uygulamalarının Belirlenmesi: Konya İl Merkezi Örneği,* Yüksek Lisans Tezi, Selçuk Üniversitesi Sosyal Bilimleri Enstitüsü, Konya.

[24] Ulusoy, B.H., Çolakoğlu, N. (2018). What Do They Know About Food Safety? A Questionnaire Survey On Food Safety Knowledge of Kitchen Employees in İstanbul, *Food and Health*, 4(4): 283-292.

[25] Şanlıer, N., Hussein, A.T. (2008). Yiyecek- İçecek Hizmeti Veren Otel Mutfakları ve Personelinin Hijyen Yönünden Değerlendirilmesi: Ankara İli Örneği, *Kastamonu Eğitim Dergisi,* 6(2): 461-468.

[26] Şanlıer,, N., Türkmen, F. (2010). Perceptions of Hygiene among Staff Working in Food Companies, *Research Journal of Medical Sciences*, 4(3): 231-237.

[27] Eksen, M., Karadağ, N., Karakuş, A. (2004). Muğla merkez ilçe gıda işyerlerinde çalışanların el ve vücut hijyeni konusundaki bilgi düzeylerinin incelenmesi, *UGBD*, 1(1): 1-21.

[28] Özmen, S.A. (2009). *İstanbul'daki bazı kasapların, şarküterilerin ve marketlerin et satışreyonlarının hijyen durumunun belirlenmesi,* Yüksek Lisans Tezi, Namık Kemal Üniversitesi Fen Bilimleri Enstitüsü, Tekirdağ.

[29] Babür, T.E. (2007). *Muğla'da ki birinci sınıf tatil köylerinde çalışan mutfak personelinin aldıkları hizmet içi eğitimi ve mutfak hijyen durumunun değerlendirilmesi,* Yüksek Lisans Tezi, Selçuk Üniversitesi, Sosyal Bilimler Enstitüsü, Konya.

[30] Erçişli, S. (2005). *Konya'da tüketime hazır yemek üreten ve bunları sunan işletmelerde çalışanların hijyen bilgisinin belirlenmesi,* Yüksek Lisans Tezi, Selçuk Üniversitesi, Sosyal Bilimler Enstitüsü, Konya.

[31] Siau, A.M.F., Son, R., Mohhiddin, O., Toh, P.S., Chai, L.C. (2015). Food court hygiene assessment and food safety knowledge, attitudes and practices of food handlers in Putrajaya, *International Food Research Journal*, 22(5): 1843.

[32] Abdul-Mutalib, N.A., Abdul-Rashid, M.F., Mustafa, S., Amin-Nordin, S., Hamat, R.A., Osman, M. (2012). Knowledge, attitude and practices regarding food hygiene and sanitation of food handlers in Kuala Pilah, Malaysia, *Food Control*, 27(2): 289-293.

[33] Demirel, S. (2009). *Hazır yemek üretimi yapan işletmelerde çalışanların hijyen bilgi düzeylerinin belirlenmesi,* Yüksek Lisans Tezi, Namık Kemal Üniversitesi Fen Bilimleri Enstitüsü, Tekirdağ.

[34] Baş, M., Ersun, A.Ş., Kıvanç, G. (2006). The evaluation of food hygiene knowledge, attitudes, and practices of food handlers in food businesses in Turkey, *Food Control*, 17(4): 317-322.

[35] Anonim, 2013. *Hijyen eğitimi yönetmeliği*. Ankara: 5 Temmuz 2013 Tarih ve 28698 sayılı Resmi Gazete.

NATURENGS
MTU Journal of Engineering and Natural Sciences
https://dergipark.org.tr/tr/pub/naturengs
DOI: 10.46572/naturengs.1022735

Quantum Chemical Calculations on Fentanyl Used as Potent Analgesic

Sümeyya SERİN[1]*, Tuğba UTKU[2], Gülşen KAYA[3]

[1,2,3]Scientific and Technological Research Center, Inonu University, Malatya, Turkey

(**Received:** 12.11.2021; **Accepted:** 14.12.2021)

ABSTRACT: This current study dealt with the quantum chemical analysis of fentanyl compound, which is a potent synthetic analgesic. First of all, the geometry optimizations were carried out via Density Functional Theory (DFT) and Hartree-Fock (HF) methods in both the gas and the water phase. The B3LYP functional and the HF method were used with the 6-31G (d,p) and 6-31++G (d,p) basis sets. Computed structural parameters were compared with the data available in the literature and consistent results were obtained for all four different methodologies. Charge distributions of each atom of fentanyl were obtained by Mulliken and natural population analysis. Accompanied by calculated molecular descriptors, the results of frontier molecular orbital (FMO) analysis and natural bond orbital (NBO) analysis were reported. Finally, molecular electrostatic potential (MEP) analysis has been performed to estimate reactive sites for electrophilic and nucleophilic attacks. Total density, ESP, MEP, and contour maps were visualized at B3LYP/6-31++G (d,p) level of theory. Gaussian 16 and GaussView 6 software packages were used to carry out all these studies.

Keywords: Fentanyl, DFT, Atomic Charges, NBO, HOMO-LUMO

1. INTRODUCTION

Fentanyl (trade name Sublimaze, N-phenyl-N-[1-(2-phenylmethyl) piperidin-4-yl] propanamide), a synthetic phenylpiperidine belonging to the 4-anilinopiperidine series, was first synthesized in the late 1950s by Janssen Pharmaceutica® in Belgium [1]. It is used as a pain reliever during anesthesia and in the treatment of postoperative pain. By the World Health Organization (WHO) ranking, it is an analgesic in the 3rd degree among narcotic substances. Although its chemical structure is similar to pethidine, it is known to be about 80 times more effective and potent than meperidine, and about 80 times more effective than morphine, which is not a pethidine derivative. It is also a potent, synthetic, narcotic, analgesic opioid with fewer side effects [2, 3]. It began to be used in medical studies in the 1960s as an intravenous anesthetic under the trade name Sublimaze. Fentanyl's active ingredient, which is in the form of Fentanyl Citrate in the preparations, produces its analgesic effect by mimicking the effect of endogenous opioid neurotransmitters on specific receptors [3, 4].

Fentanyl, a basic amine with a pKa of 8.43, is an effective opioid because of its high lipophilicity and rapid and effective distribution. It can be administered to people in different ways such as intramuscular, intravenous, transdermal, transmucosal and respiration [5-7]. Although 1 ng/mL plasma concentration may cause respiratory depression according to individual characteristics, 1.5–2 ng/mL concentration provides good postoperative analgesia.

*Corresponding Author: sumeyya.alatas@inonu.edu.tr
ORCID number of authors: [1] 0000-0002-4637-1734, [2] 0000-0001-7034-2725, [3] 0000-0003-2537-8117

Its effect starts in 30-60 seconds and lasts 30-60 minutes. The maximum level of analgesic effect is achieved within 3–6 minutes. In repetitive and long-term applications, the duration of action is prolonged as the inactive tissues are saturated [8]. In addition, Fentanyl metabolites do not have significant pharmacological activity, so it is a therapeutically important drug substance. For this reason, various methods for the synthesis of fentanyl have emerged in the literature, and its molecular characterization has been explored using different experimental and theoretical methods [9-15]. In these studies, FT-IR, ^{1}H NMR, ^{13}C NMR, normal Raman (NR), surface-enhanced Raman spectroscopy (SERS) analyses of fentanyl were examined in detail.

Some physicochemical properties of a drug, such as pKa, lipophilicity, solubility, hydrogen bonding, and permeability, have a significant effect on its pharmacological activity, and therefore, a good understanding of these properties, their measurements and the agreement of their estimations are very important for a successful drug design [16]. In this context, it is highly advantageous to make use of quantum chemical descriptors. The 3D molecular descriptors characterize primarily properties that are bounded with the 3D conformation of the molecule. The main ones are descriptors such as chemical potential, chemical hardness, softness, molecular volume, electronegativity, and polar surface area. From this point of view, this study is aimed to examine the charge distribution analysis, frontier molecular orbital analysis, natural bond orbital analysis and molecular electrostatic surface properties of fentanyl using quantum chemical calculations.

2. COMPUTATIONAL METHODS

All geometry optimizations and frequency calculations of fentanyl were performed utilizing Gaussian 16 [17] and GaussView 6 software packages [18]. Computations were repeated in the water (ε=78.36) phase to investigate the solvent effect. No imaginary frequency was observed in any of the calculations made with Becke, three-parameter, Lee-Yang-Parr (B3LYP) and HF methods with two different basis sets that are 6-31G (d,p) and 6-31++G (d,p) [19-22]. In this way, the stability of the structure is verified. The SMD universal method (**S**olvent **M**odel based on **D**ensity), a parametrized self-consistent reaction field (SCRF) based solvation model developed by Truhlar and coworkers, has been used to obtain thermochemical parameters [23].

3. RESULTS AND DISCUSSION

3.1. Geometry optimization

The optimized molecular structure of fentanyl with the numbering and labeling scheme is represented in Figure 1. The optimized bond lengths and bond angles values that are calculated using B3LYP and HF methods with two different basis sets are given in Table 1 and Table 2. The theoretical values in the tables are accompanied by the experimental values. The experimental bond lengths and bond angles are obtained from reference [15]. Linear correlation coefficients (R^2) were calculated for each methodology to examine the strength of the relationship between theoretical structural parameters and experimental values. While it was seen that the R^2 value was around 0.92 for bond lengths, this value increased to 0.96 for bond angles. This situation shows that the theoretical and the experimental values are in good agreement.

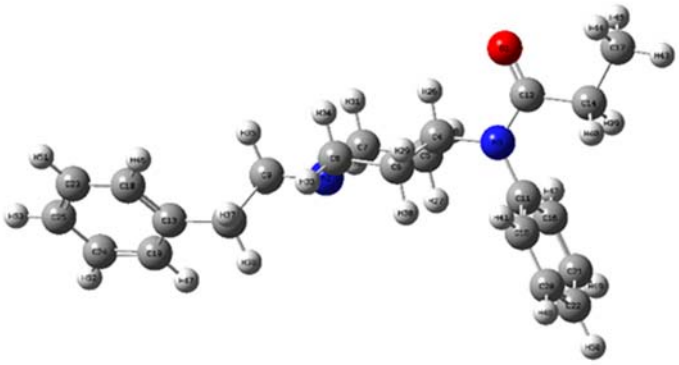

Figure 1. The optimized molecular structure of fentanyl

Table 1. Selected experimental and calculated bond length values of fentanyl

Bond Length (Å)	Exp.	B3LYP		HF	
		6-31G (d, p)	6-31++G (d, p)	6-31G (d, p)	6-31++G (d, p)
C24-C25	1.38	1.39	1.39	1.39	1.39
C25-C23	1.41	1.40	1.40	1.39	1.39
C24-C19	1.40	1.40	1.40	1.39	1.39
C19-C13	1.40	1.40	1.40	1.39	1.39
C13-C18	1.40	1.40	1.40	1.39	1.39
C13-C10	1.53	1.51	1.51	1.51	1.51
C18-C23	1.33	1.39	1.39	1.39	1.38
C9-N2	1.52	1.46	1.46	1.45	1.45
N2-C7	1.50	1.47	1.47	1.46	1.46
C8-C6	1.51	1.53	1.53	1.52	1.52
C6-C4	1.55	1.54	1.54	1.53	1.53
C4-C5	1.51	1.53	1.53	1.53	1.53
C4-N3	1.48	1.48	1.49	1.48	1.48
C5-C7	1.55	1.53	1.53	1.53	1.53
N3-C11	1.43	1.43	1.44	1.43	1.43
N3-C12	1.39	1.39	1.39	1.37	1.37
C11-C16	1.38	1.40	1.40	1.39	1.39
C15-C20	1.37	1.39	1.39	1.39	1.38
C20-C22	1.38	1.40	1.39	1.39	1.39
C21-C16	1.41	1.40	1.40	1.39	1.39
C12-O1	1.23	1.23	1.23	1.20	1.21
	R^2	**0.92**	**0.92**	**0.90**	**0.92**

Table 2. Selected experimental and calculated bond angle values of fentanyl

Bond Angle (°)	Exp.	B3LYP		HF	
		6-31G (d, p)	6-31++G (d, p)	6-31G (d, p)	6-31++G (d, p)
C23-C25-C24	118.9	119.5	119.5	119.4	119.4
C25-C23-C18	119.8	120.1	120.1	120.2	120.2
C23-C18-C13	120.3	120.9	121.0	121.0	121.0
C18-C13-C19	118.1	118.3	118.2	118.2	118.2
C18-C13-C10	119.0	120.9	121.0	120.9	120.9
C19-C13-C10	122.4	120.8	120.8	120.8	120.8
C13-C19-C24	121.7	121.0	121.0	121.0	121.0
C25-C24-C19	121.0	120.1	120.1	120.2	120.2
C13-C10-C9	110.6	111.9	112.0	111.9	112.0
C10-C9-N2	112.7	113.2	113.5	113.0	113.1
C9-N2-C8	110.6	112.8	112.8	113.0	113.0
C9-N2-C7	109.4	111.7	111.5	112.3	112.1
C8-N2-C7	110.2	110.3	110.5	110.9	110.9
N2-C8-C6	110.8	111.2	111.3	111.3	111.4
C8-C6-C4	110.9	110.5	110.5	109.9	110.0
C6-C4-C5	110.3	109.7	109.7	109.4	109.5
C5-C4-N3	112.8	113.1	113.1	112.9	112.9
C4-C5-C7	109.6	110.4	110.3	110.6	110.6
N2-C7-C5	109.4	111.1	111.4	111.0	111.2
C4-N3-C11	119.8	119.6	119.5	120.1	120.1
N3-C11-C15	119.8	120.4	120.4	120.1	120.2
C15-C11-C16	120.4	119.2	119.3	119.2	119.1
C11-C16-C21	118.9	120.3	120.3	120.4	120.4
C21-C22-C20	118.5	119.8	119.7	119.7	119.6
C22-C20-C15	119.9	120.2	120.1	120.1	120.1
C20-C15-C11	119.9	120.4	120.3	120.5	120.5
N3-C12-C14	117.8	116.9	117.0	117.6	117.7
	R^2	**0.96**	**0.96**	**0.95**	**0.95**

For each calculation level, the calculated thermodynamic parameters for not only the gas phase but also the water phase were tabulated. According to Table 3, the lowest total energy, enthalpy and Gibbs free energy values were obtained by using B3LYP/6-31++G(d,p) level of theory.

Table 3. Thermodynamic parameters of fentanyl calculated for each methodology (in Hartree)

	Gas Phase			Water Phase		
	ΔE_{Total}	**ΔH**	**ΔG**	**ΔE_{Total}**	**ΔH**	**ΔG**
B3LYP/6-31G(d,p)	-1039.989153	-1039.503861	-1039.586078	-1040.004146	-1039.518981	-1039.599860
B3LYP/6-31++G(d,p)	-1040.023219	-1039.538979	-1039.621841	-1040.042067	-1039.558099	-1039.639363
HF/6-31G(d,p)	-1033.231049	-1032.715185	-1032.793744	-1033.251792	-1032.736328	-1032.813857
HF/6-31++G(d,p)	-1033.253170	-1032.738158	-1032.816920	-1033.276390	-1032.761853	-1032.839734

3.2. Charge distribution analysis

Mulliken population analysis is one of the most widely used population analysis methods because it helps to determine atomic charges that affect the properties such as molecular polarizability, dipole moment, electronic structure of a particular molecule [24]. The results of the Mulliken population analysis through all the methodologies used in this study provide the total atomic charges of fentanyl. In addition, the results of natural population analysis [25] provide the natural charges of fentanyl. Mulliken and natural atomic charges calculated for both vacuum and water environments are listed in Table 4 and Table 5.

Table 4. Calculated Mulliken atomic charges of fentanyl

	B3LYP/6-31G (d, p)		B3LYP/6-31++G (d, p)		HF/6-31G (d, p)		HF/6-31++G (d, p)	
Atom	**Gas**	**Water**	**Gas**	**Water**	**Gas**	**Water**	**Gas**	**Water**
O1	-0.506137	-0.603495	-0.443960	-0.609848	-0.618134	-0.715916	-0.531865	-0.673607
N2	-0.436828	-0.459074	0.084116	-0.070023	-0.621626	-0.654513	-0.093399	-0.203193
N3	-0.535823	-0.536514	0.307839	0.502940	-0.789867	-0.781804	0.095556	0.151605
C4	0.069289	0.056932	-0.854872	-1.081967	0.099399	0.094953	-1.299758	-1.257451
C5	-0.187207	-0.186661	0.456119	0.484692	-0.219089	-0.217433	0.547768	0.519386
C6	-0.192398	-0.185543	0.305018	0.335853	-0.219075	-0.223426	0.389264	0.401574
C7	-0.031935	-0.036774	-0.502892	-0.622205	-0.013197	-0.019371	-0.232789	-0.170966
C8	-0.034510	-0.040100	-0.504425	-0.544000	-0.020464	-0.022746	-0.215059	-0.390232
C9	-0.004157	-0.011786	-0.776137	-0.958977	0.010071	0.008519	-0.406118	-0.681489
C10	-0.258487	-0.252722	-0.044888	0.022829	-0.237849	-0.226924	-0.056317	-0.021824
C11	0.185324	0.194622	-2.213747	-1.181195	0.200088	0.203863	-0.220998	-0.224546
C12	0.568671	0.594619	0.567311	0.851059	0.776280	0.805148	0.167876	0.398789
C13	0.109406	0.093517	0.333703	0.316035	-0.006812	-0.038387	0.866377	0.818180
C14	-0.265349	-0.272587	0.144041	0.042029	-0.319567	-0.324986	0.195443	0.067645
C15	-0.062260	-0.085761	0.265895	0.609133	-0.122140	-0.139708	0.114379	0.033195
C16	-0.064567	-0.085844	0.195609	0.542186	-0.124311	-0.141686	0.119856	0.103711
C17	-0.301701	-0.331080	-0.850957	-0.851367	-0.313305	-0.347106	-0.498632	-0.546349
C18	-0.109362	-0.144380	-0.244974	0.217621	-0.154645	-0.182544	-0.439361	-0.074407
C19	-0.122258	-0.144561	-0.528625	-0.497480	-0.165476	-0.183237	-0.697265	-0.594542
C20	-0.104666	-0.127008	-0.122862	-0.198435	-0.158702	-0.184583	-0.312041	-0.352425
C21	-0.105666	-0.126720	-0.133497	-0.158679	-0.159238	-0.186084	-0.322033	-0.407560
C22	-0.070444	-0.099686	-0.300435	-0.162166	-0.146307	-0.170991	-0.177491	-0.203227
C23	-0.092415	-0.115047	0.021849	-0.376652	-0.143746	-0.174552	-0.075556	-0.390819
C24	-0.088097	-0.114922	-0.094972	-0.228074	-0.142704	-0.174521	-0.165271	-0.284384
C25	-0.084660	-0.117932	-0.313338	-0.205820	-0.160198	-0.189763	-0.329749	-0.246711

Table 5. Calculated natural atomic charges of fentanyl

	B3LYP/6-31G (d, p)		B3LYP/6-31++G (d, p)		HF/6-31G (d, p)		HF/6-31++G (d, p)	
Atom	**Gas**	**Water**	**Gas**	**Water**	**Gas**	**Water**	**Gas**	**Water**
O1	-0.61872	-0.70723	-0.63097	-0.73266	-0.72792	-0.81380	-0.73221	-0.82651
N2	-0.51056	-0.52923	-0.55546	-0.57459	-0.57237	-0.59311	-0.61833	-0.63996
N3	-0.50392	-0.48258	-0.51775	-0.49269	-0.60496	-0.58109	-0.62534	-0.60026
C4	-0.06338	-0.06078	-0.07181	-0.07117	-0.02063	-0.01727	-0.02051	-0.01681
C5	-0.48151	-0.48573	-0.46221	-0.46609	-0.45444	-0.45386	-0.42629	-0.42768
C6	-0.47918	-0.48510	-0.45971	-0.46583	-0.45207	-0.45418	-0.42360	-0.42611
C7	-0.26174	-0.26454	-0.23978	-0.24374	-0.21182	-0.21157	-0.17987	-0.18138
C8	-0.26730	-0.26724	-0.24566	-0.24715	-0.21857	-0.21202	-0.18675	-0.18261
C9	-0.25608	-0.25321	-0.23653	-0.23586	-0.20475	-0.19835	-0.17537	-0.17199
C10	-0.47957	-0.48593	-0.46560	-0.47343	-0.44958	-0.45003	-0.42768	-0.43064
C11	0.13220	0.12554	0.13948	0.13423	0.14698	0.13858	0.15716	0.15023
C12	0.71063	0.73203	0.70605	0.73057	0.87570	0.90150	0.87183	0.90109
C13	-0.03017	-0.03667	-0.03516	-0.03955	-0.02589	-0.03505	-0.02755	-0.03508
C14	-0.55605	-0.55901	-0.53886	-0.54125	-0.53644	-0.53637	-0.51056	-0.51131
C15	-0.24420	-0.24380	-0.23902	-0.23749	-0.23668	-0.23045	-0.22932	-0.22268
C16	-0.24604	-0.24364	-0.24041	-0.23679	-0.23762	-0.23364	-0.22995	-0.22628
C17	-0.67916	-0.69278	-0.65411	-0.66695	-0.63919	-0.64865	-0.59876	-0.60810
C18	-0.24289	-0.24888	-0.24046	-0.24671	-0.24599	-0.24863	-0.24269	-0.24541
C19	-0.23667	-0.24818	-0.23510	-0.24624	-0.23964	-0.24827	-0.23746	-0.24511
C20	-0.22114	-0.24512	-0.22191	-0.24651	-0.21519	-0.24222	-0.21377	-0.24163
C21	-0.22016	-0.24504	-0.22095	-0.24648	-0.21434	-0.24213	-0.21294	-0.24130
C22	-0.24081	-0.24372	-0.23811	-0.24257	-0.23904	-0.23697	-0.23475	-0.23431
C23	-0.22470	-0.24821	-0.22322	-0.24845	-0.21075	-0.23639	-0.20641	-0.23392
C24	-0.22551	-0.24822	-0.22367	-0.24844	-0.21169	-0.23637	-0.20712	-0.23390
C25	-0.25019	-0.26061	-0.24999	-0.26169	-0.25405	-0.25979	-0.25333	-0.25997

Mulliken and Natural charge diagrams of fentanyl calculated at B3LYP/6-31G (d,p) level of theory are represented in Figure 2. When Table 4, 5, and Figure 2 are examined, it is observed that there is a general tendency in the same direction in both charge distributions for all 4 methodologies. While all hydrogen atoms are positively charged and oxygen atoms are negatively charged, differences are seen for carbon and nitrogen atoms. While the natural charges of N2 and N3 atoms are negative, positive values are also seen in Mulliken charges for B3LYP/6-31++G(d, p) and HF/6-31++G(d, p) methods.

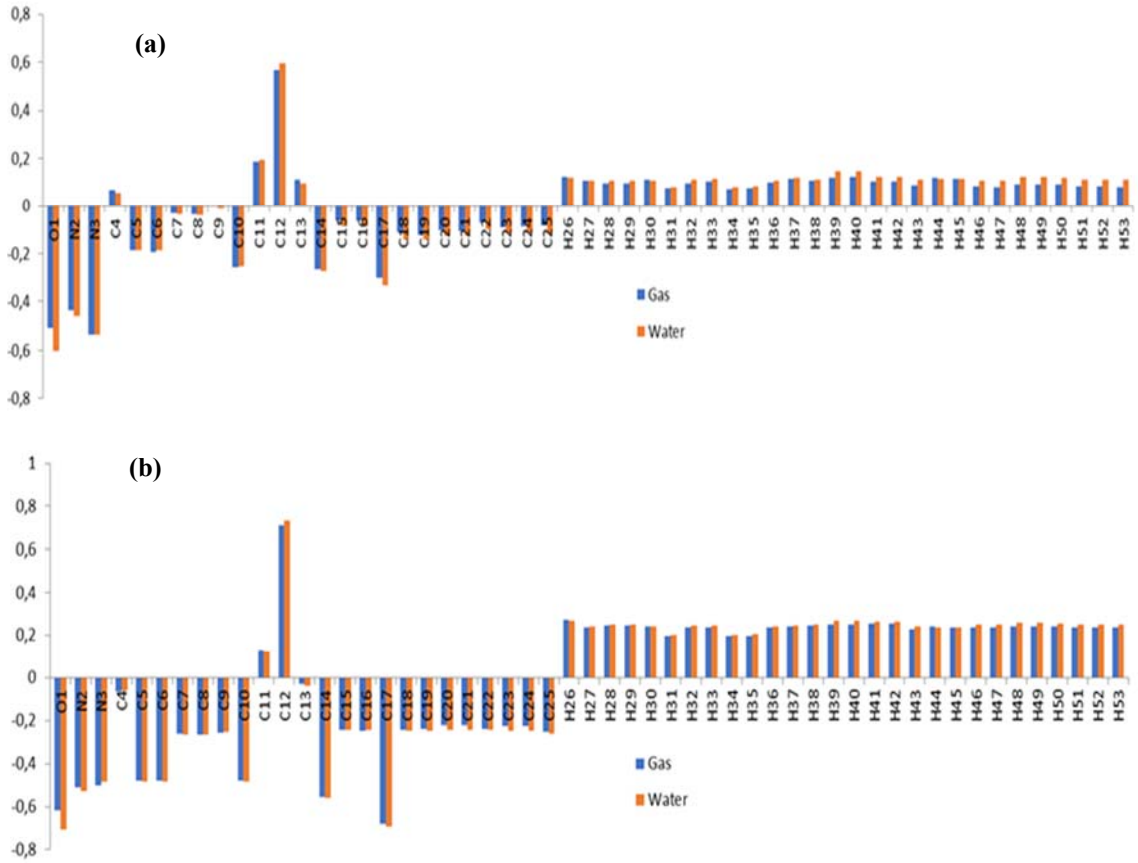

Figure 2. (a) Mulliken (b) Natural charge diagrams of fentanyl at B3LYP/6-31G (d,p) level of theory

3.3. Frontier molecular orbital (FMO) analysis

Frontier molecular orbitals, the highest occupied molecular orbital (HOMO) and the lowest unoccupied molecular orbital (LUMO), which have a crucial role in the electronic properties of a molecule, are the most critical orbitals in a molecule. While HOMO energy is related to electron-donating potential, LUMO energy is related to electron-accepting affinity [26]. The difference between the HOMO-LUMO energy values, also called the energy gap, is a significant parameter in determining the electrical properties of the molecule, as well as giving important information about its stability. The ΔE value expresses the energy required to transition from a stable ground state to an excited state. The higher the energy value, the higher the stability. Using the HOMO and LUMO energy values, some quantum chemical descriptors can also be calculated [27-29], which provide important information about the reactivity/bioactivity of a particular molecule [30-33]. The values obtained as a result of FMO analysis for fentanyl are summarized in Table 6. In Table 6, the highest ΔE values are obtained by using HF/6-31G (d, p) method and the values are equal to 12.2291 eV and 12.4770 for gas and water phases respectively. These high energy values point out the good stability of fentanyl. Also, chemical hardness, softness and energy gap values are notions related to each other. The highest chemical hardness value and the lowest softness value belong to again HF/6-31G (d, p) method.

Table 6. Calculated molecular descriptors for both gas and water phases in eV (S: eV^{-1})

	B3LYP/6-31G(d,p)		B3LYP/6-31++G(d,p)		HF/6-31G(d,p)		HF/6-31++G(d,p)	
	Gas	Water	Gas	Water	Gas	Water	Gas	Water
E_{HOMO}	-5.7797	-5.8320	-6.0535	-6.0673	-8.6921	-8.7602	-8.8502	-8.8728
E_{LUMO}	-0.4585	-0.2626	-0.9189	-0.6493	3.5369	3.7168	0.9336	1.2014
ΔE	5.3212	5.5694	5.1345	5.4181	12.2291	12.4770	9.7839	10.0742
Chemical Hardness (η)	2.6606	2.7847	2.5673	2.7090	6.1145	6.2385	4.8919	5.0371
Global Softness (S)	0.1879	0.1796	0.1948	0.1846	0.0818	0.0802	0.1022	0.0993
Chemical Potential (μ)	-3.1191	-3.0473	-3.4862	-3.3583	-2.5776	-2.5217	-3.9583	-3.8357
Electronegativity (χ)	3.1191	3.0473	3.4862	3.3583	2.5776	2.5217	3.9583	3.8357
Electrophilicity index (ω)	1.8283	1.6673	2.3670	2.0816	0.5433	0.5097	1.6014	1.4604

Molecular orbital energy level diagrams and HOMO-LUMO plots of fentanyl are displayed in Figure 3. It is clear that for both theory levels, HOMO orbitals are localized on the piperidine ring, while LUMO orbitals are localized on the aniline ring. The energy gap (ΔE) values calculated using the values obtained from the molecular orbital energy levels were found to be 5.32 eV and 5.13 eV for B3LYP/6-31G (d, p) and B3LYP/6-31++G (d, p) levels, respectively.

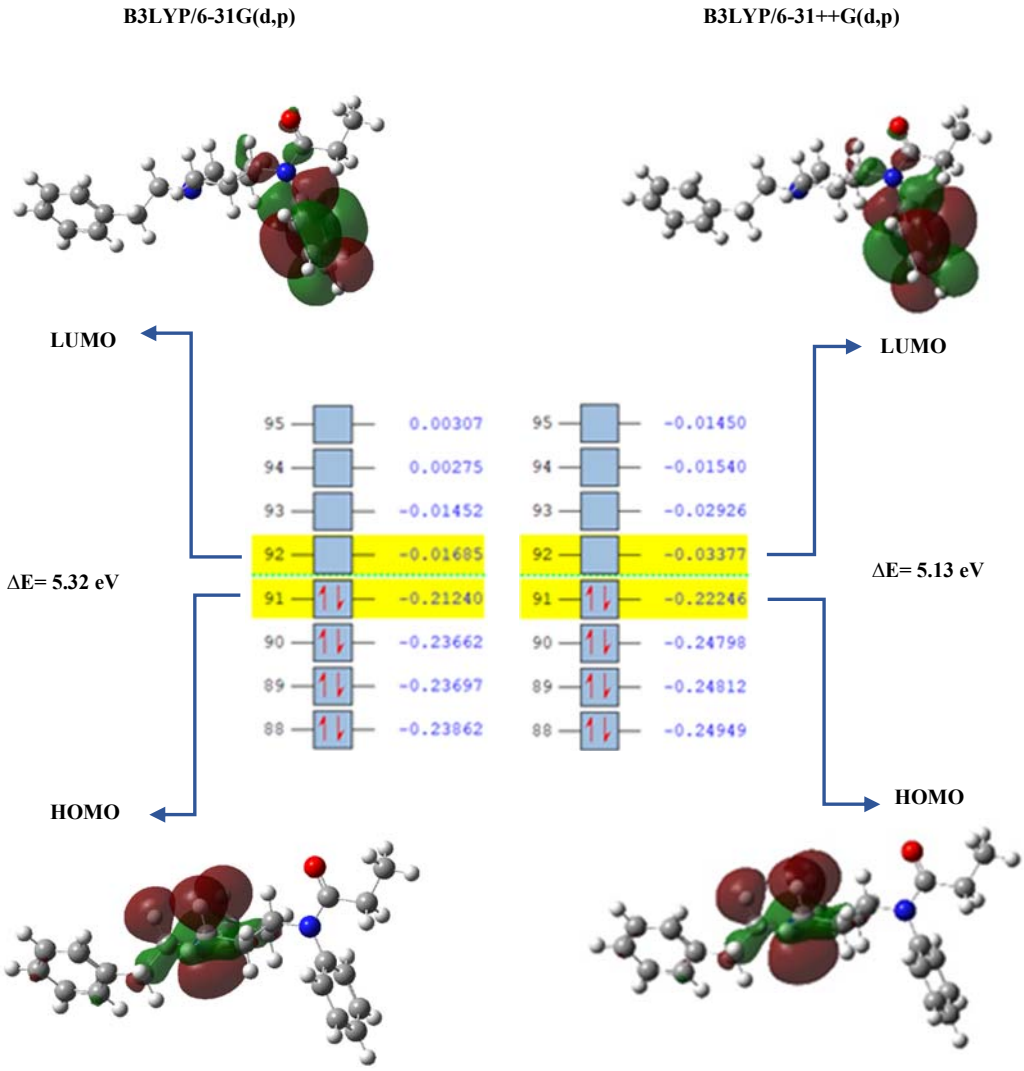

Figure 3. Molecular orbital energy diagrams and HOMO-LUMO plots of fentanyl

3.4. Natural Bond Orbital (NBO) analysis

The role of exchange transfer or intermolecular orbital interactions in a molecule can be figured out by NBO analysis. It is performed by regarding possible interactions between the whole donor (filled) and acceptor (empty) natural bond orbitals and anticipating their energetic importance with second-order perturbation theory [34, 35]. In this study, the calculated natural population analysis (NPA) and natural electronic configuration (NEC) of fentanyl at B3LYP/6-31++G (d, p) level are presented in Table 7. Moreover, the stabilization energy values calculated according to the formula (1) given below for the interactions between the donor and acceptor orbitals are shown in Table 8.

$$E^{(2)} = \Delta E_{ij} = qi\frac{(Fij)^2}{(\varepsilon j - \varepsilon i)} \quad (1)$$

The qi, εj and εi, Fij has shown in the formula represent donor bonding orbital occupancy, acceptor bond orbital energies and NBO Fock matrix element, respectively. NBO analysis of fentanyl shows that there are 11 interactions involving LP (1) N2, 10 interactions involving LP (1) N3, 3 interactions for LP (1) O1 and 6 interactions for LP (2) O1. The interactions that are important among these results are summarized in Table 8. According to Table 7, it is seen that the intramolecular charge transfer from LP (1) N3 donor to π*(O1-C12) acceptor orbital is calculated as 64.99 kcal mol^{-1}. Again, the most important ones among the π-π* interactions are shown in the table.

Table 7. Summary of NPA and NEC of fentanyl at B3LYP/6-31++G(d,p) level

	Natural Population				
Atom	**Core**	**Valence**	**Rydberg**	**Total**	**Natural Electron Configuration**
O1	1.99979	6.60980	0.02138	8.63097	[core]$2s^{1.70}2p^{4.91}3d^{0.02}$
N2	1.99945	5.52665	0.02936	7.55546	[core]$2s^{1.29}2p^{4.24}3s^{0.01}4p^{0.01}$
N3	1.99929	5.49479	0.02367	7.51775	[core]$2s^{1.21}2p^{4.29}4p^{0.02}$
C4	1.99918	4.04833	0.02430	6.07181	[core]$2s^{0.94}2p^{3.11}3d^{0.01}4p^{0.01}$
C5	1.99931	4.45013	0.01277	6.46221	[core]$2s^{1.03}2p^{3.42}4p^{0.01}$
C6	1.99932	4.44755	0.01285	6.45971	[core]$2s^{1.03}2p^{3.42}4p^{0.01}$
C7	1.99936	4.22455	0.01587	6.23978	[core]$2s^{1.01}2p^{3.21}4p^{0.01}$
C8	1.99935	4.23013	0.01618	6.24566	[core]$2s^{1.01}2p^{3.22}4p^{0.01}$
C9	1.99937	4.22069	0.01647	6.23653	[core]$2s^{1.01}2p^{3.21}4p^{0.01}$
C10	1.99929	4.45319	0.01312	6.46560	[core]$2s^{1.02}2p^{3.43}4p^{0.01}$
C11	1.99888	3.83748	0.02416	5.86052	[core]$2s^{0.84}2p^{3.00}4p^{0.01}$
C12	1.99938	3.25588	0.03869	5.29395	[core]$2s^{0.81}2p^{2.45}3d^{0.01}4p^{0.03}$
C13	1.99906	4.01854	0.01756	6.03516	[core]$2s^{0.88}2p^{3.13}4p^{0.01}$
C14	1.99926	4.53050	0.00910	6.53886	[core]$2s^{1.06}2p^{3.47}$
C15	1.99892	4.22493	0.01516	6.23902	[core]$2s^{0.96}2p^{3.27}4p^{0.01}$
C16	1.99892	4.22624	0.01525	6.24041	[core]$2s^{0.96}2p^{3.27}4p^{0.01}$
C17	1.99949	4.64556	0.00907	6.65411	[core]$2s^{1.09}2p^{3.55}$
C18	1.99901	4.22671	0.01473	6.24046	[core]$2s^{0.95}2p^{3.28}4p^{0.01}$
C19	1.99902	4.22105	0.01504	6.23510	[core]$2s^{0.95}2p^{3.27}4p^{0.01}$
C20	1.99915	4.20688	0.01588	6.22191	[core]$2s^{0.96}2p^{3.24}4p^{0.01}$
C21	1.99915	4.20593	0.01587	6.22095	[core]$2s^{0.96}2p^{3.24}4p^{0.01}$
C22	1.99914	4.22362	0.01535	6.23811	[core]$2s^{0.97}2p^{3.26}4p^{0.01}$
C23	1.99916	4.20742	0.01664	6.22322	[core]$2s^{0.96}2p^{3.24}4p^{0.01}$
C24	1.99915	4.20802	0.01650	6.22367	[core]$2s^{0.96}2p^{3.24}4p^{0.01}$
C25	1.99914	4.23484	0.01601	6.24999	[core]$2s^{0.96}2p^{3.27}4p^{0.01}$

Table 8. Second-order perturbation theory analysis of fentanyl at B3LYP/6-31++G (d, p) level in the gas phase

Donor(i)	Occupancy	Acceptor(j)	Occupancy	$E^{(2)}$ kcal/mol	E(j)-E(i)/a.u	F(i,j)/a.u
π C11-C15	1.66435	π* C16-C21	0.32505	20.27	0.28	0.068
		π* C20-C22	0.32841	19.58	0.28	0.067
π C13-C18	1.64875	π* C19-C24	0.33295	19.51	0.28	0.066
		π* C23-C25	0.33735	21.38	0.28	0.069
π C16-C21	1.65806	π* C11-C15	0.35643	20.65	0.28	0.068
		π* C20-C22	0.32841	20.11	0.28	0.067
π C19-C24	1.67111	π* C13-C18	0.34351	20.84	0.28	0.069
		π* C23-C25	0.33735	19.55	0.28	0.066
π C20-C22	1.65837	π* C11-C15	0.35643	20.80	0.28	0.068
		π* C16-C21	0.32505	20.09	0.28	0.067
π C23-C25	1.66588	π* C13-C18	0.34351	19.21	0.28	0.066
		π* C19-C24	0.33295	20.63	0.28	0.068
LP (2) O1	1.86241	σ* N3-C12	0.08361	25.55	0.69	0.121
		σ* C12-C14	0.06228	19.76	0.62	0.101
LP (1) N2	1.88258	σ* C7-H31	0.03430	7.54	0.70	0.066
		σ* C8-H34	0.03470	7.39	0.69	0.065
		σ* C9-H35	0.03222	7.48	0.70	0.066
LP (1) N3	1.69901	π* O1-C12	0.28965	64.99	0.26	0.117
		σ* C11-C15	0.02907	6.52	0.79	0.069
		σ* C11-C16	0.02892	6.39	0.79	0.068

3.5. Electrostatic surface properties

Three-dimensional shapes of the molecular electrostatic potential (MEP) surfaces that are also known as molecular electrostatic potential maps describe the 3D charge distributions within a molecule. These surfaces give a visual representation of variably charged regions of a molecule. The charge distribution information is used to determine the charge-dependent properties and the interaction of molecules with each other [36]. In the MEP map, the red region represents the electron-rich region with the lowest potential energy, while the blue region represents the electron-poor, positively charged region with the highest potential energy value. Total density, MEP, ESP, and contour maps obtained at B3LYP level with 6-31++G (d,p) as the basis set are displayed in Figure 4. According to the MEP map, it is seen that the negative potential is clearly around the O1 atom. In addition, regions with positive potential are predominantly located on C-H bonds.

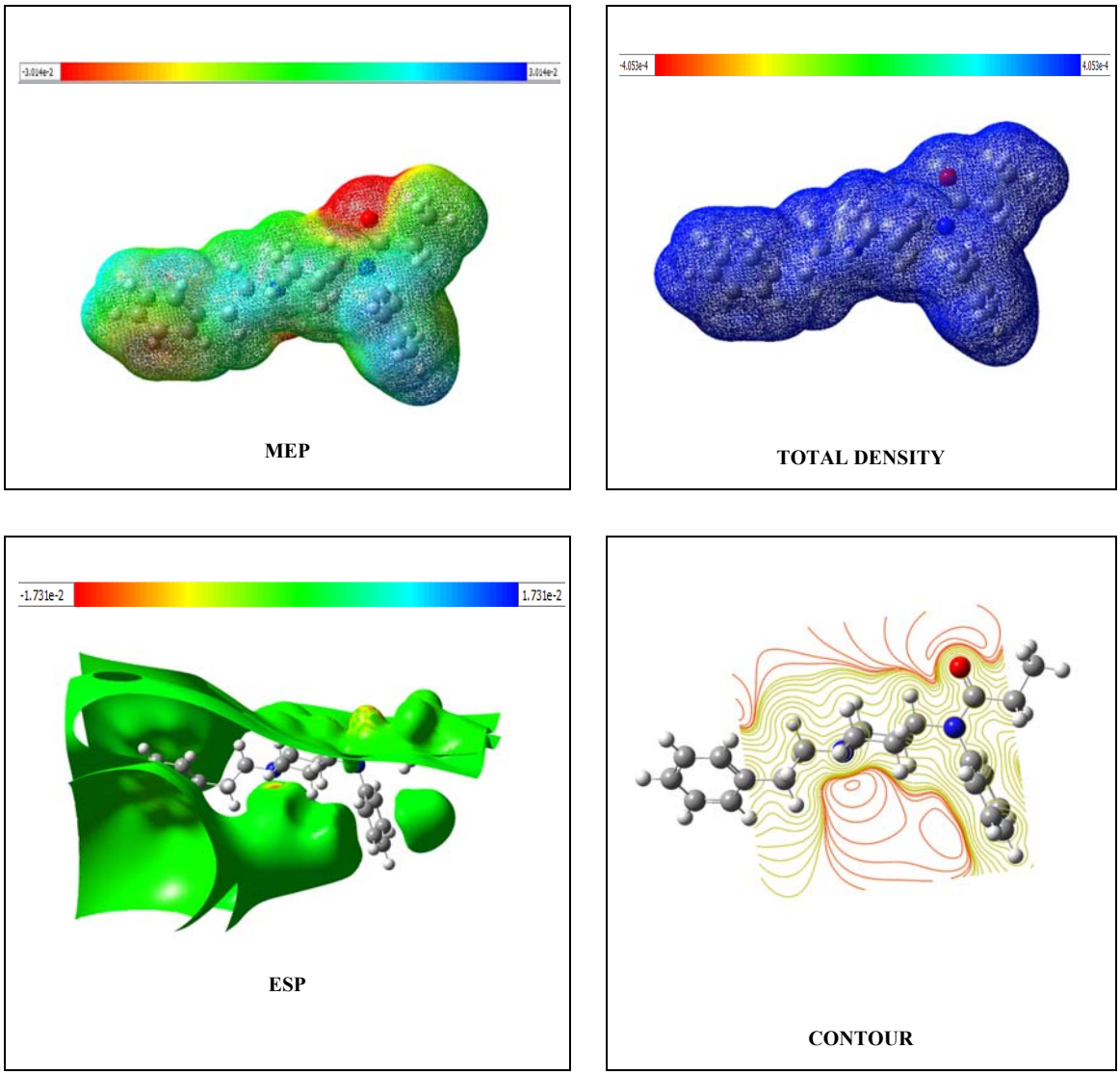

Figure 4. Molecular surfaces calculated at B3LYP/6-31++G (d, p) level of theory

4. CONCLUSIONS

It is known that the physicochemical properties of drugs affect their bioactivity. These physicochemical properties differ according to the changes in their chemical structures. The spatial arrangement of the drug molecule and how it interacts with the target determines the pharmacological activity of the drug. In the light of this information, it is a highly advantageous approach to obtain information about the relevant physicochemical properties by using computational chemistry methods to interpret the pharmacokinetic properties of a drug candidate while it is still in the design phase.

As a result, quantum chemical analysis was performed for fentanyl, a potent synthetic analgesic. Calculations were repeated for the water environment, as its behavior in the solvent environment is also important. Values compatible with the literature were obtained for bond angle and bond length. The lowest total energy, enthalpy and Gibbs free energy values from the calculated thermodynamic parameters were observed at B3LYP/6-31++G(d,p) level. Outputs of Mulliken population analysis, natural population analysis, and frontier molecular orbital

analysis are presented both as tables and diagrams. Quantum chemical descriptors were calculated from the HOMO and LUMO energy values. The energy gap, hardness and softness values that provide predictions about the reactivity of the molecule show that the compound is stable. The highest ΔE and hardness value with the lowest softness value were obtained by HF/6-31G (d, p) method. Intermolecular orbital interactions of fentanyl were figured out by NBO analysis. It was determined that the intramolecular charge transfer from LP (1) N3 donor to π*(O1-C12) acceptor orbital, which was calculated as 64.99 kcal mol^{-1}, was the strongest interaction. According to the MEP analysis, it is observed that the negative potential is clearly around the O1 atom. In addition, regions with positive potential are predominantly located on C-H bonds.

Acknowledgments

The numerical calculations reported in this paper were fully/partially performed at TUBITAK ULAKBIM, High Performance and Grid Computing Center (TRUBA resources).

REFERENCES

[1] Smialek, J.E., Levine, B., Chin, L., Wu, S.C., Jenkins, A. J. (1994). A Fentanyl Epidemic in Maryland, *J.Forensic Sci.,* 39(1): 159-164.

[2] Morgan, E.G., Mikhail, M.S., Murray, M.J., Larson, C.P. (2002). *Clinical Anesthesiology*, Mc Graw Hill Co., New York.

[3] Stanley, T.H. (1992). The History and Development of The Fentanyl Series, *J.Pain Sympt. Manage*, (7):3-7.

[4] Payne, R., Coluzzi, P., Hart, L., et al. (2001). Long-term Safety of Oral Ttransmucosal Fentanyl Citrate for Breakthrough Cancer Pain, *J. Pain Symptom Manage*. 22(1): 575–583.

[5] Kathe, K., Kathpalia, H. (2017). Film Forming Systems for Topical and Transdermal Drug Delivery, *Asian J. Pharm. Sci.,* 12(6): 487–497.

[6] Zeppetella, G. (2000). An Assessment of the Safety, Efficacy, and Acceptability of Intranasal Fentanyl Citrate in the Management of Cancer-Related Breakthrough Pain: A Pilot Study, *J.Pain Sympt. Man.* 20(4): 253–258.

[7] Mandel, L., Carunchio, M. J. (2011). Rampant Caries From Oral Transmucosal Fentanyl Citrate Lozenge Abuse. *J. Am. Dent. Assoc*., 142(4): 406–409.

[8] Ronald, D.M. (2010). *Miller's Anesthesia, Seventh Edition*, Livingstone Elsevier, Churchill.

[9] Suh, Y. G., Cho, K. H., Shin, D. Y., (1998). Total Synthesis of Fentanyl, *Arch. Pharmacol. Res*.,21(1): 70-72.

[10] Zee, S. H., Wang, W. K., (1980). A New Process for the Synthesis of Fentanyl, *J. Chin. Chem. Soc*., 27(4): 147-149.

[11] Gupta, P. K., Ganesan, K., Pande, A, Malhotra, R. C. (2005). A Convenient One Pot Synthesis of Fentanyl *J. Chem. Res.* 452-453.

[12] Asadi, Z., Esrafili, M.D., Vessally, E., Asnaashariisfahani, M., Yahyaei, S., Khani, A. (2017). A structural study of fentanyl by DFT calculations, NMR and IR spectroscopy, *J. Mol. Struct.,* (1128): 552-562.

[13] Leonardi, J., Haddad, A., Green, O., Birke, R. L., Kubic, T., Kocak, A., Lombardi, J.L. (2017). SERS, Raman, and DFT analyses of fentanyl and carfentanil: Toward detection of trace samples, *J Raman Spectrosc*., 48: 1323–1329.

[14] Wang, C.H., Terracciano, A.C., Masunov, A.E., Xu, M., Vasu, S.S. (2021). Accurate prediction of terahertz spectra of molecular crystals of fentanyl and its analogs, *Scientific Reports*, 11: 40-62.

[15] Peeters, O.M., Blaton, N.M., De Ranter, C.J., Van Herk, A.M., Goubitz, K. (1979). Crystal and molecular structure of N-[1-(2-phenylethyl)-4-piperidinylium]-N-phenylpropanamide (fentanyl) citrate-toluene solvate, *J. Cryst. and Mol. Struct*., 9(3).

[16] Ergül, M., Sayın, K., Ataseven, H. (2021). 2-Phenylethyne-1-Sulfonamide Derivatives as New Drugs Candidates for Heat Shock Protein 70 and Doublecortin-like Kinase, *Turkish Comp. Theo. Chem. (TC&TC),* 5(1): 1-12.

[17] Frisch, M.J., Trucks, G.W., Schlegel, H.B., Scuseria, G.E., Robb, M.A., Cheeseman., J.R., Scalmani, G., Barone, V., Petersson, G.A., Nakatsuji, H., et.al. (2016). *Gaussian 16 Rev. B.01*, Wallingford, CT.

[18] Dennington, R., Keith, T.A., Millam, J.M. (2016). *Gauss View, Version 6*, Semichem Inc., Shawnee Mission.

[19] Becke, A.D. (1993). A new mixing of Hartree–Fock and local density functional theories. *J. Chem. Phys.,* 98: 1372–1377.

[20] Lee, C., Yang, W., Parr, R. G. (1988). Development of the Colle-Salvetti correlation-energy formula into a functional of the electron density, *Physical Review B*., 37: 785–789.

[21] Becke, A.D. (1993). Density-Functional Thermochemistry. III. The role of exact exchange, *J. Chem. Phys.,* 98: 5648–5652.

[22] Roothaan, C. C. J. (1951). New Developments in Molecular Orbital Theory, *Rev. Mod. Phys*., 23: 69-89.

[23] Marenich, A. V., Cramer, C. J. and Truhlar, D. G. (2009). Universal Solvation Model Based on Solute Electron Density and on a Continuum Model of the Solvent Defined by the Bulk Dielectric Constant and Atomic Surface Tensions *J. Phys. Chem. B.,* 113(18): 6378-6396.

[24] Mulliken, R. S. (1955). Electron Population Analysis 0n LCAO-MO Molecular Wave Functions, *J Chem Phys*., 1833-1841.

[25] Reed, A. E., Weinstock, R. B., Weinhold, F. (1985). Natural Population Analysis, *J. Chem. Phys*., 83: 735−746.

[26] Fukui, K. (1982). The Role of Frontier Orbitals in chemical reactions, *Science*, 218: 747–754.

[27] Parr, R. G., Pearson, R. G., (1983). Absolute hardness: companion parameter to absolute electronegativity, *J. Am. Chem. Soc.,* 105(26): 7512–7516.

[28] Parr, R. G., (1986). Absolute electronegativity and hardness correlated with molecular orbital theory, *Proc. Natl. Acad. Sci.,* 83(22): 8440-8441.

[29] Parr, R. G., Szentpály L.V., Liu, S. (1999). Electrophilicity index, *J. Am. Chem. Soc.,* 121: 1922 – 1924.

[30] Serdaroğlu, G. and Elik, M. (2018). A Computational study predicting the chemical reactivity behavior of 1-substituted 9-ethyl-βCCM derivatives: DFT- Based Quantum Chemical Descriptors, *Turkish Comp. Theo. Chem. (TC&TC),* 2(1): 1-11.

[31] Sayin, K. and Üngördü, A. (2019). Investigations of structural, spectral and electronic properties of enrofloxacin and boron complexes via quantum chemical calculation and molecular docking, *Spectrochimica Acta Part A: Molecular and Biomolecular Spectroscopy*, 220: 117102.

[32] Serdaroğlu, G. and Ortiz, J. V. (2017). Ab Initio Calculations on some Antiepileptic Drugs such as Phenytoin, Phenobarbital, Ethosuximide and Carbamazepine., *Struct. Chem.,* 28: 957-964.

[33] Üngördü, A. and Sayin, K. (2019). Quantum chemical calculations on sparfloxacin and boron complexes, *Chemical Physics Letters*, 733: 136677.

[34] Weinhold, F., Landis, C. R. and Glendening, E. D. (2016). What is NBO analysis and how is it useful? *Int. Rev. Phys. Chem*., 35(3): 399-440.

[35] Reed, A. E., Curtiss, L. A. and Weinhold, F. (1988). Intermolecular Interactions from a Natural Bond Orbital, Donor-Acceptor Viewpoint. *Chem. Rev.,* 88(6): 899-926.

[36] Murray, J. S. and Politzer, P. (2011). The electrostatic potential: an overview, WIREs Comput. *Mol. Sci.,* 1: 153-322.

NATURENGS
MTU Journal of Engineering and Natural Sciences
https://dergipark.org.tr/tr/pub/naturengs
DOI: 10.46572/naturengs.1009013

Random Number Generator Based on Discrete Cosine Transform Based Lossy Picture Compression

Selman YAKUT[1*]

[1]Department of Computer Engineering, Faculty of Engineering and Natural Sciences, Malatya Turgut Özal University, Malatya, Turkey.

(**Received:** 13.10.2021; **Accepted:** 30.11.2021)

ABSTRACT: The widespread digitalization make the security of digital systems more important. Various cryptographic systems are used to ensure the security of the systems. An important part of the system is random numbers. In the article, a random number generator based on the discrete cosine transform, which is the basis of image compression algorithms, is proposed. In this generator, the difference between the original image and the compressed image produced using the discrete cosine transform is used. The original picture is transferred to the frequency domain by using the discrete cosine transform. Then, it is converted back to the space domain by using the inverse discrete cosine transform. These transformations cause some losses as certain coefficients are taken into account. Raw random numbers were generated using the differences between the original image and the compressed image. Then, the possible weaknesses in the generated random numbers were removed by passing these raw data through the hash function. The SHA-512 algorithm was used as the hash function. An important advantage of the developed system is that it can be easily implemented. The safety of generated random numbers is demonstrated by the successful result of NIST and correlation tests. In addition, the security parameters of the proposed method are shown in the discussion section.

Keywords: Discrete cosine transform, Image compression, Random numbers, Hash functions.

1. INTRODUCTION

Today, digital devices are widely used day by day. The use of the devices such as smartphones, tablets, and computers is indispensable in many areas [1]. Cyberattacks, on the other hand, abuse the weak sides of these digital devices [2]. Many cryptographic systems and protocols are used to avoid this weakness [3-5]. These systems ensure the security of both data sources and data. The basis of these systems is usually based on secret and secure parameters such as key and seed value [3]. For the security of the systems, it is important to produce these values from reliable sources [4]. Random number generators produce secure random numbers, which is the most important parameter that affects the security of these systems and data [3].

Random numbers are the most important part of many cryptographic applications [6]. Private-public key pair, secret key, seed value are among them. Since this value has critical importance on the whole system, it is important to produce them. In addition, there are security parameters that random numbers must provide to be used in cryptographic systems. These parameters are

*Corresponding Author: selman.yakut@ozal.edu.tr
ORCID number of authors: [1] 0000-0002-0649-1993

expressed as R1-R4 and guarantee the safety of the numbers used. R1-R4 parameters are briefly described in Table 1.

Table 1. The security requirements for secure random number generators

R1:	Random numbers should not contain any statistical weaknesses
R2:	Knowing the subsequences of random numbers should not allow the calculation or prediction of the preceding and succeeding random numbers
R3:	It should not be possible to compute the previous random numbers with the possibility of prediction when the internal state value is known, or even if the internal state value is unknown
R4:	It should not be possible to compute the next random numbers with the possibility of prediction when the internal state value is known, or even if the internal state value is unknown

Various methods and sources are used for random number generation. However, random number generators are divided into three sub-classes: true random number generators (TRNG), pseudo-random number generators (SRSU), and hybrid random number generators (HRNG). TRNG generators use physical and non-repeatable sources such as electronic noise and radioactive decay [7]. PRNG are generators based on some calculations which use a specific algorithm and seed value [8-10]. HRNG, on the other hand, is an approach based on the use of these two approaches together [11].

Many post-processing algorithms are used to eliminate possible weaknesses in random numbers generators [6]. Post-processing algorithms are widely used to make the generator more secure [12-16]. There are many post-processing algorithms in the literature [13-15]. Cryptographic hash algorithms are widely used as post-processing algorithms in random number generation [15]. The important reason for this is that these algorithms are resistant to collisions and are one-way functions. In addition, these algorithms produce data with a uniform distribution and strong statistical properties [16].

Data generated from digital data sources are subjected to compression processes to reduce the data load in transmission and storage processes. Compression is divided into two classes such as lossy and lossless compression [17-18]. Lossless compression is that the original image is compressed without any loss of the image. On the other hand, Lossy compression causes some loss on the original image and the original image does not reproduce. The most widely used method of lossy compression is to compress the original image by converting it to the frequency domain. Discrete cosine transform, which is used in many algorithms such as JPEG, is an important transform method.

Discrete cosine transform is a widely used method in data compression [19-22]. In the method, data is first converted into the frequency domain. Then, in the frequency domain, some coefficients that take into account the human visual sense are kept, while some coefficients are not taken into account [23]. Thus, significant compression of the data is done by using a series of processes that are not noticed or barely noticed by the human eye [24]. When converted to this compressed image, the original image does not reproduce because of some loss [19-22].

In the study, a random number generator based on the discrete cosine transform, which is the basis of image compression algorithms, is proposed. Random numbers are generated by using the difference values between the original image and the compressed image using the discrete cosine transform. These numbers are passed through cryptographic hash algorithms, ensuring that they have a uniform distribution and become safe. It can be used as a random number generator in many digital applications with the proposed method. In addition, it is shown that generated random numbers are safe by statistical tests.

The rest of this paper is organized as follows: In the second part, the structure of the proposed method, the entropy source used, and the operations performed were examined. In the next section, the safety evaluation of the numbers produced and the method used were made. The last section contains the results.

2. MATERIAL AND METHODS

In the study, secure random numbers, which are an important part of many applications, are generated. The proposed approach is given in Figure 1. Firstly, the original picture is transformed into the frequency domain by using the DCT. Then, the data in the frequency domain is transformed back to the space domain by going through IDCT and the compressed image obtained. The compressed image is subtracted from the original image and the difference matrix is obtained. Then, raw random numbers are produced by converting the data in each row and column in this matrix to binary number format. Then, these raw data are passed through the cryptographic hash algorithm and possible correlations and weaknesses are removed.

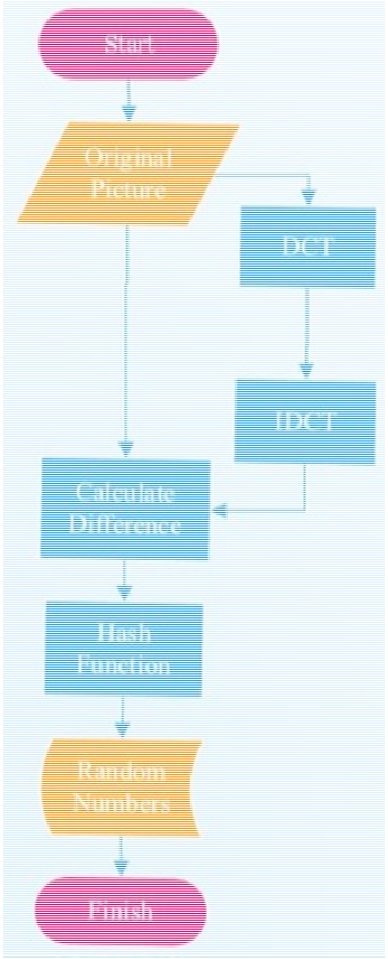

Figure 1. The general structure of the proposed method

DCT is a Fourier-based method that converts data from the space domain to the frequency domain. In the method, original data is represented with fewer coefficients without any significant difference in terms of human visual psychology. In the method, compressed data is created by giving some losses from the original data. First, the original data is transferred to the frequency domain by DCT transform. The data transferred to this domain is expressed by the

coefficient matrix. Some values of this coefficient matrix are preserved by considering human visual psychology and some values are neglected. Then, the data in the frequency domain is transferred to the space domain by using the IDCT transform, and compressed data is obtained. The difference between the original and the compressed image is taken as an entropy source.

A random number generator is designed by using the difference between the original data and the compressed data as an entropy source. Firstly, the original image pixel value is subtracted from the compressed image pixel value and the difference matrix is calculated. Then these difference matrix values are taken as positive and converted to binary. A binary bit sequence is converted to binary and added in a row. Finally, these binary bit string values are given as input to the hash algorithm and random numbers are generated.

Transferring images from the space domain to the frequency domain is widely used in steganography techniques. Many transformations are used for this transfer process. DCT is one of the commonly used transformations based on mathematical operations. The formulas used for DCT and IDCT transformations are given in Eq. (1), Eq. (3) respectively. First of all, transformation matrices were produced using the equations. Using these matrices, transformations are made from the space domain to the frequency domain.

$$C(u,v) = \mathrm{a(u)a(v)} \sum_{x=0}^{N-1} \sum_{y=1}^{N_1} f(x,y) \left(a_n \cos \frac{(2x+1)\pi x}{2N} + b_n \sin \frac{(2y+1)\pi x}{2N} \right) \quad (1)$$

Here the values of *a(u)* and *a(v)* are prepared Eq. (2)

$$a(k) = \begin{cases} \sqrt{\frac{1}{N}} & k = 0 \; ise \\ \sqrt{\frac{2}{N}} & k \neq 0 \; ise \end{cases} \quad (2)$$

The inverse discrete cosine transform is performed as shown in Eq. (3). IDCT transfers input images or data from the frequency domain to the space domain. With this inverse transformation, the data is compressed. Compressing is done without significant visual differences between the compressed data and the original data.

$$C(u,v) = \mathrm{a(u)a(v)} \sum_{x=0}^{N-1} \sum_{y=1}^{N_1} f(x,y) \left(a_n \cos \frac{(2x+1)\pi x}{2N} + b_n \sin \frac{(2y+1)\pi x}{2N} \right) \quad (3)$$

Potential weaknesses in these numbers are removed by using hash functions in the designed generator. The SHA-512 function, which is used in many applications and has a secure structure, is used as a cryptographic hash function [25]. These functions extract a summary of a given message, which can be expressed as a fingerprint. During this process, both data are compressed and passed through some logical and algebraic operations. With the help of these

processes, possible weaknesses in these data are removed and safe summary values are produced. The general structure of these functions is given in Figure 2.

By using the structure of hash functions as in Figure 3, random numbers larger than the hash value are generated. The hash value taken at each step is used to generate random numbers and to calculate new data.

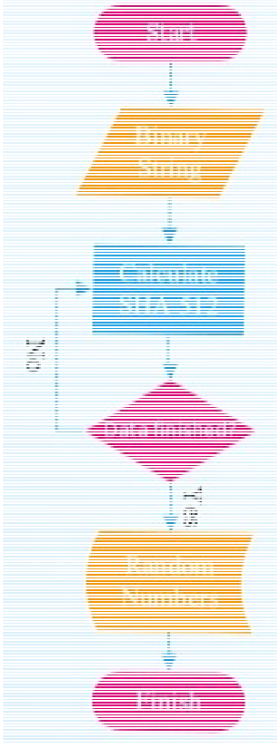

Figure 2. The post-processing structure of the proposed method

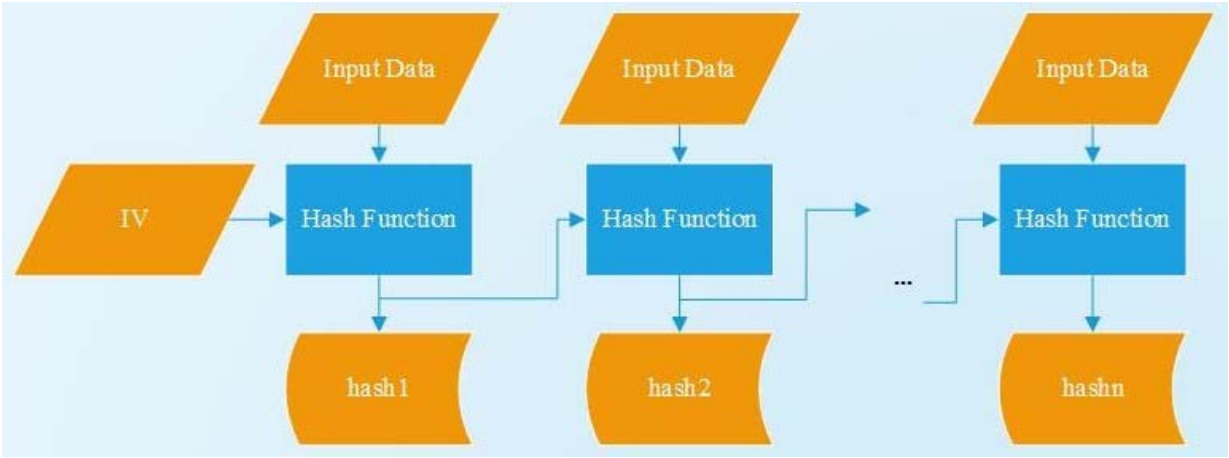

Figure 3. Cascade structure using cryptographic hash functions of the proposed method

3. RESULTS AND DISCUSSION

The security of applications used in many areas depends on the security of random numbers. Random numbers are an important part of the applications. Therefore, various security parameters must be met for the numbers used in these fields to be considered safe. The first of these parameters is that the source and method of the random numbers should be safe. Secondly, the numbers do not contain any statistical weakness. Another important parameter is that these numbers should meet the security requirements for cryptographic applications. In addition, the production cost of these numbers is another important parameter.

The proposed approach is based on the DCT method, which is widely used in lossy compression operations. Compressed data obtained with this approach is created with some loss from the original data. Here, the amount of loss varies according to the compression ratio in the original image. However, since some coefficients of the data transferred to the frequency space are not taken into account, the original picture is not produced from the compressed picture. Thus, the difference values between the compressed data and the original data can be used as an entropy source. In this study, raw random numbers are generated by using the entropy source. Here, is original image value, compressed image value, and difference matrix value is given in Table 2, Table 3, and Table 4 respectively.

Table 2. Original image value

	1	2	3	4	5	6	7	8
1	225	226	225	226	227	228	228	228
2	224	225	225	226	227	228	227	228
3	224	225	226	226	227	228	228	227
4	224	225	225	228	227	226	228	228
5	222	225	224	226	226	228	227	228
6	223	224	224	226	226	226	227	227
7	224	224	225	226	226	226	226	226
8	223	223	224	225	226	226	227	227

Table 3. Compressed image value

	1	2	3	4	5	6	7	8
1	221	224	225	229	229	228	230	225
2	222	227	225	226	227	227	231	229
3	222	228	227	228	227	227	231	231
4	229	229	224	225	224	225	225	227
5	224	224	223	223	224	228	229	231
6	223	228	226	225	227	229	227	229
7	218	223	226	226	225	224	221	223
8	220	219	224	227	226	227	223	222

Table 4. Difference matrix value

	1	2	3	4	5	6	7	8
1	4	2	0	3	2	0	2	3
2	2	2	0	0	0	1	4	1
3	2	3	1	2	0	1	3	4
4	5	4	1	3	3	1	3	1
5	2	1	1	3	2	0	2	3
6	0	4	2	1	1	3	0	2
7	6	1	1	0	1	2	5	3
8	3	4	0	2	0	1	4	5

In the proposed approach, cryptographic hash functions are used to remove any possible statistical weaknesses and biases in the generator. The use of these functions guarantees the security of the generated numbers. Primarily, these functions meet the requirements for cryptographic systems. These requirements, expressed as R1-R4, are parameters such as the numbers produced do not contain any statistical weakness, do not reproduce, and do not be reversed. These requirements are briefly explained in Table 1. Hash functions meet these requirements because they are both unidirectional and conflict-proof.

Random number generators should not contain any statistical weaknesses because of security reasons. The weaknesses make possible various attacks on these numbers. So the numbers used in critical applications do not contain any statistical weaknesses. Various tests are used to statistically examine the random number generators. These tests have similar structures generally. The 800-22 test suite, proposed by NIST, and the autocorrelation method are widely used. The 800-22 test suite contains 15 different tests [26]. This test suite statistically analyzes the random numbers. The safety of the numbers is carried out using these tests. The successful test results are given in Table 5 show the safety of the proposed method.

Table 5. Statistical test results of the proposed method

Statistical tests	*P*-value	Results
Frequency Test	0.3751	Successful
Block-frequency Test	0.4972	Successful
Runs Test	0.5137	Successful
Test for the Longest Run of Ones in a Block Test	0.3254	Successful
Binary Matrix Rank Test	0.6176	Successful
Discrete Fourier Transform Test	0.1865	Successful
Non-overlapping Template Matching Test	0.3268	Successful
Overlapping Template Matching Test	0.6249	Successful
Maurer's Universal Statistical Test	0.7630	Successful
Linear Complexity Test	0.4534	Successful
Serial Test1	0.3017	Successful
Serial Test2	0.4782	Successful
Approximate Entropy Test	0.2164	Successful
Cumulative Sums Test	0.6595	Successful

The autocorrelation test is used to decide whether the produced random numbers are self-contained. The mathematical expression of the test is given in Eq. (4), where $\oplus$ is the *XOR* operation; n is the dimension, and d is an integer value in the range of $0 \leq d \leq n/2$. Eq. (5) shows the relationship between zero and one number. The results of the equation being in the range of $|X\_5\neg|<1.6449$ show that the proposed generator is successful [4]. Table 6 shows the successful results obtained using the method.

$$A(d) = \sum_{i=0}^{n-d-1} (b_n \oplus b_{n+d}) \quad (4)$$

$$X_5 = \frac{2[\mathrm{A(d)} - \frac{\mathrm{n-d}}{2}}{\sqrt{\mathrm{n-d}}} \quad (5)$$

Table 6. Autocorrelation test results

Test	D value	X5 value	Results
Autocorrelation	8	-0.4234	Successful
	10	0.5029	Successful
	13	-0.5341	Successful
	16	1.1878	Successful
	20	-0.7347	Successful
	25	-0.8628	Successful
	100	0.9652	Successful
	500	-0.9443	Successful
	1000	-1.2024	Successful

4. CONCLUSIONS

Random numbers form an important part of many algorithms. These numbers can be generated from different sources such as atmospheric phenomena and electrical noise. In the study, random numbers are generated by using lossy compression operations based on the discrete cosine transform. In the transformation, any data in the space domain is transferred to the frequency domain. In the coefficient matrix produced by this transfer process, some important coefficients are preserved and the unimportant ones are neglected, taking into account human visual psychology. These operations cause differences between the original image and the compressed image. In the study, random numbers are generated by using these differences as an entropy source. The cryptographic hash function is used to remove any possible weaknesses in these generated numbers. This function is unidirectional and conflict-proof, which makes the numbers safe. Thus, the generated numbers meet the security requirements for many areas, especially cryptographic applications. In addition, the NIST and autocorrelation tests are used to show that the produced numbers do not contain any statistical weakness. Thus, the generated random numbers can be used in many fields.

REFERENCES

[1] Flores-Vergara, A., Garcia-Guerrero, E. E., Inzunza-González, E., López-Bonilla, O. R., Rodríguez-Orozco, E., Cardenas-Valdez, J. R., Tlelo-Cuautle, E. (2019). Implementing a chaotic cryptosystem in a 64-bit embedded system by using multiple-precision arithmetic, *Nonlinear Dynamics*, 96(1): 497-516.

[2] Yu, J.-Y., Lee, E., Oh, S.-R., Seo, Y.-D., Kim, Y.-G. (2020). A Survey on Security Requirements for WSNs: Focusing on the Characteristics Related to Security, *IEEE Access*, 8: 45304–45324.

[3] Koç, Ç. (2009). *Cryptographic Engineering*. Springer, New York.

[4] Menezes, A.J., van Oorschot, P.C., Vanstone, S.A. (1996). *Handbook of Applied Cryptography, 1st edn*., CRC Press, Boca Raton.

[5] Paar, C., Pelzl, J. (2009). *Understanding cryptography: a textbook for students and practitioners*, Springer, Bochum.

[6] Yakut, S. (2019). Design and Analysis of Real Random Number Generators, Ph.D. Thesis, Fırat University Institute of Science and Technology, Elazığ.

[7] Bakiri, M., Guyeux, C., Couchot, J. F., Oudjida, A. K. (2018). Survey on hardware implementation of random number generators on FPGA: Theory and experimental analyses, *Computer Science Review*, 27: 135-153.

[8] Aljohani, M.; Ahmad, I.; Basheri, M.; Alassafi, M.O. (2019). Performance Analysis of Cryptographic Pseudorandom Number Generators, *IEEE Access*, 7: 39794–39805.

[9] García-Martínez, M., Campos-Cantón, E. (2015). Pseudo-random bit generator based on multi-modal maps, *Nonlinear Dynamics*, 82(4): 2119–2131.

[10] Avaroglu, E. (2017). Pseudorandom number generator based on Arnold cat map and statistical analysis. *Turkish J. Electr. Eng. Comput. Sci.,* 25: 633-643.

[11] Avaroglu, E., Tuncer, T., Özer, A.B., Türk, M. (2015). A new method for hybrid pseudo random number generator, *J. Microelectron. Electron. Compon. Mater*., 44: 303–311

[12] Yakut, S., Tuncer, T., Özer, A. B. (2020). A New Secure and Efficient Approach for TRNG and Its Post-Processing Algorithms. Journal of Circuits, Systems and Computers.

[13] Avaroğlu, E., Tuncer, T. (2020). A novel S-box-based postprocessing method for true random number generation, *Turk. J. Elec. Eng. & Comp. Sci*., 28: 288–301.

[14] Garipcan, A. M., Erdem, E. (2020). A GRSÜ using chaotic entropy pool as a post-processing technique: analysis, design and FPGA implementation, *Analog Integrated Circuits and Signal Processing*, 103(3): 391-410.

[15] Łoza, Sz., Matuszewski Ł., Jessa M. (2015). A Random Number Generator Using Ring Oscillators and SHA-256 as Post-Processing, *Int. Journal of Electronics and Telecommunications*, 61(2): 199-204.

[16] Aljohani, M., Ahmad, I., Basheri, M., Alassafi, M. O. (2019). Performance analysis of cryptographic pseudorandom number generators, *IEEE Access*, 7: 39794-39805.

[17] Starosolski, R. (2020). Hybrid Adaptive Lossless Image Compression Based on Discrete Wavelet Transform, *Entropy*, 22(7): 751.

[18] Hudson, G., Yasuda H., Sebestyen I. (1988). The international standardization of a still picture compression technique, *IEEE Global Telecommunications Conference and Exhibition. Communications for the Information Age*, Hollywood, 1016-1021.

[19] Fuad, M., Ernawan F. (2020). Video steganography based on DCT psychovisual and object motion, *Bulletin of Electrical Engineering and Informatics*, 9(3): 1015-1023.

[20] Wedaj, F. T., Kim S., Kim H. J., et al. (2017). Improved reversible data hiding in JPEG images based on new coefficient selection strategy, *Eurasip Journal on Image & Video Processing*, (1): 63.

[21] Ajmera, A., Divecha M., Ghosh S. S., Raval I. and Chaturvedi R. (2019). Video Steganography: Using Scrambling- AES Encryption and DCT, DST Steganography, *2019 IEEE Pune Section International Conference (PuneCon)*, Pune, 1-7.

[22] Mao, B.H., Wang, Z.C., Zhang X.P. (2019). Asymmetric JPEG Steganography Based on Correlation in DCT Domain, *Computer Science*, 46(01):203-207.

[23] Ahmed, N., Natarajan T. and Rao K. R. (1974). Discrete Cosine Transform, *IEEE Transactions on Computers*, 23(1): 90-93.

[24] Al-Roithy, B.O., Gutub, A. (2021). Remodeling randomness prioritization to boost-up security of RGB image encryption, *Multimed Tools Appl*., 80: 28521–28581.

[25] Sumagita, M., Riadi I., Soepomo J.P., Warungboto U. (2018). Analysis of secure hash algorithm (SHA) 512 for encryption process on web based application, *Int J Cyber-Secur Digital for (IJCSDF),* 7(4): 373–381.

[26] Rukhin, A., Soto, J., Nechvatal, J., Smid, M., Barker, E., Leigh, S., Levenson, M., Vangel, M., Banks, D., Heckert, A., Dray, J., Vo, S. (2010). *A statistical test suite for random and pseudorandom number generators for cryptographic applications*, NIST Special Publication, Gaithersburg.

NATURENGS
MTU Journal of Engineering and Natural Sciences
https://dergipark.org.tr/tr/pub/naturengs
DOI: 10.46572/naturengs.1007532

Comparison of Standard and Pretrained CNN Models for Potato, Cotton, Bean and Banana Disease Detection

Soner KIZILOLUK[1*]

[1] Department of Computer Engineering, Faculty of Engineering and Natural Sciences, Malatya Turgut Özal University, Malatya, Turkey.

(**Received:** 09.10.2021; **Accepted:** 10.12.2021)

ABSTRACT: Plant diseases lead to a significant decrease in product efficiency and economic losses for producers. However, early detection of plant diseases plays an important role in preventing these losses. Today, Convolutional Neural Network (CNN) models are widely used for image processing in many fields such as face recognition, climate, health, and agriculture. But in these models, the weights of the layers are randomly initialized during training, which increases training time and decreases performance. With the method known as Transfer Learning in the literature, CNN models are trained on large databases such as ImageNet. Then, pretrained CNN models are created using the weights obtained in this training. Thus, training time decreases while performance improves. In this study, standard and pretrained versions of popular CNN models DarkNet-19, GoogleNet, Inception-v3, Resnet-18, and ShuffleNet have been used for automatic classification of diseases from leaf images of potato, cotton, bean, and banana. In the experimental study, the classification performances of all these standard and pretrained CNN models are presented comparatively. Experimental results have shown that the performance of CNN models is significantly improved by transfer learning, even in a small number of epochs.

Keywords: Convolutional Neural Network, Transfer Learning, Disease Detection, Classification.

1. INTRODUCTION

In parallel with the rapid increase in the world's population, the demand for agricultural products also increases. Increased productivity in agricultural products is very important to meet this demand. However, plant diseases lead to decreases in crop productivity, economic losses, and an inability to meet the increasing demand. However, early detection of plant diseases plays an important role in preventing these losses. Experts and laboratories are required to detect plant diseases. However, this increases the transaction costs and leads to time loss [1]. Today, methods based on image processing technology are frequently used for the detection of plant diseases [2]. Convolutional Neural Network (CNN) models, one of the most up-to-date image processing technologies, are widely used in many areas such as face recognition, climate, health, and agriculture.

There are many CNN-based studies for the detection of plant diseases in the literature. Chen et al. [3] proposed a CNN model called Mobile-Atten, which is based on the MobileNet-v2 CNN model. In the study, they performed disease detection and classification using rice leaves with the Mobile-Atten model. In another study focusing on disease detection using rice leaves,

*Corresponding Author: soner.kiziloluk@ozal.edu.tr
ORCID number of authors: [1] 0000-0002-0381-9631

Shrivastava et al. [4] used AlexNet architecture. In the study, they reached a 91.37% classification accuracy rate. Abbas et al. [5] proposed a method called C-GAN based on the DenseNet CNN model for disease detection using tomato leaves and achieved a 99.51% success rate. Türkoğlu et al. [1] suggested a new CNN model consisting of 18 layers for disease detection using apricot images. Sert [6] proposed a new method called Faster R-CNN-GC, which is based on image compositing, GoogleNet, and Faster R-CNN. In the study, the detection of pepper and potato leaves was carried out and the type of disease was determined from these leaves. On the other hand, Khan et al. [7] proposed an approach called CCDF for disease detection using apple and banana leaf images. In this approach, feature extraction from apple and banana images is performed with pretrained VGG-16 and AlexNet models, and then classification is performed with the Support Vector Machine (SVM). Aksoy et al. [8] performed disease detection with AlexNet, DenseNet-121, Resnet-34, Squeezenet, and VGG-16 CNN models using apple leaf images and compared the performances of these models. Hassan et al.[9]performed disease detection with Inception-v3, InceptionResNet-v2, MobileNet-v2, and EfficientNet-b0 CNN models using leaf images of 14 different plants. Arivazhagan and League [10] proposed a 7-layer CNN model for disease detection using leaf images of the mango plant. The proposed model was found to classify the test data correctly at a rate of 96.67%. Priyadharshini et al. [11] performed disease detection using corn leaf images with the modified LeNet model and achieved a success rate of 97.89%. Dinata et al. [12] achieved a 63.7% success rate with the CNN model they proposed for disease detection using strawberry leaf images.

In this study, DarkNet-19, GoogleNet, Inception-v3, Resnet-18, and ShuffleNet models, which are popular CNN models, have been used for automatic classification of diseases from leaf images of potato, cotton, bean, and banana. In addition, pretrained versions of these models have also been used in the study. Experiment results show that the performance is significantly increased even in a small number of epochs with “Transfer Learning.”

The rest of the study has been organized as follows. In the Material and Methods section, CNN models, the concept of transfer learning, the datasets, and the workflow of the study are presented. In the Results and Discussion section, experimental study and results are given in detail. In the last section, the obtained results are discussed.

2. MATERIAL AND METHODS

2.1. Convolutional Neural Networks (CNN)

CNN is a special type of Neural Networks (NN). It was developed by drawing inspiration from the biological model of the visual cortex of animals. CNNs are frequently used in image and audio processing due to advantages such as highly accurate identification, automatic feature extraction, and learning [13]. CNNs consist of many layers. Its basic layers are the convolution layer, pooling layer, and classification layer. In the convolution layer, feature extraction is carried out by hovering small filters over the image. The pooling layer is used to reduce the size of the features. The final layer of CNN and the layer in which classification is carried out is the classification layer [1].

In this study, DarkNet-19, GoogleNet, Inception-v3, Resnet-18 and, ShuffleNet CNN models have been used. The DarkNet-19 model was proposed by Redmon [14]. It consists of 19 layers in total and the image input size is 256. The GoogleNet model was proposed by Szegedy et al. [15] and the image input size and number of layers are 224 and 22, respectively. In the Inception-v3 model proposed by Szegedy et al. [16], the image input size is 299 and it consists of 48 layers. The ResNet-18 model with an image input size of 224 and 18 layers was proposed

by He et al. [17]. In the ShuffleNet model proposed by Zhang et al. [18], the image input size is 224 and it consists of 50 layers.

In this study, pretrained versions of CNN models created with the Transfer Learning method have also been used. In CNN models, the weights in the layers are randomly initialized during training. This leads to a longer training period and decreased performance. Transfer Learning is a learning approach that examines the use of the information learned during the training phase of machine learning systems in different or similar problem solutions [19]. With the Transfer Learning method, CNN models are first trained on large databases such as ImageNet. Then, pretrained CNN models are created using the weights obtained in this training. Thus, training time decreases while performance improves.

2.2. Image Datasets

In this study, 4 different datasets on potato, cotton, bean, and banana, obtained from Kaggle, have been used [20-23]. The potato dataset consists of 3 classes, Early Blight, Healthy, and Late Blight, and 2152 images. The cotton dataset consists of a total of 4 classes, bacterial blight, curl virus, fusarium wilt, and healthy, as well as 1711 images. The bean dataset consists of 3 classes, angular leap spot, bean rust, and healthy, as well as 1296 images. The banana dataset consists of 4 classes, Cordana, Healthy, Pestalotiopsis, and Sigatoka, as well as 936 images. Samples images from both datasets are shown in Figure 1.

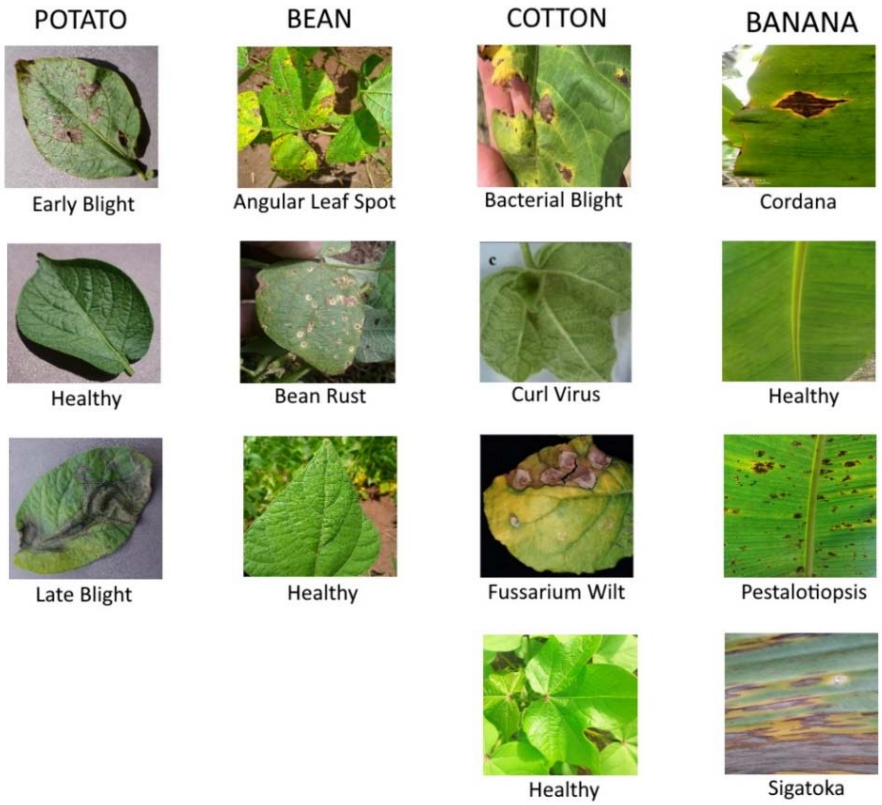

Figure 1. Sample images from datasets

2.3. Methods

In this study, standard and pretrained versions of DarkNet-19, GoogleNet, Inception-v3, Resnet-18, and ShuffleNet CNN models have been used for automatic classification of diseases using leaf images of potato, cotton, bean, and banana. In all datasets, %80 and %20 images have been used for training and testing processes, respectively. In addition, 10% of the training data have been selected for train validation. The workflow diagrams of the study have been given in Figure 2 for standard CNN models and in Figure 3 for pre-trained CNN models. In standard CNN models, the weights of the layers have been initialized randomly during training. On the other hand, In pretrained CNN models, standard CNN models are first trained on large databases such as ImageNet. Then the weights of the layers obtained from the training are transferred.

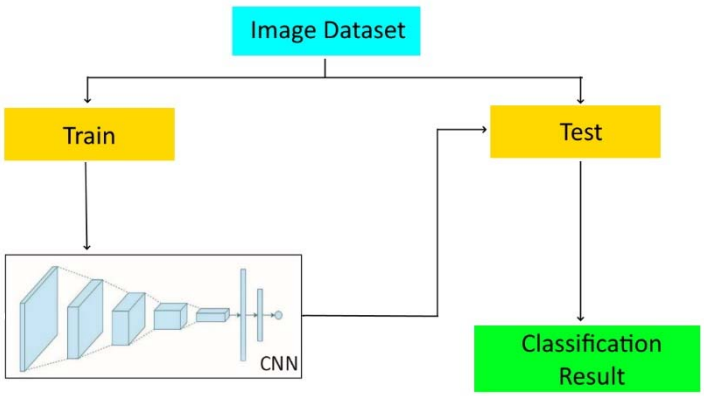

Figure 2. Workflow for standard CNN models

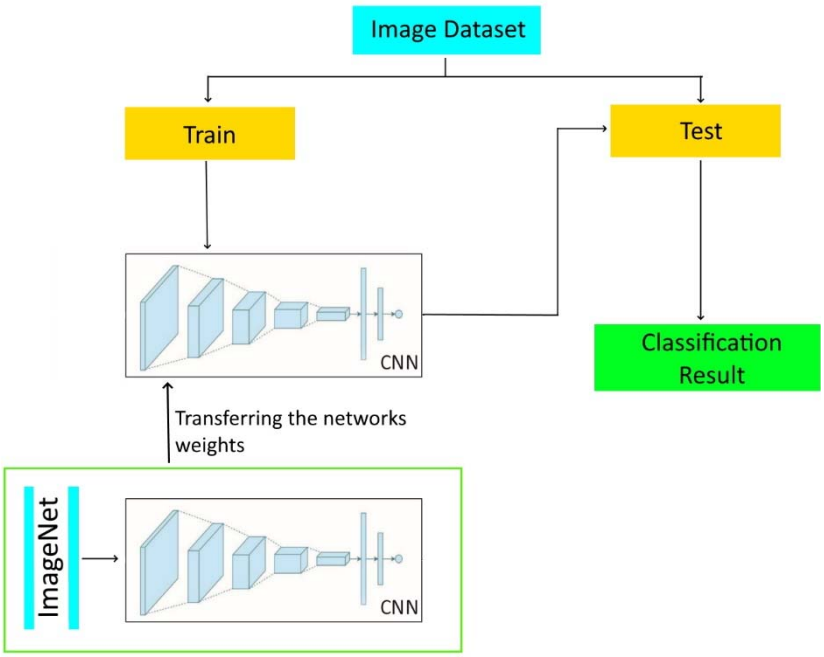

Figure 3. Workflow for pretrained CNN models

3. RESULTS AND DISCUSSION

For all CNN models, the max epoch value, the mini-batch size value, and the initial learning rate value have been selected as 5, 25, and 0.001, respectively. In addition, all CNN models have been run ten times on all datasets, and comparison has been carried according to the mean and maximum accuracy values obtained in train validation and testing processes. Additionally, mean training accuracy curves, confusion matrices, and ROC curves of each CNN model have been presented comparatively.

Table 1 shows the results obtained from the potato dataset. When the results are examined, it is seen that Pretrained-DarkNet-19 had the best performance with 99.59 mean accuracy and 100 maximum accuracy values for training validation. For the test, Pretrained-ResNet-18 had the best results with 99.67 mean accuracy and 100 maximum accuracy. Standard GoogleNet had the worst performance for both training validation and testing. In addition, it is easily seen that the performance of standard CNN models has increased by up to 7% with the transfer learning method.

Table 1. Results for the Potato dataset

	TRAIN VALIDATION			**TEST**		
	Acc. (mean)	**Acc. (max)**	**Std.Dev.**	**Acc. (mean)**	**Acc. (max)**	**Std.Dev.**
DarkNet-19	98.63	99.13	0.48	98.49	99.30	0.55
GoogleNet	92.65	96.51	3.66	93.14	96.05	2.44
Inception-v3	95.70	97.38	1.26	95.67	96.98	0.86
ResNet-18	98.20	99.13	0.65	97.44	97.91	0.49
ShuffleNet	94.39	96.80	1.25	94.37	96.74	1.45
Pretrained-DarkNet-19	**99.59**	**100.00**	0.46	99.56	**100.00**	0.43
Pretrained-GoogleNet	99.01	99.42	0.53	98.81	99.53	0.79
Pretrained-Inception-v3	99.10	99.42	0.29	99.30	99.77	0.36
Pretrained-ResNet-18	99.45	**100.00**	**0.29**	**99.67**	**100.00**	**0.22**
Pretrained-ShuffleNet	98.90	99.71	0.49	99.12	99.77	0.46

Table 2 shows the results obtained from the cotton dataset. When the results are examined, it is seen that Pretrained-GoogleNet had the best results in all values except mean accuracy for the test. In addition, it is easily seen that the performance of standard CNN models has increased by around 25% with the transfer learning method.

Table 3 shows the results obtained from the Bean dataset. When the results are examined, it is seen that Pretrained-DarkNet-19 had the best performance with 94.54 mean accuracy and 97.1 maximum accuracy for training validation, and 94.22 mean accuracy and 96.9 maximum accuracy for testing. In addition, it is easily seen that the performance of standard CNN models has increased by 20% with the transfer learning method.

Table 2. Results for the Cotton dataset

	TRAIN VALIDATION			TEST		
	Acc. (mean)	**Acc. (max)**	**Std.Dev.**	**Acc. (mean)**	**Acc. (max)**	**Std.Dev.**
DarkNet-19	71.46	77.01	3.43	73.56	80.76	4.51
GoogleNet	66.24	72.99	4.98	65.34	74.93	6.54
Inception-v3	69.23	74.45	3.01	63.85	77.55	5.82
ResNet-18	75.69	80.66	3.80	75.10	79.59	4.03
ShuffleNet	70.11	74.45	3.59	65.25	73.47	5.24
Pretrained-DarkNet-19	71.28	87.96	12.83	69.59	87.76	10.58
Pretrained-GoogleNet	**92.85**	**95.62**	2.52	91.05	**94.17**	1.91
Pretrained-Inception-v3	89.60	91.24	0.99	**91.95**	93.88	**1.49**
Pretrained-ResNet-18	89.89	90.88	**0.89**	89.42	93.29	2.06
Pretrained-ShuffleNet	88.21	90.51	1.76	89.10	91.84	1.85

Table 3. Results for the Bean dataset

	TRAIN VALIDATION			TEST		
	Acc. (mean)	**Acc. (max)**	**Std.Dev.**	**Acc. (mean)**	**Acc. (max)**	**Std.Dev.**
DarkNet-19	75.27	77.78	2.71	74.61	79.46	2.33
GoogleNet	69.66	74.40	3.38	65.08	69.38	2.69
Inception-v3	71.11	74.40	2.08	68.80	71.71	2.89
ResNet-18	72.90	78.26	2.93	71.32	76.36	3.78
ShuffleNet	65.02	69.57	4.37	63.37	67.44	3.93
Pretrained-DarkNet-19	**94.54**	**97.10**	1.55	**94.22**	**96.90**	1.84
Pretrained-GoogleNet	91.01	92.27	2.01	91.36	93.41	1.89
Pretrained-Inception-v3	91.93	92.75	**0.60**	93.37	94.19	**0.62**
Pretrained-ResNet-18	94.30	96.14	1.01	94.69	96.51	1.14
Pretrained-ShuffleNet	92.13	94.20	1.64	91.82	94.19	1.28

Table 4. Results for the Bean dataset

	TRAIN VALIDATION			TEST		
	Acc. (mean)	**Acc. (max)**	**Std.Dev.**	**Acc. (mean)**	**Acc. (max)**	**Std. Dev.**
DarkNet-19	89.47	92.67	3.45	87.82	93.09	3.68
GoogleNet	69.87	81.33	10.19	70.90	81.38	7.97
Inception-v3	82.80	86.00	3.40	81.65	86.70	4.47
ResNet-18	87.40	90.67	3.96	85.64	91.49	3.82
ShuffleNet	76.87	82.67	4.66	75.96	85.11	5.88
Pretrained-DarkNet-19	92.73	98.00	4.47	89.31	94.15	2.69
Pretrained-GoogleNet	**96.60**	**98.67**	**1.06**	**93.30**	**95.21**	1.65
Pretrained-Inception-v3	94.33	96.00	1.23	91.38	93.09	**1.25**
Pretrained-ResNet-18	94.33	97.33	1.78	90.59	93.09	2.08
Pretrained-ShuffleNet	92.53	94.67	1.36	89.26	92.55	2.09

Table 4 shows the results obtained from the Banana dataset. When the results are examined, it is seen that Pretrained-GoogleNet had the best performance. In addition, it is easily seen that the performance of standard CNN models has increased by around 10% with the transfer learning method.

Mean training accuracy curves of all models obtained from the Potato, Cotton, Bean, and Banana datasets are shown in Figure 4, Figure 5, Figure 6, and Figure 7, respectively. When the figures are examined, it is seen that the accuracy values of the pretrained CNN models reach high values even in the early iteration. In standard CNN models, it is seen that accuracy values do not increase much even in later iterations.

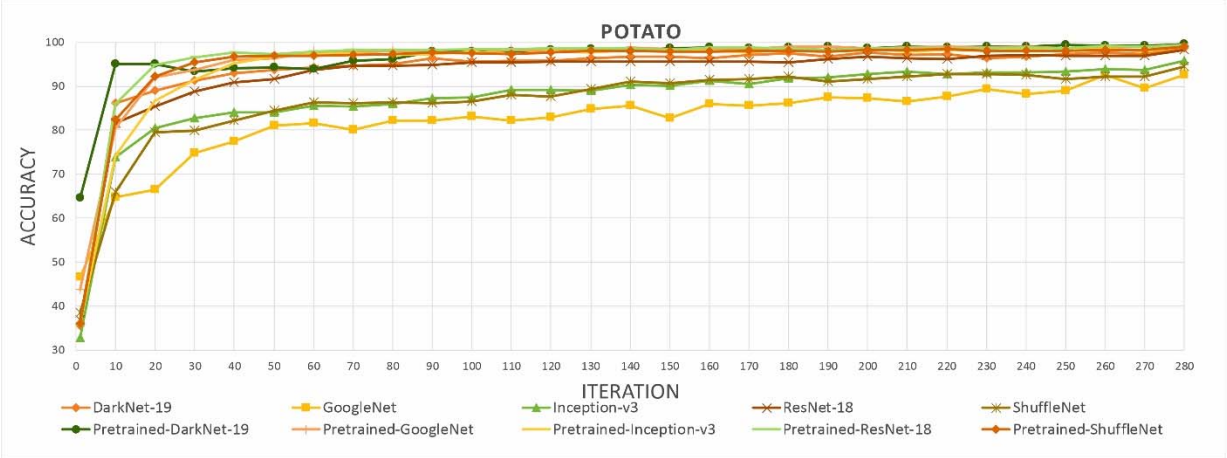

Figure 4. Mean training accuracy curves for the Potato dataset

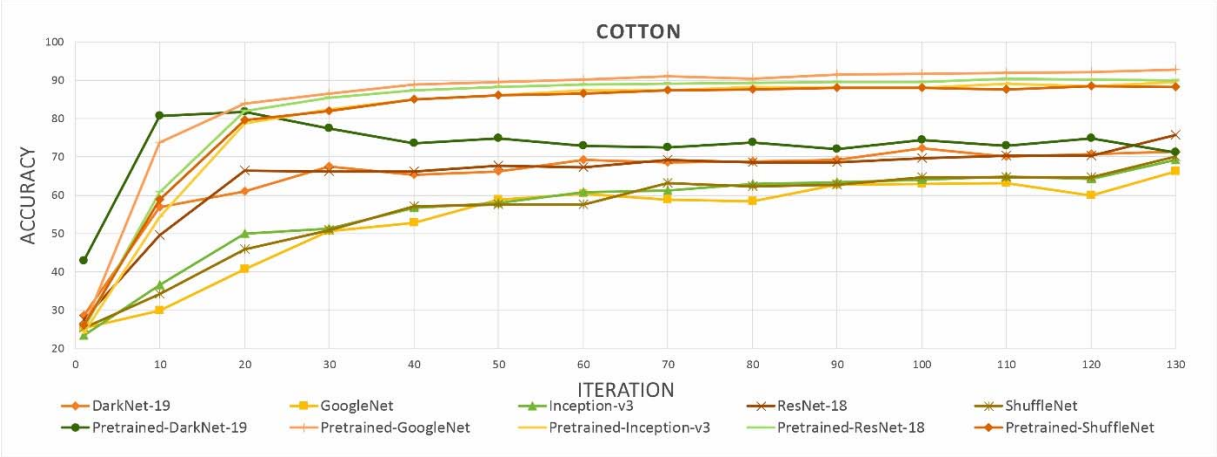

Figure 5. Mean training accuracy curves for the Cotton dataset

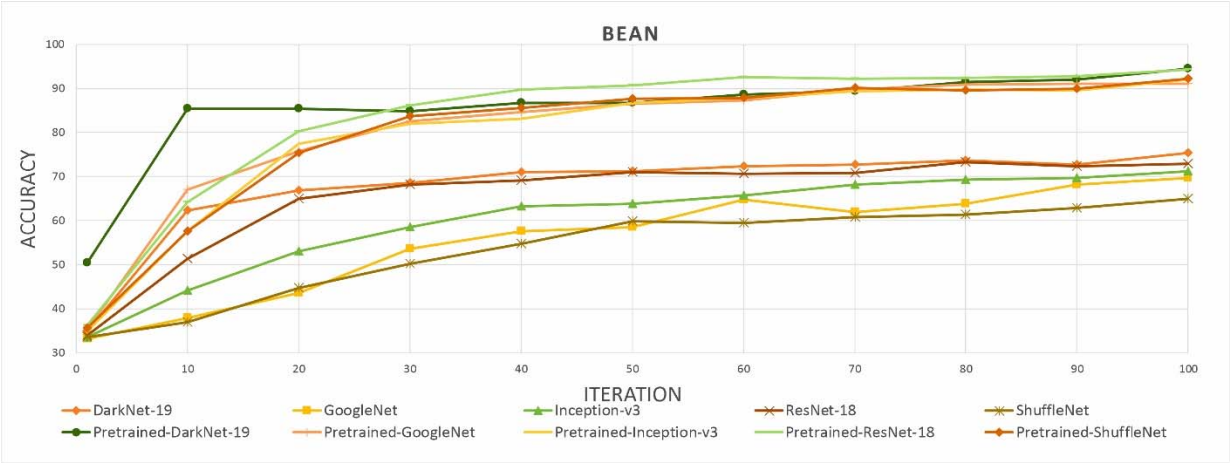

Figure 6. Mean training accuracy curves for the Bean dataset

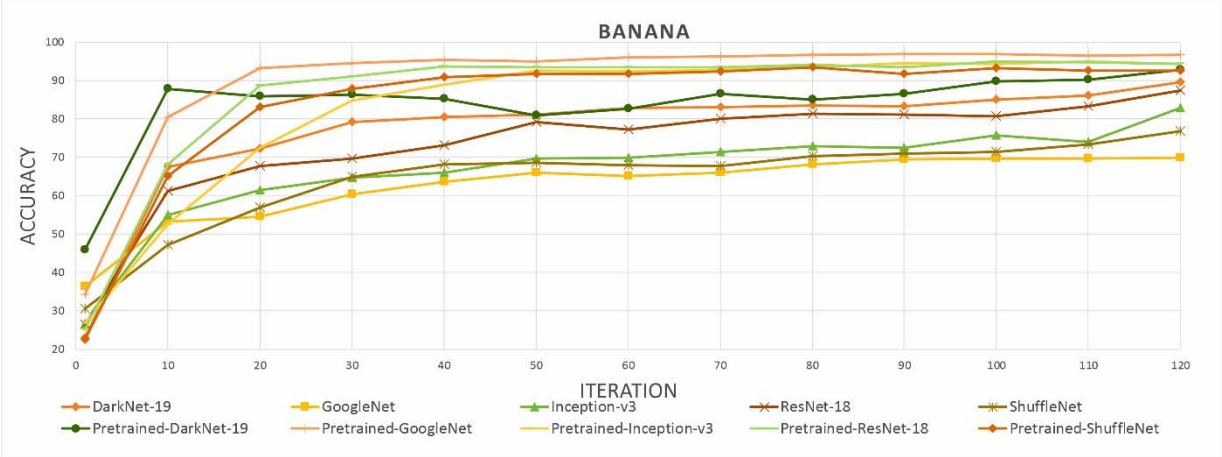

Figure 7. Mean training accuracy curves for the Banana dataset

Confusion matrices obtained from the tests of potato, cotton, bean and, banana datasets in all CNN models are given in Figures 8, 9, 10, and 11, respectively. A confusion matrix is a table that is used to describe the performance of a model by referring to its accuracy rates in each class. The rows in the confusion matrix show the predicted class (Output Class) and the columns show the true class (Target Class). When the matrixes are examined, it is easily seen that the class-based correct prediction rates of the pretrained CNN models are higher than the standard CNN models.

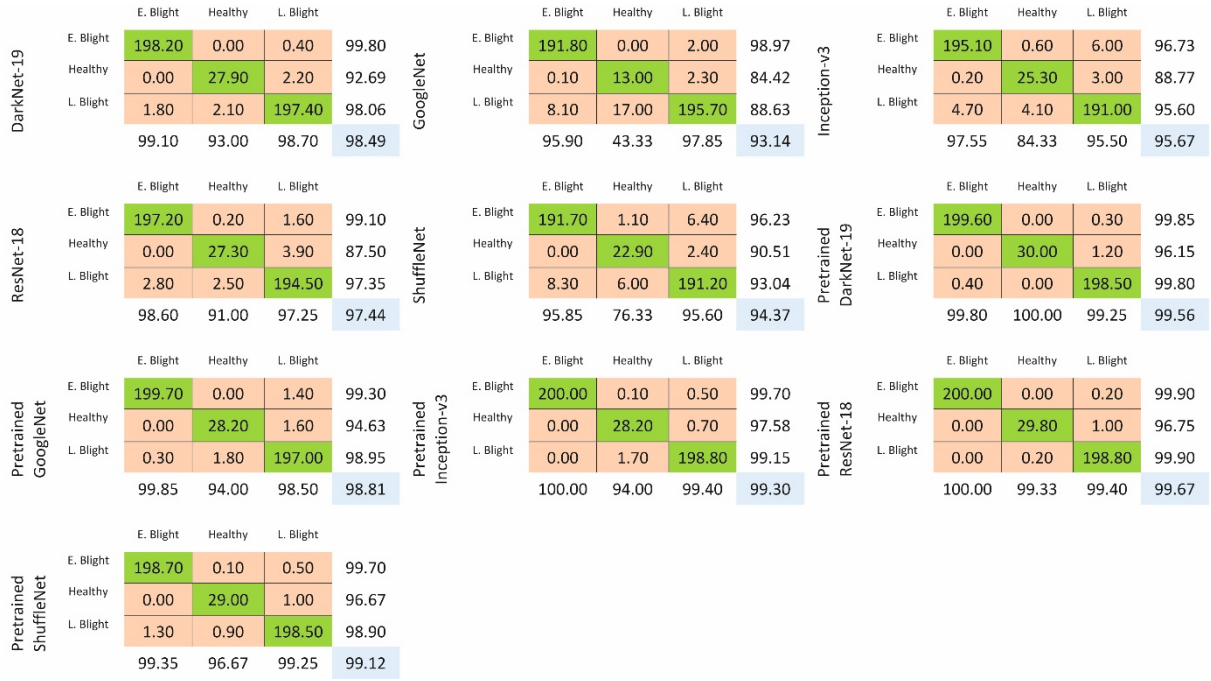

Figure 8. Confusion matrices of Potato dataset

Figure 9. Confusion matrices of Cotton dataset

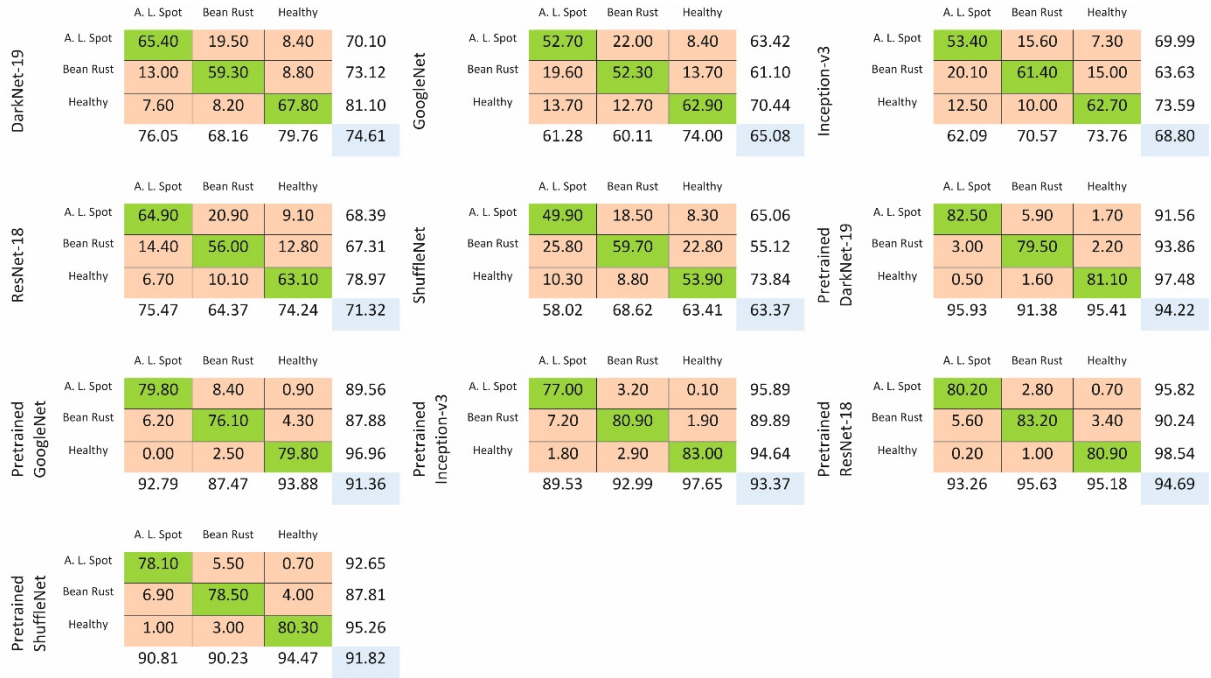

Figure 10. Confusion matrices of Bean dataset

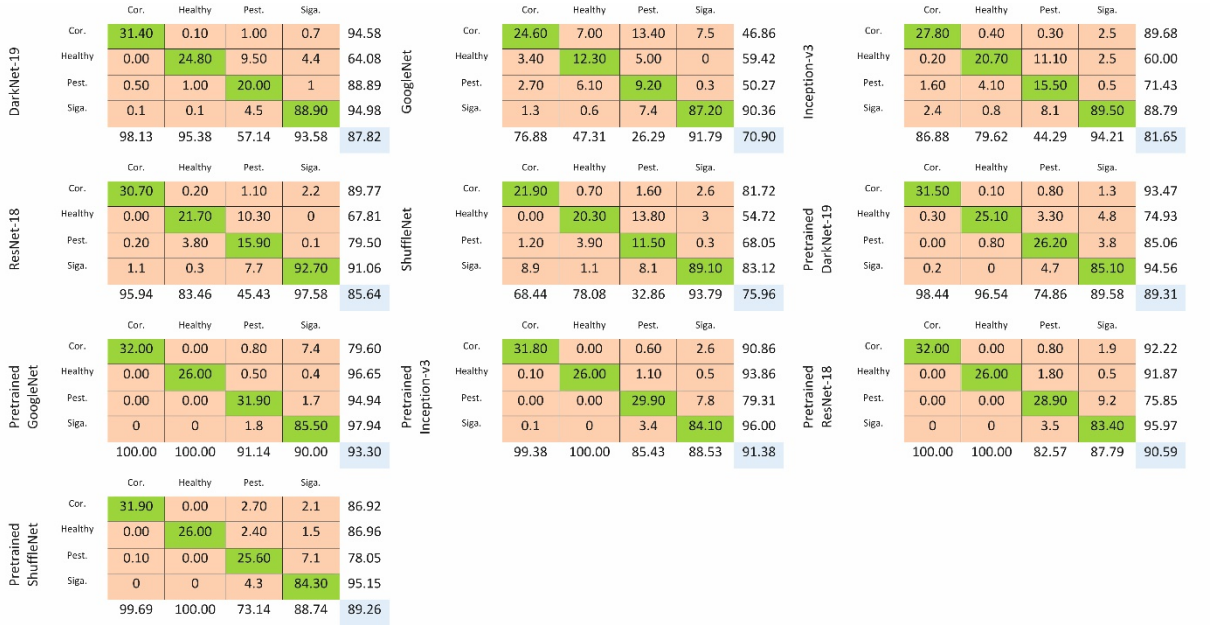

Figure 11. Confusion matrices of Banana dataset

The Receiver-Operating Characteristic (ROC) curves obtained from potato, cotton, bean, and banana datasets are shown in Figures 12, 13, 14, and 15, respectively. ROC curves show the relationship between the false-positive rate (FPR) and the true-positive rate (TPR). It is seen that pretrained CNN models have higher true-positive rates in all datasets.

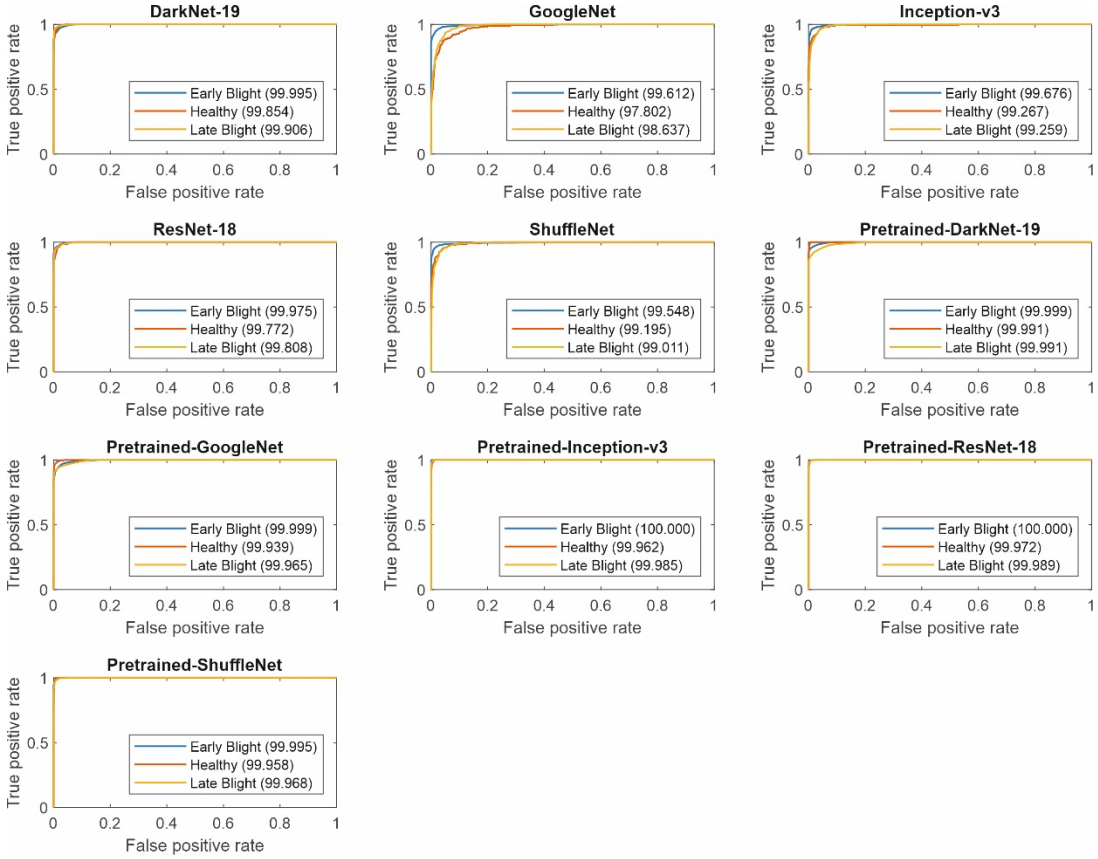

Figure 12. ROC Curves for Potato dataset

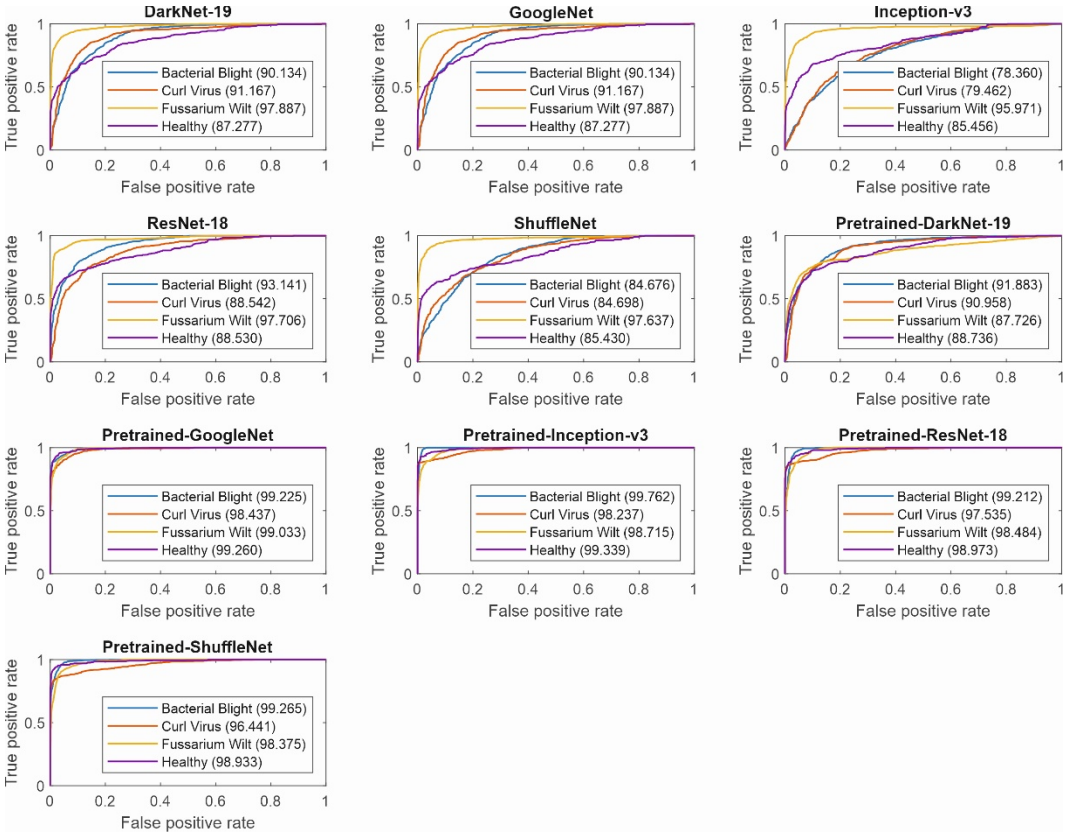

Figure 13. ROC Curves for Cotton dataset

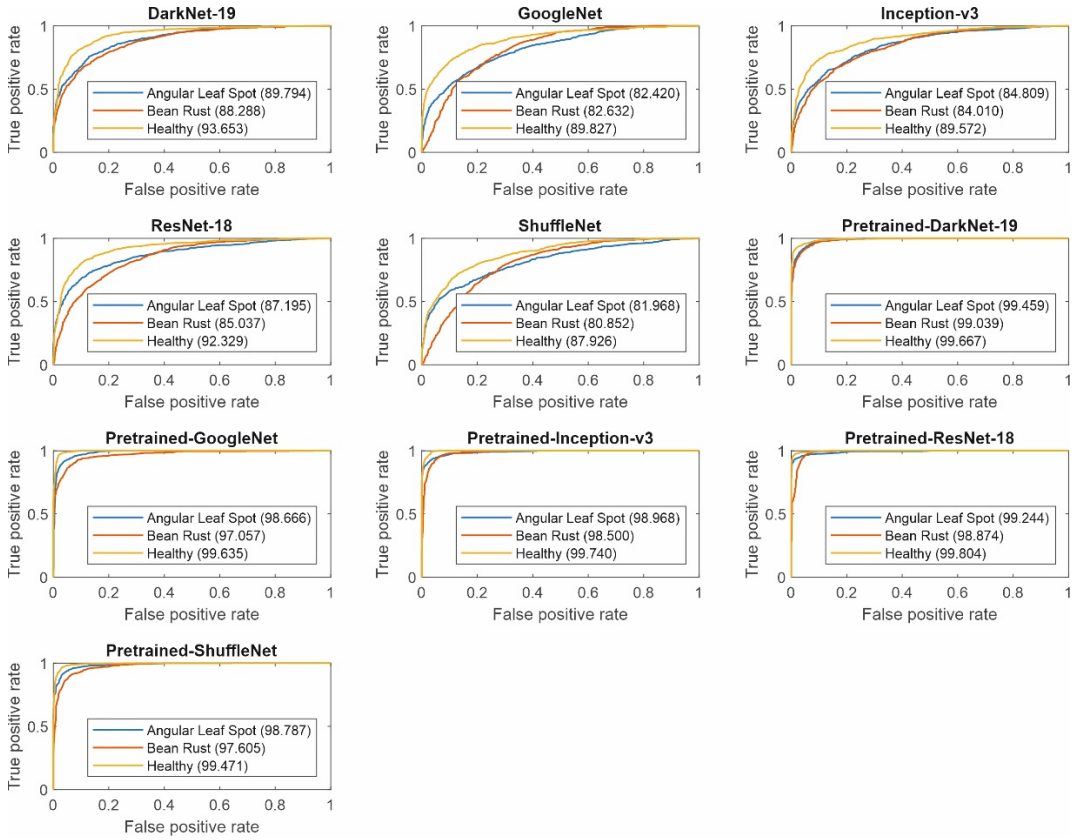

Figure 14. ROC Curves for Bean dataset

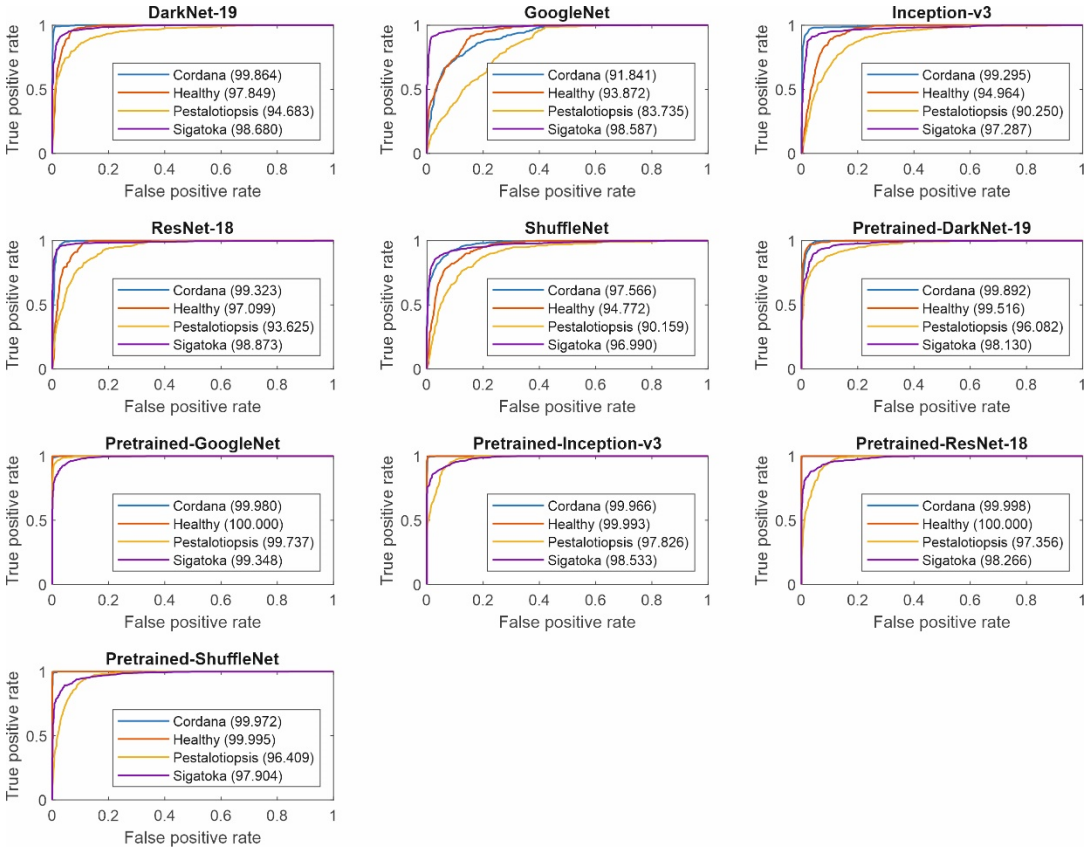

Figure 15. ROC Curves for Banana dataset

4. CONCLUSIONS

Plant diseases lead to decreases in crop productivity, economic losses, and an inability to meet the increasing demand. However, early detection of plant diseases plays an important role in preventing these losses. Methods based on image processing technology play an important role in the detection of plant diseases. In this study, DarkNet-19, GoogleNet, Inception-v3, Resnet-18 and, ShuffleNet models, which are popular CNN models, have been used for automatic classification of diseases from leaf images of potato, banana, cotton, and bean. In addition, pretrained versions of these models, the weights of which were previously trained in different large databases with the "Transfer Learning" method, have also been used in the study. When the experiment results were examined in general, it was seen that the Pretrained-DarkNet-19 and Pretrained-GoogleNet models had the highest performance. In addition, the experiment results revealed that the success rates of standard CNN models increase by 7% to 25% with the transfer learning method, even at very low numbers such as 5 epochs. In future studies, features can be extracted from plant disease images with CNN and various classification algorithms can be used in the classification phase.

REFERENCES

[1] Türkoğlu, M., Hanbay, K., Sivrikaya, I. S., and Hanbay, D. (2021). Derin Evrişimsel Sinir Ağı Kullanılarak Kayısı Hastalıklarının Sınıflandırılması, *Bitlis Eren Üniversitesi Fen Bilimleri Dergisi*, 9(1): 334-345.

[2] Aslan, M. (2021). Derin Öğrenme ile Bitki Hastalıklarının Tespiti, *Avrupa Bilim ve Teknoloji Dergisi*, 23: 540-546.

[3] Chen, J., Zhang, D., Zeb, A., and Nanehkaran, Y. A. (2021). Identification of rice plant diseases using lightweight attention network, *Expert Systems with Applications*, 169: 114514.

[4] Shrivastava, V. K., Pradhan, M. K., Minz, S., and Thakur, M. P. (2019). Rice plant disease classification using transfer learning of deep convolution neural network, *International Archives of the Photogrammetry, Remote Sensing & Spatial Information Sciences*, 3(6): 631–635.

[5] Abbas, A., Jain, S., Gour, M., and Vankudothu, S. (2021). Tomato plant disease detection using transfer learning with C-GAN synthetic images, *Computers and Electronics in Agriculture*, 187: 106279.

[6] Sert, E. (2021). A deep learning based approach for the detection of diseases in pepper and potato leaves, *Anadolu Tarım Bilimleri Dergisi*, 36(2): 167-178.

[7] Khan, M. A., Akram, T., Sharif, M., Awais, M., Javed, K., Ali, H., and Saba, T. (2018). CCDF: Automatic system for segmentation and recognition of fruit crops diseases based on correlation coefficient and deep CNN features, *Computers and electronics in agriculture*, 155: 220-236.

[8] Aksoy, B., Halis, H. D., and Salman, O. K. M. (2020). Elma Bitkisindeki Hastalıkların Yapay Zekâ Yöntemleri ile Tespiti ve Yapay Zekâ Yöntemlerinin Performanslarının Karşılaştırılması, *International Journal of Engineering and Innovative Research*, 2(3): 194-210.

[9] Hassan, S. M., Maji, A. K., Jasiński, M., Leonowicz, Z., and Jasińska, E. (2021). Identification of Plant-Leaf Diseases Using CNN and Transfer-Learning Approach, *Electronics*, 10(12): 1388.

[10] Arivazhagan, S., and Ligi, S. V. (2018). Mango leaf diseases identification using convolutional neural network, *International Journal of Pure and Applied Mathematics*, 120(6): 11067-11079.

[11] Priyadharshini, R. A., Arivazhagan, S., Arun, M., and Mirnalini, A. (2019). Maize leaf disease classification using deep convolutional neural networks, *Neural Computing and Applications*, 31(12): 8887-8895.

[12] Dinata, M. I., Nugroho, S. M. S., and Rachmadi, R. F. (2021). Classification of Strawberry Plant Diseases with Leaf Image Using CNN, *International Conference on Artificial Intelligence and Computer Science Technology (ICAICST) IEEE*, Yogyakarta, Indonesia, 68-72.

[13] Qin, Z., Yu, F., Liu, C., and Chen, X. (2018). How convolutional neural network see the world-A survey of convolutional neural network visualization methods. *arXiv preprint* arXiv:1804.11191.

[14] Redmon, J., and Farhadi, A. (2017). YOLO9000: better, faster, stronger. *In Proceedings of the IEEE conference on computer vision and pattern recognition*, Honolulu, HI, USA, 7263-7271.

[15] Szegedy, C., Liu, W., Jia, Y., Sermanet, P., Reed, S., Anguelov, D. and Rabinovich, A. (2015). Going deeper with convolutions, *In Proceedings of the IEEE conference on computer vision and pattern recognition*, Boston, USA, 1-9.

[16] Szegedy, C., Vanhoucke, V., Ioffe, S., Shlens, J., and Wojna, Z. (2016). Rethinking the inception architecture for computer vision, *In Proceedings of the IEEE conference on computer vision and pattern recognition*, Las Vegas, USA, 2818-2826.

[17] He, K., Zhang, X., Ren, S., and Sun, J. (2016). Deep residual learning for image recognition, *In Proceedings of the IEEE conference on computer vision and pattern recognition*, Las Vegas, USA, 770-778.

[18] Zhang, X., Zhou, X., Lin, M., and Sun, J. (2018). Shufflenet: An extremely efficient convolutional neural network for mobile devices, *In Proceedings of the IEEE conference on computer vision and pattern recognition*, Salt Lake City, USA, 6848-6856.

[19] Fırıldak, K., and Talu, M. F. (2019). Evrişimsel Sinir Ağlarında Kullanılan Transfer Öğrenme Yaklaşımlarının İncelenmesi, *Computer Science*, 4(2): 88-95.

[20] Nath, S. (2021). Potato Leaf Disease Detection. Kaggle Data, version 1. Retrieved September 20, 2021 from https://www.kaggle.com/sayannath235/potato-leaf-disease-detection/metadata.

[21] Karim, S. (2021). Cotton Leaf Disease Dataset. Kaggle Data, version 1. Retrieved September 20, 2021 from https://www.kaggle.com/seroshkarim/cotton-leaf-disease-dataset/metadata.

[22] Rastogi, P. (2021). Bean leaf dataset. Kaggle Data, version 1. Retrieved September 20, 2021 from https://www.kaggle.com/prakharrastogi534/bean-leaf-dataset/metadata.

[23] Mahmud, K. A. (2021). Banana Leaf Dataset. Kaggle Data, version 2. Retrieved September 20, 2021 from https://www.kaggle.com/kaiesalmahmud/banana-leaf-dataset.